JAAS

Accepted Manuscript

Volume 31 | Number 1 | January 2016 | Pages 1–346

JAAS

Journal of Analytical Atomic Spectrometry
www.rsc.org/jaas

Themed Issue: Celebrating the 30th Anniversary of JAAS

ISSN 0267-9477

ROYAL SOCIETY
OF CHEMISTRY

CRITICAL REVIEW
Timur A. Labutin et al.
Femtosecond laser-induced breakdown spectroscopy

175 YEARS

ROYAL SOCIETY
OF CHEMISTRY

rsc.li/jaas

ICP-MS for the Analysis at the Nanoscale – A Tutorial Review

Björn Meermann[1*] and Volker Nischwitz[2]

[1]Federal Institute of Hydrology, Department G2 - Aquatic Chemistry, Am Mainzer Tor 1, 56068 Koblenz, Germany. *E-Mail: meermann@bafg.de

[2]Central Institute for Engineering, Electronics and Analytics, Analytics (ZEA-3), Forschungszentrum Juelich, 52425 Juelich, Germany.

Keywords

Abstract

This tutorial review focuses on the use of ICP-MS based techniques for metal-containing nanoparticle analysis.

Within the **first part** the capabilities of "stand alone" ICP-MS for total metal analysis and the suitability of stable isotopes for nanoparticle tracking (stable isotope labelling and naturally occurring variation in isotope ratios) are introduced (chapter 3). Special focus was given on single particle ICP-MS (sp-ICP-MS) mode (chapter 4). Upon a brief introduction into the theoretical concept, critical aspects such as calibration strategies, dwell time as well as ionic background were discussed and practical advice is given. References to current data assessment sheets are provided. Furthermore, a brief chapter on general sample preparation aspects is included within the first part (chapter 2).

The **second part** is dedicated to fractionation/separation systems, such as field-flow fractionation (FFF), hydrodynamic chromatography (HDC), high performance liquid chromatography (HPLC) and capillary electrophoresis (CE) coupled on-line with ICP-MS detection for metal-based nanoparticle analysis (chapter 5). Each section starts with an introduction into the theoretical concept of the respective fractionation/separation system, followed by practical hints regarding method development (e.g. selection of appropriate carrier/mobile phase, membrane/stationary phase) as well as critical aspects and limitations. Particular attention is payed to laser ablation ICP-MS (LA-ICP-MS) for spatially resolved nanoparticle analysis. Each section concludes with selected application examples of the respective analytical technique from the most relevant fields of nanoparticle use or exposure (consumer products, food, medicine and environment), highlighting the performance of each technique in metal-based nanoparticle analysis. In addition a brief chapter on general considerations regarding sample preparation is provided to sensitise for this issue.

Chapter 6 is dedicated to aspects of quality assurance. Various critical points regarding method development and validation, mass balance, size calibration and quantification from the previous sections are revisited, discussed and practical advice is given.

Finally, the authors provide some concluding remarks and future perspectives (chapter 7). Furthermore, a flow-chart is included as a "hands-on" overview on all ICP-MS based techniques discussed within this tutorial review intended as a "method-decision tool" for users.

1. Introduction

Since its commercial introduction in 1983, inductively coupled plasma-mass spectrometry (ICP-MS) evolved as one of the leading techniques in the field of elemental (ultra-)trace analysis of metals and metalloids in numerous matrices. Given its unique properties, such as: (i) high sensitivity, (ii) multi-element capabilities, (iii) a wide linear range and (iv) the possibility to obtain isotopic information, numerous applications in various fields, e.g. geochemistry, environment, clinical and biological materials, food as well as industry have been published until now.

In the beginning ICP-MS instruments were based on quadrupole-mass analysers, comprising a low mass resolution, thus struggling with spectral interferences. Upon the introduction of ICP-sector field MS (ICP-SFMS) in 1989 improved limits of detection (LODs) as well as high mass resolution was feasible. First, due to high costs, the technique was restricted to specialised laboratories. The breakthrough of ICP-SFMS came with the introduction of multi collector-ICP-MS (MC-ICP-MS).[1] MC-ICP-MS allowed for truly simultaneous measurements of ions with a precision which rivalled or exceeded that achieved by thermal ionisation mass spectrometry (TIMS) - thus, perfectly suited for the investigation of isotope-ratios as well as related effects.[2] As the plasma source is capable in ionisation of geochemically-relevant elements, applications (mainly) in the area of geochemistry and cosmology appeared. Nowadays, MC-ICP-MS found its way into further fields of research - e.g. medicinal applications as a promising "diagnostic tool" to study the genesis and/or development of diseases.[3]

In the 1980s the first collision cell ICP-MS systems were described which enabled tackling of spectral interferences.[4,5] A few years later this instrumentation experienced a boom.[6] A recent innovation and advancement of quadrupole-based collision cell instruments (launched in 2012) was the development of triple-quadrupole ICP-MS systems (ICP-MS/MS), which allow for a better control over reactions taking place in the reaction cell and thus improved coping with spectral interferences.[7] Next to the aforementioned SF-MS as well as common quadrupole-based mass-analysers, an ICP-time of flight-mass spectrometer (ICP-ToF-MS) was introduced in the 1990s. ICP-ToF-MS systems allow for a (quasi) simultaneous detection over the whole mass-range, which is especially beneficial in terms of fast transient signals in conjunction with multi-element detection as well as isotope ratio analysis.[8,9] Just recently ICP-ToF-MS experienced a renaissance.

The chemical properties, toxicological and biological importance of many metals and metalloids depend greatly on their chemical structure, oxidation state and/or isotopic distribution; namely, their elemental species.[10] Thus, next to (ultra)trace bulk analysis, in 1986 one of the first applications of the on-line coupling of HPLC and ICP-MS was published to study elemental species.[11] Since then the number of publications in the field increased exponentially mainly related to environmental-speciation applications (e.g. As, Hg, Pb, Se, Sn).[12] Throughout the 1990s efforts were focused on separating species and coupling chromatographic systems to various detectors.[13] Beginning in the year 2000 CE was coupled on-line to ICP-MS (e.g. As speciation). GC on-line with collision-cell ICP-MS instruments allowed not only for speciation analysis of organometallic compounds, but also for organophosphorus species. As metals play an important role in life processes (e.g. every third protein is believed to require a metal co-factor)[14] ICP-MS evolved as an integral powerful complementary tool in life-sciences: the field of Metallomics appeared.[14,15] In addition the application of stable isotopes in speciation analysis comprises beneficial advantages (e.g. species-tracing, -quantification).[16]

However, ICP-MS exhibits a severe restriction: structural information of the (bio-) molecule/species gets lost within the plasma; which is indispensable for species identification - thus, from the late 1980s complementary molecular-mass spectrometry was explored for its potential in speciation analysis. Since mid of the 1990s electrospray-ionisation mass spectrometry (ESI-MS) has been applied with great success for elemental speciation analysis within the research areas of environmental chemistry, health, nutrition and bioinorganic chemistry; real, simultaneous complementary ESI-MS and ICP-MS approaches were developed.[17] Ongoing instrumental developments, e.g. recently mass cytometry instruments in combination with metal-stable isotope tagging drive life-science applications (multiplex and absolute biomolecule quantification) ahead.[18,19]

Laser ablation ICP-MS (LA-ICP-MS) pushed the range of applications deeper into medical questions and enabled either the direct determination/quantification of elements in biological samples (e.g. metal binding proteins) or via "metal labelling" upon gel electrophoresis.[20,21] In addition, bioimaging methods of e.g. tissues or bones allowed for the investigation of metal distributions.[22,23]

Within the aforementioned fields of applications, ICP-MS was applied for the investigation of analytes, which comprise clearly delineated properties (e.g. elemental species, biomolecules) and the information demanded can be quantitative, as well as qualitative. A class of analytes where the situation is more complex are metal-based nanoparticles: (i) quantitative information can be mass, molar or number concentration (as required in the current EU definition of nanomaterials)[24]; (ii) qualitative information includes not just detection of nanoparticles as such, but also to provide chemical (core, coating composition) and physical characterisation (size, shape, aggregation/agglomeration). As nanoparticles are not a class of distinct analytes, common properties are merged and designated as "fractions".[10] However, when it comes to e.g. the release of ions from nanoparticles, various elemental species may be formed - hence, speciation analysis is needed as well; the fields of elemental speciation analysis and fractionation are then overlapping. Aggravating the situation, high background concentrations of ubiquitous elements or the presence of natural nanomaterials (e.g. natural colloids) covering the same size range as engineered nanoparticles need to be taken into account; in this case advanced strategies are required allowing for nanoparticle tracing in complex matrices.

The fields of application of metal-based engineered nanoparticles (ENPs) are numerous, e.g. consumer products, food, medicine, environment and a broad variety of materials comprising high (estimated) production volumes is in use (see Figure 1). In 2006 the World Economic Forum included the specific topic "nanoparticle toxicity" for the first time to its global risk report, making the assessment of the ecotoxicological effects of engineered nanomaterials a major concern.[25] Thus, as repeatedly stressed in several publications, analytical techniques for ENPs analysis in complex matrices are needed.
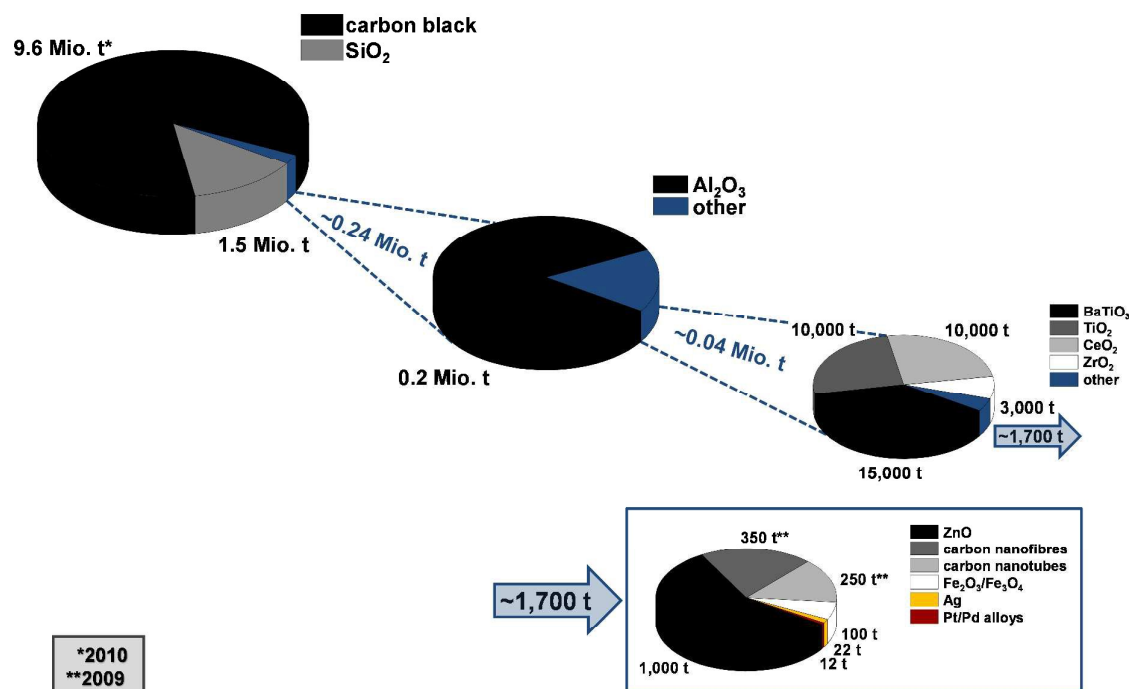
Figure 1: Overview of estimated production volumes in tons (t), or million tons (Mio. t) of nanomaterials. Data based on Ref..[26]

The performance of ICP-MS based techniques for the analysis of ENPs was demonstrated in numerous publications. However, tackling the challenging task of nanoparticle analysis is in most cases only feasible by complementary use of a set of analytical techniques and generating the whole picture from the obtained individual information like a mosaic. As displayed in Figure 2 blending of ICP-MS-based techniques is needed to a greater extend in metal-based nanoparticle analysis than speciation analysis which represents a particular challenge. For a better overview, cross-references to the respective chapters within this tutorial review are given. In addition, **Figure 2** is intended as a **Table of Content** of this Tutorial Review. Microscopy- as well as light scattering- based methods are mentioned within Figure 2, but are beyond the scope of this tutorial review; thus, the reader is referred to the respective literature e.g. light scattering[27], microscopy.[28,29,30,31,32]
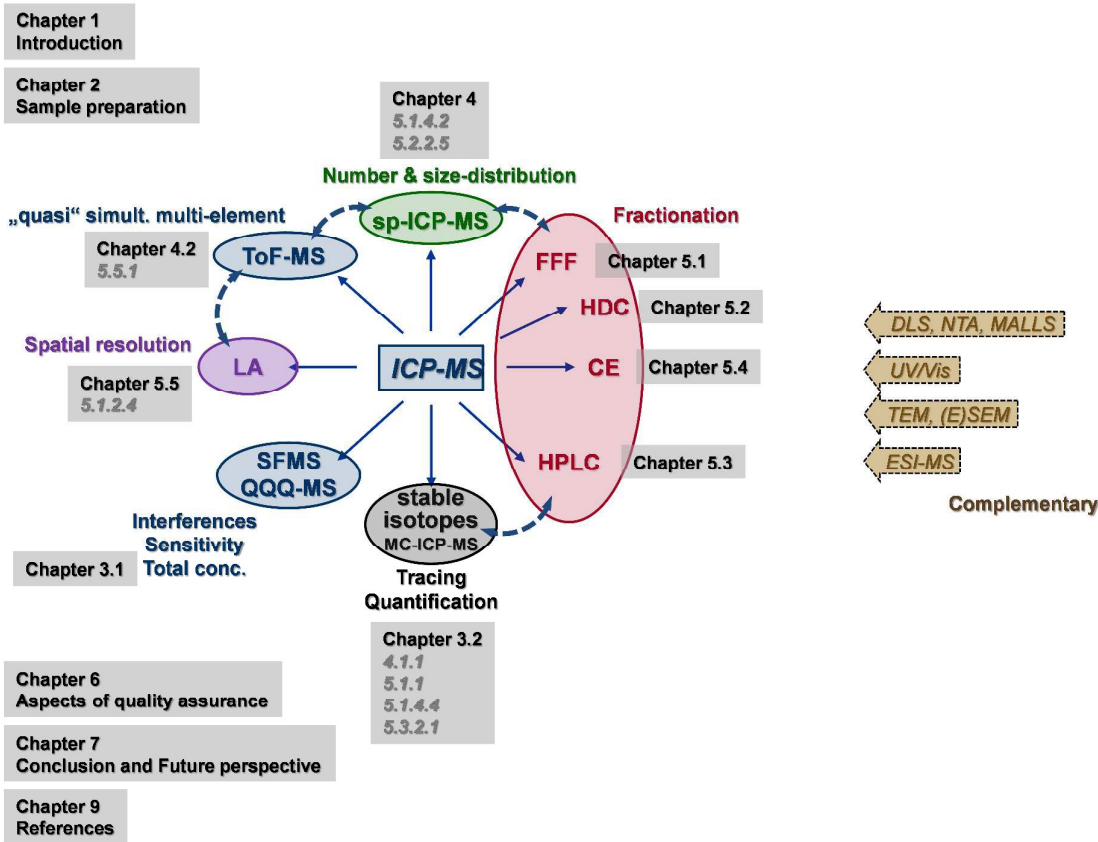
Figure 2: "**Table of Content**" as well as overview of the versatility of ICP-MS in terms of ENPs analysis. Furthermore, cross-references to the respective chapters within this tutorial review are given (cross-references given in **grey**, referring to further chapters, were the respective technique is mentioned/applied, too).

The scope of this tutorial review is (i) to provide an overview on the most common ICP-MS based techniques for the analysis of ENPs (and natural nanoparticles/colloids) subdivided into: a) "stand alone" ICP-MS and b) hyphenated techniques; (ii) highlighting the benefits and pitfalls of each technique as well as providing practical advice regarding method development; (iii) illustrating the possibilities and limits of each technique by the example of practical applications from the recent literature.

The pre-selection of practical application examples was based upon a thorough literature search. The authors find some applications in the field of nanoparticle analysis particularly interesting, and regret any inadvertent omission of references to further publications. A comprehensive compilation of application-related literature in the field of nanoparticle analysis is out of the scope of this tutorial review.

2. Sample preparation

A detailed discourse covering all aspects of sample preparation of ENPs/(natural) colloids is out of the scope of this tutorial review. However, sample preparation is a critical issue in ENP/(natural) colloid analysis, thus, the intention of this chapter is to sensitise for this issue and provide cross-references to further literature.

The general requirements for sample preparation for nanomaterial analysis by direct introduction ICP-MS and hyphenated techniques are the same as for total elemental analysis and for elemental speciation. First, the analytical information of interest must not be changed or even lost and second the sample matrix and properties need to be compatible with the respective analytical technique.

In case of total elemental mass determination of ENPs/(natural) colloids in suspension direct introduction into the ICP-MS is possible provided that there is no interfering matrix and the particle size is well below about 2 µm. A detailed discussion of particle-size limits in ICP-MS detection can be found within chapters: 3.1 and 4.1.4. For larger particles, significant organic matrix content and for solid samples digestion prior to analysis by ICP-MS is required. Risk of loss of information may occur for volatile elements during digestion. However, in general only the total element content in the sample is obtained independent if present in particulate or other form.

When using LA-ICP-MS (see chapter 5.5) the sample preparation for example for nanoparticles in tissue slices is practically identical to routine conditions. There is no special adaption required. However, also in this case only the total elemental content across the sample surface is obtained and nanoparticles are only clearly detected if there are no significant other species of the same element in the background.

More critical is the preparation of samples for sp-ICP-MS. Optimum dilution is needed to achieve individual monitoring of nanoparticles per dwell time (see chapter 4.1.2). Critical is the removal of interfering matrix to minimise background noise and changes of the transport efficiency. This works well for suspensions of ENPs, but is challenging for real sample matrices. Therefore, combination of sp-ICP-MS with a fractionation/separation technique is an elegant way to overcome such limitations and to obtain improved results.

The majority of applications for ENPs/(natural) colloid analysis with ICP-MS detection uses on-line hyphenation with liquid based separation systems (see chapters 5.1-5.4). Aqueous suspensions of nanomaterials can be directly injected onto the fractionation channel, separation column or capillary if they fulfill the principle matrix compatibility requirements well-known from elemental speciation analysis for CE and HPLC. Requirements for FFF are even less critical. However, specific conditions for nanomaterials need to be considered to avoid changes in the aggregation/agglomeration state and thus particle size distribution and to define the upper particle size limit to match the fractionation/separation range of the chosen technique. The latter can be achieved by centrifugation to sediment large particles or by membrane filtration. In case of filtration there is the risk for samples with high particle concentration that the membrane is partially clogged and even particles with sizes well below the filter pore size/cut-off are retained. Maintaining the aggregation/agglomeration state is more challenging. One strategy is to include surfactants in the carrier/mobile phase/electrolyte of the fractionation/separation system to stabilise the particles and avoid aggregation/agglomeration. This works in case the sample contains only primary particles initially. Otherwise initially existing aggregates/agglomerates might be dissociated upon interaction with the surfactant. The alternative strategy is to adapt the carrier/mobile phase/electrolyte as much as

possible to the sample matrix which is particular suitable for aqueous extracts without any on purpose added stabilisers.

Particular attention is required for extraction of nanoparticles from solid matrices such as soil, biomedical tissues, food and consumer products. Suspension in aqueous extractants is usually most suitable optionally with sonication for dissociation of agglomerates and improved extraction efficiency. Challenging matrix such as fatty sunscreen or high amount of organic compounds in food or biomedical samples can be overcome by defatting with hexane or acidic or enzyme-based digestion of the matrix. Careful method optimisation and validation is required to prove that the target particles are not changed during such procedures. In case of non-surface stabilised particles with significant solubility, for example Ag nanoparticles, only gentle sample preparation conditions are possible. Detailed discussion of sample preparation protocols and their advantages as well as limitations are available in the literature - general remarks on sample preparation[25,33], clinical samples[34], soils[35], consumer products, biological and environmental samples[36] and food[37].

3. "Stand alone" ICP-MS

The majority of ENPs and natural nanoparticles and colloids contain significant amounts of metals/metalloids in their core structure, for example Ag, Au, TiO_2 and SiO_2 nanoparticles and clays (Al-, Fe-oxides), or metals attached to their surface functional groups, for example humic acid complexes with various metals. This offers the possibility for sensitive elemental detection using ICP-MS to identify and quantify these nanomaterials. In addition, the isotope selective detection capability of ICP-MS enables isotope ratio measurements to characterise changes in isotopic composition in particular when using isotopically enriched nanomaterials as tracers or for calibration (spike). Complex mixtures of nanomaterials of various sizes as well as mixtures of nanomaterials and further low molecular mass species/fractions of the same target element require separation prior to ICP-MS detection (see chapter 5) for species/fraction (size) selective detection and quantification. Exceptions are mixtures with simple aqueous matrix which can be diluted and directly introduced using the single particle option of ICP-MS (sp-ICP-MS, see chapter 4). Apart from this the main capability of direct introduction ICP-MS is the determination of total elemental concentrations for mass balance purpose, to study extraction efficiencies from solid samples or to characterise monodisperse purified nanoparticle standards. In the following the general aspects of (nano)particle detection by ICP-MS are introduced and discussed, which are equally relevant for detection of nanomaterials eluting from the hyphenated techniques discussed in chapter 5.

3.1 Total concentration

Determination of total elemental contents of ENPs is most reliably performed by digestion of the sample to mineralise any possibly interfering matrix compounds, in particular organic molecules, and to achieve dissolution of the particles. Microwave digestion in closed vessels is the most frequently applied method, for example using a mixture of nitric acid, hydrogen peroxide and hydrofluoric acid for titanium dioxide particles in sunscreen.[38] Validation of the method was performed by digestion and analysis of certified reference materials (CRMs) in the same way. The work flow, quality control and validation are the same as for determination of total elemental contents in any other matrix loaded liquid or solid sample.

Alternatively, an aqueous suspension of (nano)particles can be directly introduced into the ICP-MS in case the non-particulate matrix is compatible, i.e. low concentration of salts and organic compounds. The work flow is simplified because

the digestion step can be omitted and thus reagent blanks are not critical. However, quality control and validation are more challenging because it needs to be proven, that the particle generates the same number of ions in the plasma leading to the same signal as the respective solution of the particle after digestion. It can easily be concluded that the process of atomisation and ionisation of a particle in the plasma is becoming more and more difficult with increasing particle size considering the limited residence time within the plasma. In addition there is a second critical effect when using a routine sample introduction system with concentric nebuliser and spray chamber. Particles in the order of about 2-10 µm are of similar size as the droplets generated within the spray chamber. Droplets larger than about 10 µm are on purpose removed from the spray chamber to send only the fine aerosol towards the plasma which works perfectly for analysing solutions but bears the risk of selectively losing the larger particles when directly introducing a suspension (see also chapter 4.1.4).[39] However, not all systems filter larger droplets - there are total consumption systems, which heat the spray chamber and reduce the droplet size.[40]

When looking into the history of ICP-techniques the direct introduction of suspensions and slurries of difficult to digest geological materials was performed in the 1980s.[41] The optimisation, experience, validation and limitations of such studies can partly be transferred to the nanoparticle suspensions of nowadays analytical tasks. Laird *et al.* studied the recovery of elemental determination of clay by slurry ICP-OES compared to analysis after total digestion. Clay size fractions <0.2 µm and 0.2 to 2 µm reached >90% recovery when suspending the sample in 0.1 mol L^{-1} NaCl using sonication. For larger size fractions of 2 to 10 µm and 10 to 45 µm maximum recoveries were only 70% and 24%, respectively.[42] Those results are in good agreement with the initial work from Halicz and Brenner analysing suspensions of clay (0.5 to 2 µm size) in distilled water by ICP-OES. The obtained signal steadily increased with increasing grinding time of the sample indicating a particle-size dependent response.[41]

Halicz *et al.* reported recovery rates for slurry analysis of a series of geological reference materials with ICP-OES in a range from 70 to 110%. The slurry was prepared at 1% solid concentration and quantified against a calibration with dissolved aqueous standards.[43] Goodall *et al.* proposed the "single particle occupancy" model claiming that analyte transport of an aqueous dissolved standard and a slurry are the same in case there is only one particle present in each aerosol droplet formed from the nebulisation of the slurry. Based on this model a theoretical upper particle size limit of about 2 to 2.5 µm is derived which agrees with the experimental data. The model was tested on slurries of ground plant materials (<2 µm) and provided at first rather low recoveries. It was found that dispersion of the fine primary particles was incomplete leading to much larger aggregates. When the concentration of anionic surfactant was increased, aggregate formation was avoided and analysis of the slurry by ICP-OES provided excellent recoveries for Ca, Mg, Mn, P and Al.[44] The review of Ebdon *et al.* summarised varies ICP-OES application but also studies using ICP-MS for slurry analysis. In this case the slurry concentration was reduced to about 0.05% to avoid clogging of the cones. Various types of nebulisers and spray chambers were discussed but in summary it was concluded that a high solids nebuliser with a standard double pass spray chamber is suitable for a wide range of slurries. Sample introduction by flow injection was recommended as option to reduce the matrix load entering the ICP and thus improving long-term stability.[45]

Twelve years later, Allabashi *et al.* reported the quantification of Au nanoparticles of 5 nm to 20 nm size by direct introduction to ICP-MS regarding their total elemental content. The results were not significantly different from those obtained after

digestion of the nanoparticles is omitted. The sample preparation was found to be an important step to avoid instability and precipitation of the particles. Dilution in 1% hydrochloric acid provided the best results.[46] Motellier *et al.* investigated the recovery for direct analysis of metal oxide nanoparticle suspensions with ICP-MS and found significant differences in the performance depending on the nanoparticle composition. For example, complete recovery was obtained for 20 nm ZnO and 20 nm SiO_2 when suspended in 0.1% HNO_3 or 1 mmol L^{-1} NaOH, respectively. More stable particles like up to 150 nm TiO_2 and 25 nm CeO required 10% nitric acid to achieve recoveries around 90%. In case of 50 nm Al_2O_3 a maximum of 80% recovery was obtained under the applied conditions.[47] Different behaviour of metal and metal oxide (nano)particles was also found by Hubbard and Zigmond when combining an aerosol generation and electrostatic size classification device with ICP-MS to study the detection efficiencies for well-defined aerosols of Au, Ag, aluminium oxide, cerium oxide and yttrium oxide particles. Volatile species showed generally higher detection efficiencies compared to the refractory species. However, above a critical diameter the detection efficiency decreased for the volatile species with increasing particle size due to incomplete dissociation and ionisation in the plasma which is in agreement with other studies. Modelling of the detection efficiencies was performed for the metallic particles but requires additional work for the more complex metal-oxide particles.[48] In summary, the generally observed upper particle size limit for efficient introduction via conventional nebuliser and spray chamber is about 2-3 μm.[49] Consequently, the direct introduction for the typical range of studied nanoparticles including agglomerates/aggregates is well below this critical limit. In spite of this, full detection efficiency is not necessarily obtained in particular not for refractory metal oxide particles. This needs to be considered for direct analysis of suspensions and digestion may be required for reliable quantification and validation.

Apart from the discussed aspect of particle behaviour in the plasma, there are the general requirements and limitations of ICP-MS to be considered for reliable, accurate and precise quantification of nanoparticles. State of the art instrumentation including quadrupole instruments with collision cell for kinetic energy discrimination, ICP-SFMS with mass resolution up to about 10,000 and the recently introduced quadrupole based MS/MS technique (ICP-QQQ) allowing targeted reactions of preselected ions, providing a broad range of options to minimize spectral interferences. More specifically, the ICP-QQQ introduces precursor ion scan, product ion scan and neutral loss/gain scan well known from organic mass spectrometry into elemental mass spectrometry opening novel strategies for eliminating spectral interferences.[50] For example, ICP-MS/MS detection was applied for the determination of Cd, Zn, Se ($\Leftrightarrow$ $^{40}Ar^{40}Ar]^+$) and S ($\Leftrightarrow$ $[^{16}O^{16}O]^+$) in quantum dots using oxygen as reaction gas to convert S^+ to $[^{32}S^{16}O]^+$ and Se^+ to $[^{80}Se^{16}O]^+$ which could be monitored interference-free at *m/z* 48 and 96, respectively, while Cd and Zn remained as non-oxidised elemental ions.[51] Once the particles are decomposed, atomised and ionised in the plasma, these interferences and their minimisation are the same as for classical analysis of dissolved (low molecular mass) elemental species. Therefore, detailed discussion is available in specific reviews. The same quality aspects discussed for the direct analysis apply also for the use of ICP-MS as on-line detector for hyphenated separation techniques and for the sp-ICP-MS approach.

3.2 Stable isotopes

Undoubtedly, ICP-MS is a powerful tool to investigate total elemental concentrations of ENPs in several matrices. However, the differentiation between such ENPs and

artefacts from natural or background-level metals (especially with regard to ubiquitous elements and elevated background concentrations) as well as the identification and tracking of nanomaterials in e.g. environmental fate, transformation, bioaccumulation studies by means of "stand alone" ICP-MS is a major challenge. For an unambiguous tracing of ENPs in a sample, the ENPs should preferably generate elevated elemental concentrations that exceed the natural background level by a factor of 10 or more, if possible. This recommendation follows from the observation that the uncertainty of concentration measurements of nanoparticles is likely to exceed 10% close to the detection limit. Thus, exposure studies at realistic concentrations are not feasible. In addition, variable background concentration levels hamper a valid quantification in particular for biological samples, which can vary by more than ±10%.[52]

Thus, an unambiguous labelling of the nanoparticles is necessary to tackle the influence of variable background. Labelling of the nanoparticles by means of an "exogenous" surface label (e.g. fluorescence dyes) has the disadvantage that the particle properties may change (e.g. surface charge,…) and that the labels could possibly be cleaved or lost from the particle. A further approach is based on possible "natural occurring" elemental-encoding. In comparison to ENPs, natural colloids may comprise accompanying elements. Multi-element analysis of "elemental-fingerprints" enables identification/tracing of ENPs in this case (see also chapter 4.2). A labelling approach without changing the nanomaterials´ properties is the intrinsic labelling either by means of radiolabel or stable isotopes. Intrinsically labelled nanoparticles comprise the same chemical composition as well as surface chemistry as unlabelled nanoparticles, but offer the crucial advantages of traceability. Radiolabels are ideally suited for *in situ* imaging of particles in e.g. individual tissues or cells. However, the shortcomings of radioactive isotopes for nanoparticle labelling include possible radiocontamination, require a special working permission, sample handling and facility. Detection is conducted by means of e.g. γ-spectrometry, scintillation counter or imaging techniques such as autoradiography, positron emission tomography or single photon emission computed tomography. In addition long-term exposure studies for investigating the transformation of nanoparticles in environmental matrices is hampered by radioisotopes comprising a short half-life period. Thus, applications dealing with radiolabels are out of the scope of this tutorial review and the reader is referred to the recent literature.[53]

The focus of the following section is placed on metal stable isotopes with regard to (i) the addition of a tracer and/or (ii) the investigation of naturally occurring differences between stable isotopes.

3.2.1 Stable isotope labels

The approach of stable isotope labelling in nanomaterial analysis was suggest by Gulson and Wong[54] and is based on the incorporation of a stable, non-radioactive isotope into the nanoparticle whose abundance is different from that occurring naturally. The shifted isotope ratio equips the respective nanomaterial with an unambiguous fingerprint allowing for a distinction from the matrix. Deploying enriched isotopes that are low in natural abundance decreases the limits of detection (nevertheless, enriched isotopes with a low natural abundance are typically more expensive than those with higher abundances) even below the natural background levels of the respective element. However, the contribution of the respective isotopically enriched metal is only detectable when the isotope ratio of the sample

clearly exceeds (i) the precision of the isotopic measurement and/or (ii) natural occurring isotope fractionation effects. Depending on the conditions and the factor of enrichment quadrupole-based ICP-MS (ICP-QMS) systems are applicable. However, ICP-SFMS and in particular MC-ICP-MS allow for isotope ratio determination with an extremely high precision[2], thus even a minor uptake of the tracer will produce analytically resolvable changes in the isotopic composition. However, the application of MC-ICP-MS systems for high precision isotope ratio measurements necessitates the nanoparticle separation from complex matrix as natural occurring isotope fractionation effects can become relevant. Laycock *et al.* conducted a model calculation (using the example of [107]AgNP) and stated that, due to the higher precision obtainable by means of MC-ICP-MS a tracing factor enhancement (compared to commonly employed bulk concentration measurements, mostly limited by natural background concentrations) of about 4,000 is achievable.[55] In addition dissolution of nanoparticles can be tracked, as the released ions carry the same isotopic fingerprint as the former nanoparticles. Thus, stable isotopes bridge the gap between fractionation and speciation analysis.[10]

Most of the metals relevant for ENPs comprise of more than one stable isotope, which is a prerequisite for isotope labelling.[56] For detailed information about natural abundances of stable isotopes of the elements the reader is referred to the website of the Commission on Isotope Abundances and Atomic Weights (CIAAW).[57]

Although stable isotopes allow for nanoparticle tracking, potential interferences (both spectral and/or non-spectral) have to be taken into account while choosing the enriched isotope. The isotope ratio should be measured at low concentrations, thus minor interference could influence the accuracy of the measurement (e.g. ^{48}Ti $\Leftrightarrow$ ^{48}Ca). Isotopically enriched metals are commercially available as elemental metal, metal oxides or metal salts. Whilst synthesis protocols for non-labelled nanomaterials are abundant in literature, some special considerations during application for the synthesis of isotopically-labelled nanoparticles need to be taken into account; given the non-negligible cost of isotopically enriched metals, nanoparticle synthesis must be optimised with a focus on small-scale synthesis and high yields. Thus, customised preparation protocols are scarce. A thorough investigation of possible influences from isotopically enriched precursors on nanoparticles´ properties was conducted by Laycock *et al.*.[55] No systematic differences were observed for the example of ^{107}Ag *versus* natural Ag. Apart from ^{107}Ag nanoparticles some further synthesis protocols from the literature are summarised in the following: Synthesis of ^{29}Si enriched nanoparticles starting from ^{29}Si elemental pellets (99.73% enrichment in ^{29}Si)[58], synthesis of ^{67}ZnO nanoparticles starting from ^{67}Zn metal powder (89.6% enrichment in ^{67}Zn)[59], ^{57}Fe nanoparticles starting from ^{57}Fe metal powder (95.06% enrichment in ^{57}Fe)[60] and ^{65}Cu nanoparticles starting from ^{65}CuCl$_2$·2H$_2$O (99% enrichment in ^{65}Cu)[61]. So far, stable isotope labelled ENPs have been applied in studies focussing on consumer product safety and on environmental transport and bioaccumulation. Mostly isotopically enriched Zn nanoparticles have been used; only a few investigations deal with Ti, Ag, Cu or Fe enriched nanoparticles.

Consumer product safety

The first application of stable isotope labels in nanoparticle tracing study is the investigation of ZnO nanoparticle uptake from sunscreens via human skin conducted by Gulson *et al.*.[62] The authors investigated two different size ranges (approximately 19 nm and 110 nm) of isotopically enriched ^{68}ZnO nanoparticles (> 99% enrichment in ^{68}Zn) incorporated into an oil-water formulation using a commercial process for

preparing sunscreens. Blood and urine samples from male and female volunteers were analysed by MC-ICP-MS for varying Zn isotope ratios. The uptake of small amounts of Zn from ZnO nanoparticles through human skin was detectable in blood and urine samples. These results were verified by further studies.[63,64] Although, in all cases, the natural background of Zn was high, small uptake rates of ZnO nanoparticles were detectable - in case of Larner *et al.* about a factor of 20,000 lower tracer concentration was detectable next to natural zinc concentration.[64]

Environmental/ bioaccumulation
ZnO nanoparticles
To investigate possible bioaccumulation of ZnO nanoparticles in freshwater organisms after short dietary exposure, Dybowska *et al.* fed freshwater snails with diatoms and ^{67}ZnO nanoparticles (89.6% enrichment in ^{67}Zn). Afterwards, they fed the snails with unlabelled food to clear their gut and snails were analysed upon acid digestion. Zn concentrations as low as 1 µg g^{-1} were detectable by this approach in contrast to a minimum detectable Zn exposure concentration of about 5,000 µg g^{-1} without using a tracer.[59] Khan *et al.* conducted exposure studies with ^{68}ZnO to estuarine snails and analysis by MC-ICP-MS concluding that bioaccumulation of nanoparticles is primarily dependent upon solubility.[65]
Corophium volutator, a sea water mudshrimp, was used as test organism within a further ^{68}ZnO nanoparticle bioaccumulation study by Larner *et al.*.[66] *C. volutator* is an important component of coastal ecosystems where river-borne particles will accumulate and is used in toxicity assessments. Zn uptake from the ^{68}ZnO nanoparticles occur via the aqueous phase or ingestion of sediment particles with adsorbed ^{68}Zn upon dissolution of ^{68}ZnO nanoparticles. Due to the high uncertainties of MC-ICP-MS measurements in this case, direct ZnO nanoparticle uptake could not be clearly proved.
Laycock *et al.* studied the uptake of ^{68}ZnO nanoparticles (99.5% enrichment in ^{68}Zn) via earthworms (*Lumbricus rubellus*) in soil by MC-ICP-MS at realistic exposure concentrations. Dermal uptake accounted for ~5% and oral uptake for ~95%. As a main finding, concentration dependent effects need to be taken into account. Stable isotope labelling allowed for low dosing at realistic concentrations.[67]
Elements comprising more than two stable isotopes enable multi-isotope tracer experiments. Via this approach e.g. sophisticated bioaccumulation studies are possible, since different forms of the same element (e.g. ionic ⇔ (nano-)particulate ⇔ different species) can be studied within a single experimental system. The number of analysed samples can be doubled; furthermore, the tracing of multiple Zn forms in a single system or organism provides results that are directly comparable, compensating potential biological variability. Laycock *et al.* dosed soil with ^{68}ZnO nanoparticles as well as soluble ^{64}ZnCl$_2$ (>99% enrichment in ^{68}Zn and ^{64}Zn) and studied the Zn bioavailability for earthworms (*Eisenia andrei*) via isotope ratios and MC-ICP-MS.[68] The uptake of ZnO nanoparticles as well as ionic Zn was indistinguishable, most likely due to rapid dissolution of ZnO nanoparticles.

Ag nanoparticles
Ag nanoparticles are rather mutual in water columns, thus Yu *et al.* also employed double stable isotope labelling for the investigation of the transformation kinetics of ^{107}Ag nanoparticles (99.5% enrichment in ^{107}Ag) and ionic ^{109}Ag$^+$ (^{109}AgNO$_3$, 99.81% enrichment in ^{109}Ag).[69] The knowledge of either (nano-)particulate or ionic state is of great interest as Ag$^+$ has shown to be much more toxic than Ag nanoparticles. As a main outcome, transformation between Ag nanoparticles and ionic Ag$^+$ was found to

be complex and greatly depended on external conditions (e.g. sunlight, dissolved organic matter, pH). Croteau *et al.* employed ^{109}Ag nanoparticles (99.7% enrichment in ^{109}Ag) for bioaccumulation studies in freshwater snails at realistic low concentrations.[70]

TiO$_2$ nanoparticles

Bourgeault *et al.* investigated the bioaccumulation of isotopically labelled TiO$_2$ nanoparticles (95.7% enrichment in ^{47}Ti) in zebra mussels.[71] Despite high environmental Ti concentrations, assimilation of TiO$_2$ nanoparticles could be detected; although assimilation efficiency was very low (3.0 ± 2.7%), suggesting that nanoparticles are mainly captured in mussel gut.

CuO nanoparticles

The bioavailability and toxicity of CuO nanoparticles as well as ionic Cu to a freshwater oligochaete (*Lumbriculus variegatus*) was investigated by Ramskov *et al.* employing ^{65}CuO nanoparticles (99% enrichment in ^{65}Cu) and ^{65}Cu^{2+}(aq) (dissolved in 0.5% HNO$_3$; 99.4% enrichment in ^{65}Cu).[72] In general, only minor differences were found between Cu added to the test system in aqueous *versus* particulate form - Cu uptake was largely similar in aqueous ⇔ (nano-)particulate form. Thit *et al.* have discovered differences in the relative subcellular distribution in *L. variegatus* of accumulated ^{65}Cu between Cu forms: ionic Cu mainly partitioned to metallothionein-like proteins (~40%) followed by cellular debris (~30%); while CuO nanoparticles related Cu was mainly found in cellular debris (~40%).[73]

3.2.2 Isotope fractionation

As a first approximation, it can be stated that isotopic abundances are constant in nature - due to the fact that all nuclides were thoroughly mixed in the solar nebula prior to the formation of the earth. Although isotopic abundances are assumed to be fairly constant in nature, variations do occur – either due to (i) the decay of naturally occurring and long-lived radionuclides, or due to (ii) natural mass fractionation effects. Different isotopes of one and the same element display the same number of electrons thus show to a large extent the same chemical behaviour. The number of neutrons is different and thereby the mass. With regard to the difference in mass isotopes of the same element may take part to a different extent in physical processes or chemical reactions. Apart from mass-dependent fractionation also mass-independent isotope fractionation can take place. However, a detailed theoretical description is out of the scope of this section - thus, we refer to specialised literature.[2]

However, the manufacturing of ENPs involves milling, wet chemical synthesis and/or high temperature condensation. Hence, isotope fractionation may occur and function as an "intrinsic label" of the nanomaterial and allowing for distinction from bulk material. As differences in isotope ratios, related to fractionation effects, are rather small, high measurement precision as well as appropriate correction for e.g. mass discrimination is a prerequisite. Instrumentation which provides the necessitated prerequisites is MC-ICP-MS. For more information, the reader is referred to the specialised literature.[2]

Up to now only a few publications exist, which employ MC-ICP-MS for the investigation of possible mass-based fractionation effects for ENPs tracking. One of the first investigations was conducted by Larner and Rehkämper. They investigated

ZnO nanoparticles with regard to possible isotope fractionation and systematically analysed 17 commercially available ZnO nanomaterials. However, neither the presence or absence of a coating nor the distribution in form of a powder versus a suspension showed any tangible systematic effect on the Zn isotopic ratios. Furthermore, the data obtained from ZnO nanoparticle measurements were indistinguishable from the values that are commonly found for Zn of geological, biological and anthropogenic origin in environmental samples. Thus, this implies that the indigenous isotopic composition of ZnO nanoparticles is not suitable for tracing in natural and experimental systems.[52] Within a further study from Laycock *et al.* CeO$_2$ nanoparticles were investigated for potential isotope-fractionation of Ce, but a distinct isotope signature was also not detectable and thus, tracing by this approach is not feasible.[74] Lu *et al.* investigated transformation processes of Ag nanoparticles by MC-ICP-MS. They found significant variations in Ag isotope ratios during formation and dissolution of Ag nanoparticles. Furthermore, engineered Ag nanoparticles show different isotope fractionation effects than their naturally formed counterparts.[75] This result reveals the possibility of determining whether the Ag nanoparticles are naturally formed or engineered. However, the question remains whether or not high-precision Ag isotope analysis may be used as a reliable technique to reveal the source of Ag nanoparticles.

The investigation of isotope fractionation effects as "indigenous" label for nanoparticles is an exciting field of research. However, up to now only a few studies were undertaken and only Ag nanoparticles show isotope fractionation effects. In spite of this, studying isotope fractionation effects related to nanoparticles is an extremely complex field and far away from being researched in depth not least because of numerous ENPs being present nowadays. However, the combination of precise isotope ratio determination by MC-ICP-MS (if the isotope ratios are diverging sufficiently ICP-SF-MS or ICP-QMS are sufficient as well) and stable isotope labelling is more promising and an ongoing increase in research activities is expected.

4. Single particle-ICP-MS (sp-ICP-MS)

In sp-ICP-MS a very dilute suspension of nanoparticles is introduced into the ICP-MS, such that statistically only one nanoparticle at a time (per dwell) enters the plasma. Within the ICP atomisation and ionisation of the nanoparticle´s constituent takes place. Transient signals are recorded which are characterised by signal flashes. The intensity of the flash of ions is a function of the size (in case of solid spherical and pure nanoparticles) or mass of the initial particle and the frequency of the flashes is a direct function of the number-concentration of the particles. A strength of sp-ICP-MS is that any commercial ICP-MS instrument can be utilised - no instrument modification is required apart from special software for data evaluation. Furthermore, sp-ICP-MS comprises superb detection capabilities - in comparison to further nanoanalytical techniques unrivalled extremely low number concentrations are detectable (10^3 cm^{-3} to 10^5 cm^{-3}).[76]

But, the technique comprises also some weaknesses: (i) limited/no multi-element capabilities using quadrupole-based ICP-MS systems, which are the most common type of mass-analysers; (ii) despite its excellent low number concentration capabilities, detection power in terms of nanoparticle size is still lacking and highly material dependent (for most nanoparticles in the range of 10-20 nm or even higher).[76] Although considerable progress has been made, sp-ICP-MS is still an emerging technique with numerous development opportunities. Some crucial steps

need to be undertaken to transfer the recorded data into a particle number versus size information histogram, which will be introduced in the following sections.

4.1 General concept/theory

The theoretical concept of sp-ICP-MS is outlined just briefly in this review. For a detailed description of the concept and the theoretical basis the reader is (amongst others) referred to several publications from Degueldre et al..[77,78,79,80,81,82,83]

For spherical, pure and solid nanoparticles, the determination of their diameter is mainly based on equation 1,[83] by relating the third power of the diameter (d^3) with the net intensity of the nanoparticle pulses ($counts_{NP}$).

$$counts_{NP} = \eta_{ion.} \cdot \eta_{interf.} \cdot \eta_{trans.} \cdot \frac{A \cdot N_{Av}}{M_M} \cdot \frac{1}{6} \cdot \pi \cdot \rho \cdot d^3 \qquad \text{Eq. 1}$$

$\eta_{ion.}$ = ionisation efficiency
$\eta_{interf.}$ = ICP-MS interface extraction efficiency
$\eta_{trans.}$ = mass spectrometer ion transmission efficiency
A = atomic abundance of the measured isotope
N_{Av} = Avogadro number
M_M = atomic mass of the target element M
ρ = density of the nanoparticle
d = diameter of the nanoparticle

In case of non-spherical/pure nanoparticles the expression for the mass related to the nanoparticle´s volume is substituted by the mass per nanoparticle (m_{NP}).

4.1.1 Calibration strategies

An appropriate calibration strategy is required to link the intensity of the signal flashes of single particles to mass information. Two common approaches exist using either (i) calibration by nanoparticle standards or (ii) employing standard solutions and determining transport efficiencies.

Approach (i) utilises different sizes of well characterised nanoparticle standards containing the same elemental composition, the same geometry as well as density as the target nanoparticle. Thus, a direct correlation between particle size and instrument response can be generated. However, the scarcity of monodisperse, well-characterised and stable nanoparticle standards limits the applicability of this approach. Several available certified nanoparticle reference materials (CNRMs) are listed in Table 1.

Table 1: Existing CNRMs. Next to material and certified size, number-concentration, the respective supplier is listed as well. Most of the information is extracted from a conference report from "Global Summit on Regulatory Science (GSRS16)" https://www.fda.gov/AboutFDA/CentersOffices/OC/OfficeofScientificandMedicalPrograms/NCTR/WhatWeDo/ucm488022.htm (assessed January 30th 2018).

Material	Name	Size [nm]/ surface [m² g⁻¹]	Reference property	Mass fraction [µg g⁻¹]	Supplier
Au nanoparticle citrate stabilised	RM8011	10	mean diameter	51.56 ± 0.23	NIST[a]
	RM8012	30	mean diameter	48.17 ± 0.33	NIST[a]

aqueous suspension	RM8013	60	mean diameter	51.86 ± 0.64	NIST[a]
Ag nanoparticle *freeze-dried **suspension	RM8017*	75	mean diameter		NIST[a]
	BAM-N001**	7 to 36	particle size distribution		BAM[b]
TiO$_2$ nanoparticle powder	SRM 1898	*55*	specific surface area		NIST[a]
	NMIJ-5713a	*76*	specific surface area		AIST/NMIJ[c]
	NMIJ-5711a	*11*	specific surface area		AIST/NMIJ[c]
	NMIJ-5712a	*57*	specific surface area		AIST/NMIJ[c]
Polystyrene Spheres aqueous suspension	SRM 1963a	101.8 ± 1.1	mean diameter		NIST[a]
	SRM 1964	60.39 ± 0.63	mean diameter		NIST[a]
	5701-a	120	mean diameter		AIST/NMIJ[c]
	5702-a	150	mean diameter		AIST/NMIJ[c]
	5703-a	200	mean diameter		AIST/NMIJ[c]
	GBW 12019	115	particle size		NIM[d]
	GBW (E)120090	84	particle size		NIM[d]
	GBW (E)120091	65	particle size		NIM[d]
Silicon nanoparticle cyclohexane stabilised suspended in toluene	RM8027	2	mean diameter	6.43 ± 0.31 (Si mass fraction)	NIST[a]
Silicon dioxide aqueous suspension	ERM-FD100	20	mean diameter		JRC[e]
	ERM-FD101b	80	mean diameter		JRC[e]
	ERM-FD102	mixture 20, 80	mean diameter		JRC[e]
	ERM-FD304	40	mean diameter		JRC[e]
nano-alumina	GBW13901	*445.4*	specific		NIM[d]

16

dry powder			surface area		
	GBW13906	*359.4*	specific surface area		NIM[d]
	GBW13907	*515.3*	specific surface area		NIM[d]

[a] National Institute of Standards and Technology (NIST), https://www-s.nist.gov/srmors/browseMaterials.cfm?subkey=42&tableid=231 (accessed January 25th, 2018) => further product details can be found in the respective reports
[b] Federal Institute for Materials Research and Testing (BAM), https://www.webshop.bam.de/default.php?cPath=2282&language=en (assessed January 26th, 2018)
[c] Japanese National Institute of Advanced Industrial Science/National Metrology Institute of Japan (AIST/NMIJ), https://www.nmij.jp/english/service/C/ (assessed January 26th, 2018)
[d] National Institute of Metrology (China) (NIM), http://en.nim.ac.cn/researchdivision/138 (assessed 26th, 2018)
[e] Joint Research Centre of the European Commission (JRC), https://crm.jrc.ec.europa.eu/c/By-analyte-group/Particle-pore-size/40487/ (assessed January 26th, 2018)

Next to the listed CRMs the European Commission´s Joint Research Centre (JRC) produces a set of representative test materials (RTMs) for the development and collection of data on characterisation, toxicological and ecotoxicological properties, as well as risk assessment and safety evaluation of nanomaterials. For further information the reader is referred to: [84]

Approach (ii) is hampered by the fact that the aerosol-transport efficiency in ICP-MS is (in most cases) not 100%. The quantification of the total metal content in one single particle by means of standard solutions requires the knowledge of the mass-flux (W) per time frame/dwell time (equation 2).[81]

$$W = c_{Std.} \cdot \eta_{neb.} \cdot Q_{sample} \cdot t_{dwell} \qquad \text{Eq. 2}$$

$c_{Std.}$ = mass concentration of the standard [mass · volume^{-1}]
$\eta_{neb.}$ = nebulisation/transport efficiency
Q_{sample} = sample flow rate [volume · time^{-1}]
t_{dwell} = dwell time [time]

The crucial part is the determination of the nebulisation/transport efficiency (η_{neb}).[85]
• A simple approach is based on the collection of the effluent waste of the spray chamber. Knowledge of the sample flow rate and waste collection time allows for the calculation of the total volume of sample that enters the ICP. However, this approach is prone to errors due to recovery losses.[86] Direct approaches, e.g. aerosol collection via cascade impactors, deliver higher accuracy and precision, but are quite laborious.[86]
• A further approach to determine η_{neb} is based on a nanoparticle suspension with a known number-based concentration. The number of flashes per second (detected via ICP-MS) is equal to the number of nanoparticles that enter the plasma. The ratio of the number of single particle peaks to the initial number-based concentration of the standard suspension is $\eta_{neb.}$. However, the number-based concentration of the standard must be accurately known; otherwise, a large error in the determination of η_{neb} occurs.
• A third approach similar to the previous one is also based on a nanoparticulate standard suspension; but here, only particle/material density, diameter as well as

shape is needed: the intensity of the detected nanoparticulate flashes can be allocated to an absolute mass-concentration, given the fact that in case of nanoparticles the transport efficiency is only affecting the number of particles transported into the ICP-MS. For the calculation of $\eta_{neb.}$ a dissolved standard solution with a known mass-concentration of the same element is delivered to the nebuliser; in this case a reduced transport efficiency is affecting the absolute mass of the dissolved standard transported into the plasma. $\eta_{neb.}$ is expressed by the quotient of signal-to-mass ratios of both the dissolved standard solution as well as the nanoparticulate standard (equation 3):

$$\eta_{neb.} = \frac{\frac{I_{Std.}}{M_{Std.}}}{\frac{I_{NP}}{M_{NP}}} \quad \text{Eq. 3}$$

$I_{Std.}$ = signal intensity of the standard [cps]
$M_{St.}$ = absolute mass-concentration of the standard [mass]
I_{NP} = signal intensity of the NP suspension [cps]
M_{NP} = absolute mass-concentration of each NP [mass]

$\eta_{neb.}$ can also be affected by non-spectral interferences - thus, an appropriate matrix-matching is mandatory.[81] Furthermore, potential diffusion losses of light (dissolved) elements (e.g. Mg) or discrete particles within the plasma need to be taken into account leading to large calibration errors; an empirical correction factor is necessary in such cases.[87] Particles of low density, low molecular weight, and low boiling point vaporise at higher rate - using dissolved elemental standard solutions for calibration is expected to be more successful then.

An alternative approach based on isotope dilution which also necessitates the determination of η_{neb} was developed by Telgmann et al.[88] for spiked AgNPs in several matrices. An [109]Ag isotopically enriched spike solution was added on-line during sp-ICP-MS analysis and quantitative data/size information was obtained based on a modified isotope dilution equation showing good agreement of particle size data compared to calibration via ionic standards. Matrix effects are directly correct for and time consuming external calibration becomes redundant. The compensation of NaCl matrix effects via this approach was investigated and confirmed by Sötebier et al..[89] But, with regard to independent single particle events it is important to collect a sufficient number of data to allow for an appropriate averaging and thus reduce errors in the isotope ratios.

As an alternative option to circumvent the determination of $\eta_{neb.}$ sample introduction systems comprising 100% aerosol transport efficiency can be employed. However, these approaches are not yet as established as the previously mentioned ones:

• Gschwind et al. investigated the use of microdroplet generators coupled to ICP-MS for the analysis of Ag and Au nanoparticles. This allows quantitative introduction of small, monodisperse single droplets into the ICP. The size/volume of a single droplet is precisely determinable. Assuming that one microdroplet contains one single particle, quantification can be accomplished by liquid standard solutions.[90]

• Another option is a drainless small-volume on-axis spray chamber in combination with a low-flow nebuliser (flow rate about 10 μL min^{-1}).[91,92,93,94] In this case the mass-flux introduced into the ICP can easily be calculated.

4.1.2 Dwell time

Conventional ICP-MS systems comprise dwell times down to 1-5 ms. However, with regard to the time duration of an ion cloud within the plasma (about 200-500 μs)[81] the

following unintentional effects can occur and need to be taken into account: (i) two nanoparticles are detected within one dwell time, leading to a size-overestimation (Figure 3, a)); (ii) nanoparticles are only partially detected, leading to a nanoparticle size-underestimation (Figure 3, c+d)). Furthermore, in case of high ionic background concentrations, long dwell times increase the size detection limits of nanoparticles.[95]
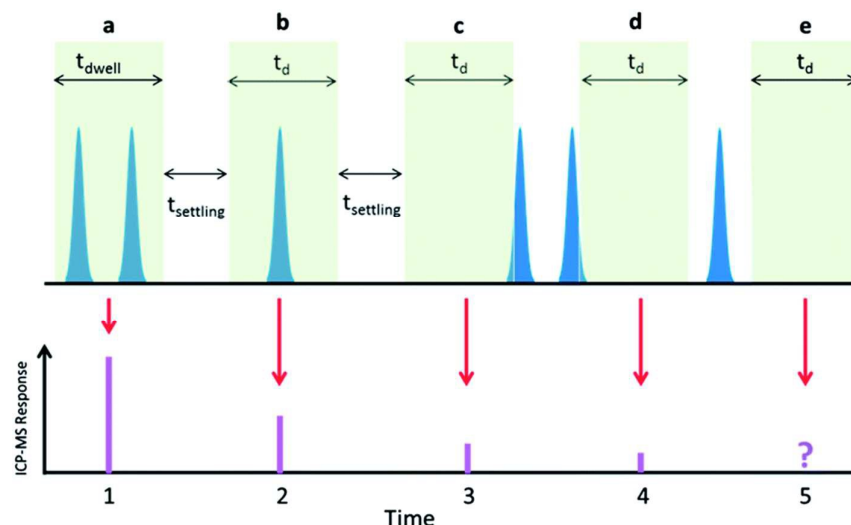

Figure 3: Effect of dwell time and settling times on single particle measurements. **a)** two particles detected; **b)** one single particle detected; **c)** the leading edge of one particle detected; **d)** the tailing edge of one particle detected; **e)** no particle detected. Reproduced from Ref.[96] with permission from the Royal Society of Chemistry.

Appropriate dilution of the nanoparticle suspension is required to minimise such effects. Furthermore, most commercial instruments invoke a settling time during data acquisition (Figure 3) where particle events are not recorded. Prolongation of the analysis time is mandatory in this case to improve counting statistics.

The newer generation of ICP-MS systems enable μs dwell times as well as acquisition times as fast as 10^5 Hz (10 μs dwell time).[96] Consequently, baseline separation of events even at high particle concentrations is possible and single particle events are time-resolved - thus, one particle event comprises several data points forming a "peak". The respective peak area can be related to the mass of the element within the nanoparticle. As long as the whole particle event occurs within one dwell, the ratio of the intensity of the particle event to the standard deviation of the ionic background increases leading to improved detection limits with shorter dwell times.[97] However, this applies only for single mass detection - if mass needs to be changed, the settling time of the quadrupole negates the benefits of low dwell times. Thorough investigations regarding dwell time effects were reported by e.g.:[96,98] Montano *et al.* demonstrated a further benefit of μs dwell times to resolve the ^{28}Si signal from SiO_2 nanoparticles from background signals generated by the isobaric molecular interference $[^{14}N^{14}N]^+$.[99]

4.1.3 Ionic background ⇔ peak identification
In particular for ubiquitously present elements a high ionic background of the target element is usually occurring. Thus, flashes induced by ENPs must be separated from background signals. A high ionic background counteracts a low ENPs size detection limit and appropriate strategies are mandatory to distinguish between ion and particle events. The definition of threshold values to decide whether the obtained signal is

originating from a particle or from background event is critical. If the threshold is set too low, false positives will occur and if the threshold is set higher, size detection limits will increase.

• Pace *et al.* employed a "3σ - criterion" where σ is the standard deviation of the whole dataset: The entire data set is averaged and all data pointes that are three standard deviations above the mean are collected. The remaining data set is averaged and again all data points 3σ above the new mean are collected. This procedure is repeated until no more data points are "3σ" above the final mean. The remaining data set represents the background while the collected data points are particle events.[85] Statistical evaluation and an error analysis of background versus nanoparticle distinction was conducted by Laborda *et al.*.[83]

• Cornelis *et al.* developed an algorithm for deconvolution of particle events from dissolved/or background signals.[100,97]

With regard to dwell times ≤100 µs time resolved ENPs events composed of individual measurement points instead of flashes are detected. Shot noise can result in the signals from a single nanoparticle going above, below, back above and then below of the respective detection threshold. Hence, signals belonging to one single nanoparticle are allocated to several nanoparticles resulting in an overestimation of the total number of nanoparticles and an underestimation of the size.

Further approaches described in literature actively remove ionic species from the nanoparticles: Hadioui *et al.* employed ion exchange resins for the removal of the ionic background and obtained a simpler and more accurate data processing as well as improved size-detection limit.[101] Tan *et al.* used the coupling of electrospray-differential mobility, which has the ability to separate ionic species from nanoparticles, on-line with sp-ICP-MS to reduce the ionic background.[102]

4.1.4 Upper size detection limits

Lower size detection limits are mainly delimited by the sensitivity of the respective ICP-MS system. A mathematical derivation of size detection limits on basis of Poisson statistics was conducted by Laborda *et al.*.[83] The same authors also presented an overview based on reported literature data.[82] Lee *et al.* evaluated the lower size detection limit for 40 elements relevant for nanoparticles.[103]

However, the upper size detection limits are also critical especially with regard to the behaviour of ionic *versus* particulate matter within an ICP (calibration strategies).

The size-threshold for nanomaterials is 100 nm - however, according to the EU-definition on nanomaterials[24] a size-number distribution information is needed to decide, whether a material is "nano" or not. Hence, particles in a given sample could also be larger than 100 nm and complete decomposition as well as atomisation of the nanoparticles needs to be guaranteed. In addition, to keep nanoparticles stable in suspension, steric or electrostatic stabilisation is mandatory. However, especially in complex matrices, destabilisation and formation of agglomerates/aggregates larger than 100 nm is most likely. To study the behaviour of nanoparticles-agglomerates/aggregates in complex matrices complete decomposition/ionisation needs to be guaranteed and "valid" upper size limits need to be known.

The linear dynamic range in sp-ICP-MS is often limited to about 3 orders of magnitude in particle mass and about 1-2 orders of magnitude in particle diameter given the fact that the mass of a particle is directly proportional to the cube of its

diameter.[87] Pertinent aspects are residence times as well as vaporisation and atomisation behaviour of nanoparticles within the plasma. Theoretical studies on the necessary residence times as a function of particle size of UO_2 colloids to reach sublimation temperature were conducted by Degueldre *et al.*.[80] Several system parameters affecting the upper size detection limits were investigated by Olesik and Gray.[95] Especially gas flow rates as well as sampling depth affect the residence time and vaporisation behaviour of nanoparticles as well as diffusion of formed ions within the plasma.[104] As boiling points and diffusion coefficients of the elements are varying depending on their mass, case-specific optimisation of the plasma parameters is mandatory. Ho *et al.* investigated the correlation between boiling points and sampling depths with elemental standard solutions and concluded that the obtained optimum sampling position allows rather accurate calibration using elemental standard solution for (nano)particle size determination. The sampling depth profile of aqueous solution can be used as a guide for the selection of the sampling depth of sp-ICP-MS. For larger discrete nanoparticles, the optimum sampling depth value shifts downstream because of longer duration for complete vaporisation of the particles.[105] For example upper size limits of about 1-2 µm were reported for SiO_2 nanoparticles [106,99], about 1 µm also for ZrO_2 colloids[78] and 2-6 µm were assumed for UO_2 colloids based on theoretical examinations.[80] In any case, 1-5 µm are the maximum sizes recommended.[82] Refer also to chapter 3.1.

The analysis of larger nanoparticles requires careful plasma parameter optimisation to avoid large error in size determination. Furthermore, particle size cut-offs of common spray chambers need to be taken into account.[44]

4.1.5 Raw data assessment - histogram
For the translation of sp-ICP-MS raw data into a histogram, several freely available single particle calculation spreadsheets exist.
• One of the first calculation spreadsheets was developed by a group at the National Institute of Food Safety - RIKILT.[106,107] Upon import of raw data of the unknown sample, measurement data for calibration, nebulisation efficiency as well as information on the material properties (e.g. density) and instrument parameters, a signal distribution and finally a particle size-distribution is obtained (Figure 4).
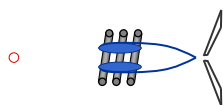

Figure 4: a) raw data/spikes; **b)** particle number concentration; **c)** particle number-*versus* size- distribution upon calibration of the system. In addition cross-references to the respective chapters are given in brackets.

• A further software "Nanocount" was developed by Cornelis[108] and a lucid data processing schematic is given by Pace *et al.*.[85]
• A "practical handbook" to establish a protocol for the determination of mean nanoparticle size, number-based size distribution, particle number concentration and mass concentration of ions in an aqueous suspension of nanoparticles using sp-ICP-

MS was published by the National Institute of Standards and Technology (NIST).[109,110]

Furthermore, ICP-MS instrument manufacturer supply evaluation software packages and/or application notes for nanoparticle analysis via sp-ICP-MS: Agilent Technologies[111], Thermo Fisher Scientific[112], Perkin Elmer[113], Nu Instruments (Cameca/Ametek)[114], TOFWERK[115].

However, despite its easy and fast applicability, sp-ICP-MS remains a screening tool[106] and *a priori* knowledge about particle composition and shape is mandatory (as the theoretical description is mostly based on the assumption of spherical shape) to draw conclusions about the true particle size. But, sp-ICP-MS is an emerging technique which has rapidly developed during the past few years and is still evolving.

4.2 Multi-element capabilities

Quadrupole mass analysers are the most common in ICP-MS (ICP-QMS). However, with regard to fast signal flashes in sp-ICP-QMS they suffer from the limitation that only one *m/z* can be acquired at a time. As introduced before, recently fast scanning ICP-QMS systems (µs dwell time) were developed, comprising dwell times much shorter than the residence time of generated atom/ion clouds from single particles within the ICP. However, even though two nuclides become detectable within an ion cloud of one nanoparticle, signals comprise a spectral skew.

To overcome this limitation and to permit multi-element measurements of short transient signals (quasi-) simultaneous mass analysers are mandatory. The simultaneous detection of several elements within one short transient signal opens up new vistas, e.g., (i) the distinction between artificial and natural nanoparticles/colloids in complex matrices is still a challenging task and would benefit from multi-element analysis revealing potential particle source specific elemental fingerprints; (ii) nanoparticles consisting of several elements (e.g. core-shell particles) can be further investigated; (iii) the analysis of isotope ratios within single particles is enabled.

Currently, multi collector (MC-ICP-MS) as well as time of flight (ICP-ToF-MS) instruments have been applied for multi-element sp-ICP-MS.

A proof of concept study was conducted by Yongyang *et al.* employing sp-MC-ICP-MS for isotope ratio measurements of erbium in single particles. Erbium oxide functions as uranium surrogate at different enrichment levels, as the isotope signatures from natural uranium to highly enriched uranium could be covered by erbium isotope range. In conventional methods, particles are separated from the liquid matrix, digested and analysed as bulk via e.g. (MC)-ICP-MS resulting in an average information from many particles covering a wide size range. Detection and isotopic analysis of individual particles in environmental matrices provides essential fingerprint information in e.g. nuclear safety and potential release of radioactive particles from nuclear facilities. Furthermore, in the field study of nuclear environment, isotopic analysis of colloids – acting as potential radionuclide carrier – supports source identification and elucidation of migration behaviour. Sp-MC-ICP-MS is suitable for sensitive detection and precise isotope ratio measurements (better than 0.3%) of an averaged set of individual particles with sizes ranging from 130 nm - 3 µm.[116]

However, MC-ICP-MS instruments are designed for the precise isotope ratio determination of one element or of a maximum of two elements with *m/z* close to one another. Simultaneous detection of all nuclides spread over the whole mass-range of

the periodic table is impossible by MC-ICP-MS, but ToF instruments are capable of this.

Borovinskaya *et al.* developed and investigated a new ICP-ToF-MS which is commercially available from TOFWERK (Thun, Switzerland) since a few years and allows for recording simultaneous multi-element full mass spectrum within about 30 µs. Droplets consisting of multi-element solutions and containing Au nanoparticles were employed to study the instrument performance for the multi-element analysis of short, transient signals.[117] Recently, Praetorius *et al.* employed the sp-ICP-ToF-MS for multi-elemental fingerprint analysis of engineered CeO_2 nanoparticles in the presence of natural Ce-containing nanoparticles/colloids in soils.[118] By sp-ICP-ToF-MS a distinction of ENPs and natural nanoparticles/colloids was enabled. In addition, a machine learning approach was developed by the authors allowing for an automated allocation whether a nanoparticle is of natural or engineered origin based on the elemental fingerprints. This combined approach of sp-ICP-ToF-MS detection with machine learning is beneficial when analysis of ENPs needs to be conducted in the presence of natural nanoparticles/colloids comprising a similar elemental composition and much higher mass/number concentration and will gain in importance in the future. However, this technique is beneficial in all kinds of applications were fast transient signals and multi-element capabilities are needed. A characterisation of figures of merit of the ICP-ToF-MS was conducted recently by Hendriks *et al.*.[119]

4.3 Applications

It is out of the scope of this tutorial review to provide a comprehensive overview of application-related publications in the field of sp-ICP-MS of recent years and thus the reader is referred to specialised reviews on this topic e.g.[81,82] In the following a selection of recent publications is presented providing an insight in the range of applications of this emerging technique. A literature search revealed that most of the application-related sp-ICP-MS publications cover questions in the environmental field closely followed by standard/model suspensions applied for method development. Approximately the other half of the application-related publications covers the topics consumer products, food and medicine.

4.3.1 Consumer products

A broad variety of cosmetics is commercially available and thus a characterisation of the products applied to the skin is necessary. In general, cosmetics involve a complex matrix including e.g. minerals, oils, fats, pigments and UV-filters. Components in the form of ENPs such as TiO_2 and ZnO are extensively used and require a "nano"-labelling according to the current cosmetic product regulation, which demands for suitable analytical techniques. De la Calle *et al.* developed a sp-ICP-MS screening method for the analysis of sixteen cosmetic products.[120] They confirmed the presence of TiO_2 nanoparticles in five samples - four of which were "nano" labelled. Within a further study from Dan *et al.* TiO_2 nanoparticles, widely used as UV filters, were investigated in sunscreen and detected in the size range of 32-40 nm.[121] Furthermore, the authors determined the TiO_2 nanoparticle mass content by a standard addition-sp-ICP-MS approach which was less time consuming and showed good agreement with conventional acid digestion ICP-MS analysis. Mackevica *et al.* investigated the release of silver nanoparticles from another widely spread consumer product - toothbrushes.[122] The use of silver nanoparticles in commercial products has become increasingly common, mostly due to their anticipated antimicrobial properties (most probably related to the release of Ag^+). Thus, release studies, in particular with regard to consumer safety and life-cycle assessment, are needed. Silver nanoparticle

release was proven from several toothbrushes in a size range of 42-47 nm. Under the assumption that a toothbrush is used 2 minutes per day for 3-4 months, the authors showed that two brands release Ag during this whole usage period.[122]

4.3.2 Food

Nanoparticles also play an increasingly important role in food - either intended or accidental. Kollander *et al.* investigated the content of lead nanoparticles in game meat upon enzymatic digestion by sp-ICP-MS analysis.[123] Game meat may contain high levels of Pb in the form of fragments from the Pb-core bullet used to cull the game and thus consumption may lead to increased Pb levels in blood. A hitherto neglected route of Pb exposure from consumption of game meat is via metallic lead nanoparticles - this might become a relevant issue especially with regard to potential gastrointestinal uptake of nanoparticles. The authors detected Pb nanoparticles in game meat with minimum detectable particle diameters of approximately 46 and 56 nm.[123] The game meat destined for consumption showed no detectable Pb nanoparticles (or were at least not detectable). However, some hunters also consume the meat close to the wound channel and thus, ingestion of Pb nanoparticles is most likely. Verleysen *et al.* investigated the release of Ag nanoparticles from decoration of pastry. E174 (silver) is a food additive approved by the European Commission and is authorised to be used to colour the coating of confectionery, for decoration of chocolates and in liqueurs.[124] Especially, in consumer products, where nanosilver is not linked to justified and tangible benefits, concerns about possible health effects arise. Furthermore, silver (E174) is included in the program for the re-evaluation of approved food additives set up by Commission Regulation (EU) no. 257/2010.[124] The authors showed that a simple treatment with water results in the release of a subfraction of Ag nanoparticles. Transmission electron microscopy (TEM) data were confirmed by sp-ICP-MS results although a substantial fraction below the size detection limit of sp-ICP-MS (13 nm) was not detected. A further application field of Ag nanoparticles related to food are plastic food containers with regard to antimicrobial properties. However, the potential migration of silver nanoparticles into food has hardly been addressed. Within a recent study Mackevica *et al.* investigated the release of silver from four different food containers.[125] Both sp-ICP-MS as well as TEM revealed the release of Ag nanoparticles from all food containers with particle sizes in the range from 10 - 100 nm in particular in contact with slightly acidic matrix.

4.3.3 Medicine

Nanomaterials are under intense development for medicinal applications such as imaging, diagnosis, treatment of diseases/drug delivery. The challenge facing biomedical research is the poor understanding of the agglomeration status as well as the fate of nanomaterials in biological systems (e.g. blood stream). Gold-based nanomaterials are candidates for diagnostic and therapeutic agents due to their bioinertness, controllable morphology, surface functionality as well as optical properties.[126] After intravenous administration the nanomaterials might change their pristine properties such as surface functionality and agglomeration/aggregation due to interaction with the complex blood matrix which requires suitable characterisation methods. Jenkins *et al.* investigated the agglomeration status of gold-nanoparticles in blood by sp-ICP-MS.[126] By means of sp-ICP-MS agglomeration of the tested Au nanoparticles in blood upon incubation was detectable. A further, interesting field of application of sp-ICP-MS are nanoparticle-encoded bioassays. Zhang *et al.* developed a method for quantification of three DNA targets associated with clinical

diseases by DNA probes labelled with Au nanoparticles (⇔ HIV), Ag nanoparticles (⇔ Hepatitis A) and Pt nanoparticles (⇔ Hepatitis B) for distinction as a proof-of-concept. Via formation of sandwich conjugates with the labelled DNA probes the DNA targets could be detected by sp-ICP-MS at about 3 orders of magnitude higher sensitivity compared to colorimetric methods.[127] The availability of several different ENPs offers the potential to extend the method as high-throughput assay of DNA with multiplex nanoparticle tags. Sp-ICP-MS also shows great potential for studying the elemental heterogeneity of cells that means the variation due to stochastic expression of genes, proteins and metabolites which can influence "cellular decision making" as well as cell fate. Just a few studies are available, for example Wang *et al.* developed an ICP-MS method for the investigation of trace-metal distribution in single cells (sc-ICP-MS).[92] This approach enabled detection of differences in the elemental distribution between normal and cancer cell lines. Sc-ICP-MS will substantially contribute to a deeper understanding of cellular processes in the future.

4.3.4 Environment

Platinum group elements (PGEs: Pt, Pd, Rh) are homogenously deposited on the inner surface of car exhaust catalysts with expected particle diameters below 10 nm, but sintering can lead to their aggregation and formation of larger particles. Due to mechanical as well as chemical impacts, PGE particles are released into the atmosphere and via rainwater also in surface waters. Investigations regarding the impact of PGE particles within the environment are rare. Folens *et al.* employed sp-ICP-MS for the investigation of Pt nanoparticles within road dust samples and found about 3.3% of the released platinum in the form of nanoparticles.[128] It is supposed, that Pt-nanoparticles are bioavailable as shown within a former study by Jiménez-Lamana *et al.* investigating the uptake of 70 nm Pt-nanoparticles in the model plants *Lepidium saliva* and *Sinapis alba* via expose studies.[129] Enzymatic digestion of the plant material was conducted to extract and subsequently analyse the Pt-nanoparticles via sp-ICP-MS. Apart from pristine Pt-nanoparticles also larger Pt-particles were observed, possibly due to agglomeration/aggregation processes, but platinum in dissolved form was not detected. The highest Pt-nanoparticle number-concentration was observed in the roots and lower concentrations in the leaves, stems and cotyledons indicating transport within the plant. Apart from ENPs released into the environment, natural particles (colloids) in size range from approximately 1 nm to 1 μm can also act as transporters for toxic metals and metalloids. The current understanding of metal/metalloid interaction with colloids and their mobilisation and transport is still limited partly by a lack of reliable analytical methods.[130] Gomez-Gonzalez *et al.* investigated the release of arsenic-bearing colloids from mine-wastes.[130] The authors combined sp-ICP-MS with synchrotron-based X-ray absorption spectroscopy (XAS) to obtain complementary information on the nature of the particles. The combined use of these techniques allowed for detection, identification and size determination of *scorodite* (FeAsO$_4$ · 2H$_2$O) particles released from mine wastes, suggesting their potential to transport arsenic. Sp-ICP-MS has the potential to make a valuable contribution to further understand the underlying processes of fate and colloid-transport of metals/metalloids within the environment. However, in the case of natural colloids, it is important to note, that sp-ICP-MS is not capable of providing direct size-information unless supplementary data (e.g. composition, shape, density) are provided by further, complementary techniques.

5. Hyphenated techniques

In order to obtain more information on nanomaterials in a given sample, ICP-MS can be coupled on-line to a fractionation/separation system. This is especially required in case the nanomaterial comprises polydisperse size-distribution and/or is suspended in a complex matrix. During the last years several fractionation and separation systems were investigated and successfully applied for nanomaterial analysis. In the following sections the most common systems field-flow fractionation (FFF), hydrodynamic chromatography (HDC), high performance liquid chromatography (HPLC) and capillary electrophoresis (CE) are introduced. In addition, laser ablation hyphenated to ICP-MS (LA-ICP-MS) is included as an option for spatially resolved imaging of nanoparticles in solid matrices. Advantages, limitations and practical hints of each technique are discussed and several application examples from the most relevant fields are highlighted.

5.1 Field-flow fractionation (FFF) - general concept & theory
FFF is a non-chromatographic, flow-based fractionation method, which was invented and theoretically described by John Calvin Giddings in 1966.[131] In FFF sample fractionation is performed inside a trapezoidal channel without a stationary phase and is the only technique that offers a continuous, high size-resolution fractionation from about 1 nm up to several μm.[39] Briefly, most of the FFF subtechniques comprise channel dimensions of 20-50 cm length, 2-3 cm width and 0.01-0.05 cm in thickness;[132] (alternatively, and mentioned for the sake of completeness, FFF in rotating coiled columns has also been described in few studies[133,134,135,136]). A pumped carrier liquid is moving the analytes/particles from the „inlet side" to the "outlet/detector side" generating a parabolic flow profile. Simultaneously a force field perpendicularly to the direction of the carrier flow is applied, which forces the analytes/particles towards the channel bottom ("accumulation wall") (see Figure 5). The nature of the force field can be manifold and according to the field, the FFF subcategory is named - e.g. sedimentation (Sd-FFF, centrifugal force), flow (Fl-FFF, flow force), electrical (El-FFF, electrical field), thermal (Th-FFF, temperature gradient), magnetic (Mg-FFF, magnetic field)-FFF.[137] The net movement of the analytes towards the external field is caused by diffusion from an area of high analyte concentration to an area with lower concentration. After a certain relaxation period, a dynamic steady state is reached. Due to the different velocity vectors of the parabolic flow profile (see Figure 5) the velocity of the particles/analytes depends on their distance from the accumulation wall. Smaller particles/analytes with larger diffusion coefficients diffuse faster in higher channel regions with faster laminar flow and consequently elute prior to larger ones. Up to now only Fl-FFF and Sd-FFF have been coupled on-line to ICP-MS for nanoparticle analysis. In Fl-FFF different types exist - symmetrical-Fl-FFF, asymmetrical-Fl-FFF (AF4) and hollow-fiber-FFF (HF5). In symmetrical-Fl-FFF the perpendicular flow is directed from the lid through the bottom of the channel (necessitating a further pump); while in AF4 the lid is impermeable and the cross-flow is generated by directing part of the channel flow through the bottom of the channel. The bottom of the channel is covered by a membrane with a given size-cut off (thus, in principle everything smaller than the size-cut off, e.g. ionic fractions/species, is not detectable; apart from few exceptions) mounted on a frit (either made of metal or ceramic). In HF5 the field is radial with the cross flow radiating outwards over the entire inner surface of the tube while the rest of the carrier liquid generates the channel flow.[138,139] Benefits of HF5 over AF4 are smaller sample injection volumes, shorter analysis times and decreased sample dilution. However, up to now (to the best of the authors´ knowledge) only PES hollow

fibers (10 kDa) are commercially available, which limits method optimisation parameters. In Sd-FFF the separation channel is spanned on a centrifugal apparatus and the field strength correlates to the centrifugal force. In general, Sd-FFF is applied for larger (nano)particles, especially, when there is a larger difference in density among the particles. In addition a membrane is missing within Sd-FFF, thus, ionic fractions are detectable as well.

Considering that AF4 is the most frequently used subcategory in nanoparticle fractionation, the following theoretical deduction is solely shown for AF4 under the assumption of normal-mode fractionation and without taking particle-particle or particle-membrane interaction into account. For further theoretical descriptions related to the other subtechniques the reader is referred to the respective literature.[137]

For theoretical description of the retention behaviour of analytes in AF4, a retention parameter λ is defined. λ is the ratio of l (the average distance of particles from the channel wall) and w (channel height; aspects regarding channel height determination are reported in literature e.g.[140]) (see also Figure 5) (equation 4):

$$\lambda = \frac{l}{w} \qquad \text{Eq. 4}$$

λ depends on particle characteristics as well as the respective perpendicular force field. Taking these two aspects into account the following general expression for λ is obtained (equation 5):

$$\lambda = \frac{k \cdot T}{F \cdot w} \qquad \text{Eq. 5}$$

k = Boltzmann constant
T = Temperature
F = perpendicular force field

In case of AF4 the perpendicular force field F is a (cross-)flow. Inserting the respective expression into equation 5 the following equation 6 of λ for AF4 is obtained. Herein, small λ values indicate a strong retention of the particles.

$$\lambda = \frac{D \cdot V^0}{\dot{V}_c \cdot w^2} \qquad \text{Eq. 6}$$

D = Diffusion coefficient
V^0 = Channel void volume
V_c = Cross flow rate

Within this equation V^0 and w are fixed physical geometries of the channel and V_c is a measurable (cross-)flow rate. Separation of particle zones within the channel is therefore solely based on the differences in diffusion coefficients of the particles. The expression for the retention parameter λ needs to be connected with experimentally observed retention times via the retention ratio R. Herein R is the ratio of the time that a non-retained particle/analyte needs to pass through the system (t^0) and the retention time of a retained particle (t_r). R and λ can be linked in good approximation (assuming small λ values, thus strong retention) according to equation 7.[137]

$$R = \frac{t^0}{t_r} = 6 \cdot \lambda \quad (R \approx 6 \cdot \lambda, if\ \lambda < 0.02) \qquad \text{Eq. 7}$$

Combining Eq. 6 and Eq. 7 as well as the Stokes expression for the diffusion coefficient, the hydrodynamic particle size d_H in AF4 can be obtained from experimental data (equation 8):

$$d_H = \frac{2 \cdot k \cdot T \cdot V^0}{\pi \cdot \eta \cdot w^2 \cdot \dot{V}_c} \cdot \frac{t_r}{t^0} \qquad \text{Eq. 8}$$

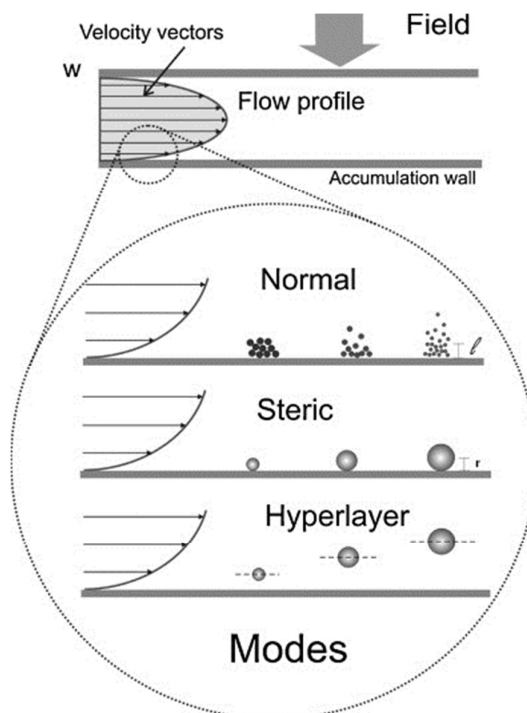η = Viscosity of the carrier

Figure 5: Separation principles of FFF. Reprinted from Ref.[132] with permission from Elsevier.

In AF4 different types of retention mode can be achieved: normal and steric/hyperlayer mode (Figure 5): Once the particle size increases beyond a certain limit (approximately 1 μm) the hydrodynamic radius (r_H; $d_H = 2r_H$) becomes greater than the layer thickness "l" (figure 5) of a cloud of smaller particles - elution order is inverted then and called "steric elution".[132] Next to steric elution particles in thin channels have long been known to experience velocity-dependent hydrodynamic lift forces, which direct them away from the channel wall. As the carrier flow is increased to a certain point, particles are forced to lift from the wall and rise to a position in the flow field where there is a complete balance between the lift as well as perpendicular force. The particles lift to a discrete, size-related position referred to as "the hyperlayer".[137] Both in steric mode and in hyperlayer formation the elution times decrease with increasing particle size. A transition from a normal to a steric/hyperlayer retention mechanism can potentially occur within the size range of the sample, giving rise to coelution of small and large particles. Steric/hyperlayer elution affects all subtechniques of FFF and requires careful interpretation of

fractograms in particular of polydisperse materials in terms of size distribution. However, in case the field strength can be selected in a way that a mixed retention mechanism is avoided, the steric/hyperlayer fractionation of large particles produces highly selective separations in short periods of time.

5.1.1 Asymmetrical flow field-flow fractionation (AF4) on-line with ICP-MS - coupling aspects

As early as 1991 Beckett proposed the on-line coupling of FFF with ICP-MS as sensitive multi-element detector.[141] In 1993, Murphy *et al.* established the on-line coupling of Sd-FFF and ICP-MS[142], and in 1999 Hasellöv *et al.* coupled AF4 to ICP-MS[143]. From this time on the number of publications is steadily increasing being further driven from about 2010 on by the exploration of the research field of ENPs.[56]

The simplest interfacing approach is to connect the outlet tubing from the FFF directly with the ICP-MS nebuliser. However, some authors suggest putting a T-piece in between for the on-line addition of acid to minimise possible memory effects.[39] In addition, an internal standard can be added via the T-piece to control the aerosol stability and correct for potential drift. Also flow-splitting has been proposed as an option to reduce the flow into the ICP-MS.[143]

Given the fact that (in most cases) low molecular mass ionic species are usually lost with the cross-flow through the membrane in AF4, tailored quantification approaches were developed: (i) injection of ionic standards post channel via a loop (same loop volume as sample loop); (ii) post channel large loop injection of ionic standards; the maximum intensities of flat-top peaks are used for data assessment[144,39,145]; (iii) off-line fraction collection upon AF4 separation and quantification of the elemental content via ICP-MS upon acid digestion.[146] A fourth approach is based on post-channel on-line isotope dilution. Herein, an isotopically enriched spike solution is added and quantification was achieved based on the determination of isotope ratios.[147]

As mentioned previously (chapter 3.1 and 4.1.4) the atomisation behaviour and detection of large particles within the ICP-MS needs to be considered. Furthermore, it needs to be kept in mind, that, ICP-MS detection delivers a mass-based information that needs to be converted into a number-based concentration. This can be accomplished based on particle size information obtained either from the AF4 theory (although membrane swelling may decreases the channel height)[148] or from the retention time using calibration with certified particle size standards (refer to Table 1). However, as will be discussed in the following section, the influence of the carrier solution, membrane type and nanoparticle characteristics can result in a shift of the retention time, as reported for Au and SiO_2 nanoparticles under identical AF4 conditions[149] as well as for polystyrene and Ag nanoparticles[150], which results in erroneous size information. Thus, Hagendorfer *et al.* suggested a multi-detector approach using different detectors coupled sequentially in-line providing a multitude of information.[151] Detectors which allow for direct size determination of nanoparticles without the need for particle size standards are light scattering detectors, e.g. multi angle laser light scattering (MALLS) and dynamic light scattering (DLS). However, it is out of the scope of this tutorial review to cover the theoretical background and applications of light scattering devices and thus the reader is referred to the respective literature e.g..[152] In case of particles that comprise plasmon resonance (e.g. Ag, Au nanoparticles) UV/Vis detection leads to additional information. In addition to on-line detectors also off-line fraction collection and subsequent TEM analysis was reported.[149] Multi-detector approaches are especially beneficial in terms

of the analysis of unknown ENPs especially in complex matrix or natural nanomaterials and colloids.

5.1.2 Method optimisation - critical aspects

In the following sections, the most crucial parameters, which need to be considered during Fl-FFF method optimisation, are discussed and some general hints are given. However, it must be kept in mind that each new type of nanomaterial requires careful optimisation of all mentioned parameters and re-evaluation is also required for each new type of matrix.

5.1.2.1 Focus time & Cross-flow

Upon sample injection into the Fl-FFF channel a focusing step is conducted. The carrier flow enters the channel simultaneously from inlet and outlet and exits the channel through the membrane. The focusing period serves to relax the sample and to narrow the width of the sample zone. On-channel preconcentration of large sample volumes is possible.[143] Focusing is a crucial part of the sample injection step as it can strongly influence the particle aggregation/agglomeration state, separation efficiency and recovery. The same applies for high cross-flow rates during separation/fractionation which could induce irreversible adsorption of nanoparticles onto the membrane.[153]

Hagendorf *et al.* observed a decrease in recovery for Au nanoparticles at a particular focusing time most probably the nanoparticles are driven too vigorously towards the membrane causing strong membrane interaction and partial immobilisation.[151] If the focusing is insufficient a void peak within the respective fractogram may occur - as reported for Au nanoparticles comprising a high negative surface charge (large negative zeta-potential values). Repulsive forces between the membrane´s surface (mostly negatively charged) and the nanoparticles are particularly pronounced and prevent proper equilibration during the focus step leading to a pre-elution of a certain amount of particles due to movement in fast regions of the parabolic flow profile (see Figure 5). In this case, harsher focusing conditions are necessary.[151] Cho *et al.* also investigated Au nanoparticles and observed an intensity decrease of the void peak with increasing flow rate.[154] However, more gentle focusing conditions are generally favoured to minimise particle-membrane interaction or possible agglomeration/aggregation. For focus-parameter optimisation it is recommended to systematically increase the time until the component of interest gives a well-shaped peak with no tendencies of peak splitting or premature elution. The effect of decreased recovery values upon the application of high cross-flow values during separation was reported by Heroult *et al.* who investigated SiO_2 nanoparticles[149].

Loeschner *et al.* conducted focusing time optimisation for Ag nanoparticles. In case the elution step begins before all particles have reached the focus zone, fractionation of the particles starts from different positions and leads to wrong size-distribution results as well as reduced resolution in particular for polydisperse samples.[155]

Another aspect investigated by Mudalige *et al.* is membrane fouling due to electrolyte rejection from the charged membrane surface in particular during focussing. Due to electrostatic repulsion polyvalent ions show higher rejection than monovalent ones and could be concentrated at the focus point during focusing leading to further reduction of the repulsion between analytes/particles and the membrane. The authors investigated the effects of citrate, EDTA and NaCl at different concentrations on regenerated cellulose (RC) and polyethersulfone (PES) membranes with different cut-offs. NaCl showed lowest rejection compared to the polyvalent ions citrate and

EDTA. The highest rejection rate was observed for the smallest pored PES membrane for any given cross-flow.[156]

5.1.2.2 Recovery

The analyte recovery (Rec.(%)) from the FFF channel is expressed as the ratio of the eluted and detected particulate elemental mass (I) and the injected mass of the target element (I_0) (equation 9). The total injected mass I_0 can either be calculated from the total elemental content of the sample and the injection volume or it can be determined via sample injection onto the FFF channel and elution without cross flow.[153] Alternatively, some authors remove the FFF channel and "short-circuit" the flow path by means of a cross-piece[157] avoiding potential interaction of the sample with the membrane and accidental release of residual material accumulated on the membrane´s surface. Due to several parameters (discussed in the following), the recovery in FFF is often below 100% and is a factor commonly used to evaluate the fractionation efficiency and may indicate if further method optimisation is mandatory. It needs to be kept in mind that low molecular mass fractions/species of the target element usually pass the membrane during focussing causing a gap in the mass balance independent from the behaviour of the particulate elemental contents in the separation channel. In case the FFF channel is not sufficiently and reproducibly cleaned after each sample run, the recovery may exceed 100% due to carry over of residual analytes from previous runs.

$$Rec.(\%) = \frac{I}{I_0} \cdot 100 \qquad \text{Eq. 9}$$

5.1.2.3 Carrier selection

A major advantage of FFF, in contrast to other fractionation/separation techniques, is the high versatility regarding carrier composition, thus perfectly adaptable to the conditions of the analyte and sample. However, the carrier composition has a strong influence on the separation conditions, thus, FFF theory may deviate from experimental observations, in particular for particles with high surface energies and careful optimisation of the carrier composition is mandatory. Particle-particle as well as particle-FFF channel/membrane interactions may occur leading to retention time shifts and thus incorrect particle sizing. With regard to ICP-MS detection, high salt contents need to be avoided.

Electrostatic repulsion of particles is reduced with increasing electrolyte concentration since stabilisation of nanoparticles typically requires a zeta potential above +30 mV or below -30 mV[155], or pH values near the isoelectric point of the particles or the membrane. As a result a pronounced increase of retention and hydrophobic sample ⇔ membrane interactions dominate.[148] In case of attractive electrostatic forces agglomerates/aggregates may occur, which may precipitate on the membrane. Two kinds of particle ⇔ membrane adsorption phenomena are reported: (i) reversible adsorption, leading to peak broadening and peak asymmetry; (ii) irreversible adsorption on the membrane, leading to reduced recovery as e.g. observed for Au nanoparticles independent from the membrane type.[151] Apart from the electrolyte concentration, also the type of electrolyte (e.g. NaCl or NaI) can matter as the different hydration properties of the anions could affect the retention behaviour. An increase in retention time of polystyrene latex particles was observed in presence of Cl^- as compared to SCN^-. Also in case of different cations, elution time effects were observed.[148] Both effects were in accordance with the lyotropic series. As observed by Schachermeyer *et al.* different cations also influence relative recovery ($Cs^+ < K^+ < Na^+$) of nanoparticles such as polystyrene.[158] Also the ionic charge state has an

influence on the separation - monovalent ions are preferred in environmental studies because it has been shown that bivalent ones increase the overall size distribution and led to aggregation in case of humic substances.[39] In general, variation of a calculated size distribution with field strength, but not with sample load, indicates possible particle-membrane/wall interactions, while a variation of a size distribution with the sample load indicates particle-particle interactions.[159]

These effects emphasise once more the need for in-line multi-detector approaches (e.g. MALLS) to achieve complementary particle size determination. However, sizes calculated from MALLS data vary widely with the model used to fit the angular dependence of the scattering intensity, and thus, both is needed: sizing based on FFF retention times as well as on light scattering data.[159]

Experimental conditions need to be adapted to the sample matrix and target particles/analytes aiming at sufficient retention avoiding elution near or in the void peak but also avoiding excessive analysis time accompanied by peak broadening and decreasing recovery.[132] To avoid elution of nanoparticles within the void peak an increase of the ionic strength of the carrier (e.g. addition of salts, changing the pH) leads to a decrease of the surface charge of the nanoparticles and thus reduced repulsive forces. As a consequence nanoparticles move closer to the membrane and in laminar flow regions of low velocity. Cho *et al.* investigated citrate carrier (0.005%, 1 mmol L^{-1}) for the fractionation of citrate capped Au nanoparticles. In comparison to deionised water, retention times were retarded and a better separation was observed (up to about 10.2 mmol L^{-1}).[154] The authors increased the citrate concentration stepwise and observed up to threefold longer retention times reaching a plateau level. Above a certain citrate concentration the stability of Au nanoparticles degrades and formation of dimers was observed.[154] Enhancing the ionic strength of the carrier beyond a certain value results in destabilisation of nanoparticles and agglomeration/aggregation occurs. Therefore, variation of the ionic strength needs to be carefully undertaken.

Apart from ionic constituents, surfactants are added frequently to the carrier. Surfactants may improve retention properties, prevent particle aggregation, and reduce loss of analyte to the accumulation membrane.[154] Heroult *et al.* tested several carrier compositions such as a commercial mixture of nonionic and ionic detergents (NovaChem), 0.1% aqueous solution of a commercial surfactant mixture (FL-70) and deionised water for the analysis of SiO_2 nanoparticles in a food matrix (coffee creamer).[149] FL-70 led to strong retention and high Si blank signals in ICP-MS. NovaChem carrier resulted in significant particle aggregate formation. Deionised water turned out as the best option, given its high compatibility to ICP-MS detection as well as being the solvent for coffee creamer in "real-life". Deionised water was also used for sample preparation, thus possible nanoparticle aggregation/agglomeration, dissolution or surface modification during FFF fractionation is reduced. Cho *et al.* investigated several surfactants for the analysis of negatively charged citrate stabilised Au nanoparticles using a RC membrane including anionic sodium dodecyl sulphate (SDS), a detergent containing both anionic and nonionic surfactants (FL-70; regarding detailed composition refer to[154]), nonionic Triton X-100 (octylphenol polyethoxylated), and a cationic cetyltrimethylammoniumbromide (CTAB).[154] The authors also investigated the impact of sodium azide (NaN_3) which is commonly added preventing the growth of bacteria and algae. Au nanoparticles eluted slightly earlier upon addition of NaN_3 (due to the enhanced ionic strength of the carrier). It turned out that SDS reduced the interaction of Au nanoparticles with the membrane, thus leading to a faster elution. Relative to SDS the elution time with FL-70 carrier was further reduced, resulting in the largest increase in hydrodynamic diameter

observed within this study, either due to cluster formation and/or adsorption of surfactants from the carrier. Thus, the surfactant activity of FL-70 is relatively strong.[154] With regard to SDS also micelle formation needs to be kept in mind. Triton X-100 exhibited unusually large void peaks (in MALLS and UV/Vis; about 80% of Au nanoparticles). Additionally, broad and distorted peaks in the MALLS were observed, potentially due to micelle formation and micelle aggregate formation. Employing CTAB (cationic surfactant) the Au nanoparticle recovery drops and a relatively large void peak appears probably due to destabilisation of Au nanoparticles (comprising a negative zeta potential) and causing precipitation on the membrane. Thus, CTAB is not applicable for Au nanoparticle analysis with AF4.[154]

5.1.2.4 Membrane selection and nanoparticle interaction

Next to the carrier a further essential part in AF4 is the membrane. The membrane has a strong influence on nanoparticle recovery as well as fractionation properties. The most common membrane materials in AF4 are regenerated cellulose (RC) and polyethersulfone (PES). Polyvinylidene-difluoride (PVDF) is a very inert membrane. The membranes are commercially available, with different size cut-offs from 0.3 kDa up to 150 kDa. However, the membranes are not designed specifically for AF4 nanoparticle applications, reflected by the molecular weight M cut-off given in [kDa]. As a rough estimation according to a FFF-supplier to transform M in nm refer to equation 10 (with particle radius r [nm] and assumed sphere density 1):

$$M = \frac{4}{3} \cdot \pi \cdot r^3 \qquad \text{Eq. 10}$$

A more general assumption is 1 kDa ≈ 1 nm. Furthermore, it needs to be kept in mind that the cut-off information reflects the average cut-off - thus membranes comprise a given size/cut-off variation. Furthermore, identical membrane materials from e.g. different batches/suppliers may behave differently during AF4 applications.[160]

Bendixen *et al.* conducted a systematic investigation of particle-membrane (RC, PES, PVDF) interaction based on zeta-potential measurements aiming at a more straightforward method development for the example of TiO_2.[161] All membranes comprised a negative zeta-potential under the investigated conditions. The zeta-potential of the TiO_2 nanoparticles is either positive or negative, depending on the carrier solution. Positively charged TiO_2 nanoparticles are completely lost, due to strong particle-membrane interactions. Furthermore, a retention time shift was observed, in dependence of the membrane material. Thus, multi-detector approaches (e.g. MALLS) and/or size calibration are highly recommended (instead of relying on size calculation from FFF theory only). The recovery rate of TiO_2 nanoparticles decreased with increasing particle size but showed no correlation to the zeta-potential of a membrane.[161]

Within a thorough investigation conducted by Cho *et al.* a hydrophilic RC membrane was compared to a hydrophobic PVDF membrane for citrate stabilised Au nanoparticle fractionation via AF4.[154] With RC membranes recovery was low and smaller size nanoparticles eluted too quickly. The fractionation of 30 and 60 nm Au nanoparticles was satisfactorily via PVDF when using a simple carrier of deionised water without additives. However, disadvantages of PVDF membranes are (i) the limited available cut-off sizes compared to RC, (ii) rapid degradation and (iii) poor performance for multi-component mixtures of Au nanoparticles.[154]

Zeta-potential of RC, PES and PVDF membranes dependent on the pH of the carrier were investigated by Ulrich *et al.*. Zeta potentials shift to negative values under basic conditions (due to pH dependent functional groups). For PVDF the effect was less

pronounced than for RC and PES.[162] This effect strongly influences repulsive or attractive membrane - nanoparticle interactions, which were also discussed on a theoretical basis.[162]

Sötebier *et al.* presented an interesting approach for the investigation of potential nanoparticles losses on the FFF membrane by LA-ICP-MS.[150] The authors performed AF4/ICP-MS analyses of Ag-nanoparticles (N-001, see Table 1) at two different concentrations employing 5 kDa PES membrane and ultrapure water as carrier. Using LA-ICP-MS imaging Ag was found in negligible amounts on the membrane close to the injection point and at the channel edges. Greatest sample loss was found to be Ag nanoparticle dissolution in the sample.[150] Deposition of nanoparticles on the membrane mainly in the region of the focus point area was also reported by Ulrich *et al.*. During the focusing step nanoparticles experience a large force in the region of the focusing point downwards to the membrane.[162] Hagendorfer *et al.* reported a significant improvement in recoveries upon several sample runs due to saturation of the membrane with the target particles. In terms of Au nanoparticles the authors observed best recoveries with PVDF and RC membranes and reported better long-term stability for PVDF membranes.[151] The same effect was reported by Ulrich *et al.* stating that an improved recovery upon several injections is probably caused by a deposition of nanoparticles in the focus zone which later prevents further deposition of nanoparticles due to repulsive forces.[162] Using 10 kDa PES membrane Loeschner *et al.* reported for Ag nanoparticles no further increase in the recovery after three injections.[155]

Membrane functionalisation of RC and PES with polystyrenesulfonate to enhance recovery and reduce nanoparticle-membrane interaction has been described by Mudalige *et al.*.[163] For the example of Au nanoparticles recoveries of about 99% were obtained as well as reduced membrane fouling. The results are promising and could be an interesting approach for membrane optimisation.

A further aspect that needs to be considered are possible interactions of nanoparticles with further surfaces present within the fractionation device, e.g. channel material (specifically the accumulation wall in Sd-FFF) and capillaries. Theoretical as well as experimental considerations were carried out by Hansen and Giddings who showed that particle-wall interactions have a significant role in perturbing the ideal relationship between retention ratio and particle size.[164] Teflon surfaces are expected to be less critical than any metal or metal oxide containing materials. But also the surface functionalisation/coating of nanoparticles influences possible interactions and need to be taken into account.

In this context, Dou *et al.* investigated possible interactions of zeolite particles with the Sd-FFF channel. Although Sd-FFF is not comprising a membrane, the Sd-FFF channel surface material is also prone to interactions with the analyte particles. It was found that the addition of NaN_3 into the carrier leads to a fouling of the channel surface.[165] Koliadima investigated Polymethylmethacrylate (PMMA) and hydroxyapatite (HAP) particles via Sd-FFF comprising a Hastelloy C surface and discussed several parameters influencing the interactions of particles with the channel wall.[166]

5.1.2.5 Sample overload

In addition sample overload is critical in FFF as demonstrated by Martin *et al.* reporting a shift in retention time with increasing sample amount.[167] Depending on the sample composition they observed positive as well as negative deviations of retention. Under specific conditions high sample concentrations are not avoidable - for instance, in order to allow satisfactory detection of analytes with low response

factors or in case of fraction collection via preparative FFF. High local sample concentration near the accumulation wall induced by the applied perpendicular field can affect the migration behaviour of the target particles. Two opposite effects are discussed: (i) mean distance effect - at high analyte amount, particles are more repelled from the accumulation wall. As a consequence, particles are displaced towards fast flow streamlines near the channel centre which tends to increase the average migration velocity of the analytes. (ii) viscosity effect: as the suspension viscosity increases with increasing analyte concentration, the viscosity is larger near the accumulation wall where the analyte concentration is higher. Accordingly, the flow velocity profile is distorted leading to lower streamline velocity close to the accumulation wall and decreased average migration velocity of the analytes. Only in case of hard spheres the mean distance effect overcomes the viscosity effect, thus the average migration velocity is increased with increasing particle concentration. In case of analytes behaving like random coils, the viscosity effect dominates.[167] To avoid undesirable effects regarding sample overload, it has been recommended to compare retention time and recovery rates for sample masses that differ at least by a factor of five. If the obtained results show no increase or decrease of retention times with increasing injected mass, no significant effect of the sample load occurs within the mass range tested.[155] It has also been reported that overloading effects can be minimised with increasing addition of salt to the carrier solution as the repulsive forces between particles and the membrane are decreased and thus particles can move closer to the membrane.[168]

5.1.3 Nanoparticle sizing

In summary, it is recommended to combine (either on-, in-line, or off-line) different FFF-detectors to derive a fraction-related size information. Loeschner *et al.* provided a clear and comparative presentation of different sizing approaches: (i) size calibration by nanoparticle standards of a different material (see Table 1); (ii) conversion of retention times to hydrodynamic diameter based on AF4 theory (see also chapter 5.1); (iii) off-line TEM measurements upon fraction collection; (iv) on-line size determination by light scattering detectors (e.g. DLS, MALLS); (v) size determination based on AF4/ICP-MS data.[155] Qu *et al.* tested polystyrene nanoparticles as size-standards for Au nanoparticles which comprise different surface coatings. They found that the sizing error can be up to 33%, depending on the analysis conditions and the size of the analyte. In conclusion, they recommend employing appropriate standards having an identical surface coating as the analyte.[169] Sizing natural nanoparticles (NOM) by means of polystyrene sulfonate (PSS) was investigated by Neubauer *et al.* reporting that great caution is required and an error of up to 20% can be expected.[168] However, under well controlled and documented conditions this approach could represent a move away from the paradigm "same FFF-conditions (e.g. carrier composition, injection volume,…) for standards and sample" which is not always feasible.[168]

5.1.4 Applications

The following section provides an overview of the broad applicability of AF4/ICP-MS in nanoparticle analysis. It is out of the scope of this tutorial review to provide a comprehensive overview on all fields of applications of AF4/ICP-MS. The selection of application examples is based on a pre-selection upon a thorough literature search. About half of the papers are related to environmental applications, almost one third deal with nanoparticle standard applications for e.g. method development/fundamental aspects and the remaining focus on the field of consumer

products, food and medicine. The authors find some applications particularly interesting.

5.1.4.1 Consumer products

A widespread class of nanoparticles used in a number of applications including food contact materials, cosmetics, wall paints, textiles and biocide sprays are based on silver due to their antimicrobial properties as well as low cost. It is believed that these antimicrobial properties are mainly due to a release of Ag ions. However, several aspects, including possible *in vivo* transformation, accumulation and interaction with enzymes and biomolecules need to be clarified.[170] Furthermore, products that contain nanoparticles required to carry a "nano" declaration according to the EC definition.[24] Thus, reliable methods are needed with regard to product safety. Cascio *et al.* investigated six commercially available antimicrobial products for external use declared to contain nano- or colloidal silver. Next to AF4/UV-Vis/ICP-MS the authors employed TEM and batch light scattering for validation of the sizing results. TEM confirmed the presence of quasi-spherical nanoparticles in 5 products with a particle-size range between 11-14 nm, while one product comprised a more polydisperse distribution. AF4/UV-Vis/ICP-MS was conducted using a 10 kDa RC membrane and basified ultrapure water (pH 9.2) as carrier achieving AgNPs channel recoveries in the range of 70-96% (based on UV/Vis detector data). The mass content of Ag-nanoparticles within the products varied from about 5-25 mg L^{-1}, while it was even lower in one product (2% of total Ag).[170] Mass to number - size conversion was accomplished upon calibration with Ag nanoparticle size standards as well as additional data on the mass content, the density of bulk silver and the assumed spherical geometry.[170] According to the results more than 50% of the detected particles are present in the size range below 100 nm and based on the EC definition 5 out of 6 products contained nanomaterials. The results were in general agreement with the TEM observations.

A further widespread nanomaterial in consumer products is TiO_2, which is used in e.g. coffee creamers, toothpaste and sunscreens to improve their optical appearance or as UV filter. However, due to the broad application range, concerns have arisen that the toxicological risk has not been investigated sufficiently. Thus, for reliable toxicological assessment a physicochemical characterisation is essential for correlation of observed effects and particle properties. Nischwitz and Goenaga-Infante developed an extraction as well as AF4/ICP-MS method for the analysis of TiO_2 nanoparticles in sunscreens.[38] Four commercially available sunscreen samples with sun-protection factors (SPF) 10, 15, 30 and 50 were analysed. The authors employed hexane as first step for defatting of the sunscreen matrix, followed by suspension of the TiO_2 nanoparticles in water supported by sonication. Upon extraction in water, a small volume of hexane was added for nanoparticle disaggregation. Extraction efficiencies of 68-110% were obtained. The developed AF4/ICP-MS method employed deionised water as carrier and a 10 kDa RC membrane. Ti mass quantification was determined using a post-channel calibration approach relying on aqueous Ti standards. For size calibration NIST Au nanoparticles of 10, 30 and 60 nm were used and it was demonstrated that size determination based on the FFF theory produced similar results.[38] The results showed that the sunscreen with SPF 10 did not contain TiO_2 nanoparticles while the sunscreens with SPF 15, 30 and 50 revealed the presence of TiO_2 nanoparticles in a size-range from 16-39 nm.[38]

5.1.4.2 Food

The addition of nanomaterials in food has increased for example to enhance color or flavor, for preservation or to facilitate manufacturing processes. Heroult *et al.* developed a method for the analysis of SiO_2 nanoparticles in coffee creamer.[149] SiO_2 is often used as anticaking agent to maintain flow properties in powder products. The authors investigated commercially available coffee creamer and conducted spiking experiments with SiO_2 nanoparticles for quality control of the sample preparation as well as for AF4/ICP-MS method optimisation. Quantification of Si was conducted via post-channel ionic Si standard addition. Given the complexity of the matrix, an in-line multi-detector approach, comprising AF4/MALLS/ICP-MS was conducted. In addition, off-line TEM analysis with energy-dispersive X-ray detection (EDAX) was carried out upon fraction collection. The authors employed a RC membrane (10 kDa cut-off) and deionised water as carrier. Internal standard as well as diluted nitric acid was added post-channel before the carrier effluent was introduced into the ICP-MS. The combination of FFF/ICP-MS with TEM-EDAX allowed for quantification, size fractionation as well as size determination of SiO_2 nanoparticles.[149]

An interesting approach published recently by Hetzer *et al.* is based on the on-line coupling of AF4 with sp-ICP-MS (AF4-sp-ICP-MS) for the investigation of Ag nanoparticle release from food contact materials (food packaging systems).[171] Although Ag-containing food packaging offers significant benefits in terms of food freshness and shelf life of food products, the market growth is hindered due to public concerns regarding exposure to potentially released Ag. The authors investigated the migration of Ag nanoparticles from model films into food simulants. Using AF4-sp-ICP-MS enhanced sensitivity was achieved. As discussed in section 4.1.3 high ionic backgrounds hamper sensitive detection and low nanoparticle size detection limits in sp-ICP-MS. However, by AF4 the ionic silver fraction is removed from the sample via the cross flow through the membrane and thus only nanoparticles reach the ICP-MS for subsequent improved sp-ICP-MS detection. Furthermore, Ag nanoparticles are "pre-" fractionated by AF4 providing an additional information level especially with regard to larger particle fractions such as agglomerates or aggregates and matrix removal from size-fractions of interest is achieved. For AF4 fractionation ultrapure water was used as well as a 10 kDa RC membrane. Migration tests were performed with ultrapure water, 3% acetic acid and 10% ethanol as food simulant solutions for an incubation time of 2 h at 70 °C in the dark. The much lower background of sp-ICP-MS analysis on-line with AF4 enabled the detection of Ag nanoparticles in ultrapure water extracts with pristine sizes and also larger sizes, but no significant Ag nanoparticle migration in acetic acid extracts was observed.[171] AF4-sp-ICP-MS is beneficial in terms of nanoparticles with high ionic matrix load, large size distribution as well as complex matrices and will definitely gain in importance in the near future, also with regard to technical developments in the field of sp-ICP-MS.

5.1.4.3 Medicine

Metalloproteins account for approximately one third of all proteins found in nature and play crucial roles in respiration, storage/transport of proteins and signal transduction. Although metals are present at trace levels, imbalances in metal concentration or lack of essential metals are likely to alter the function and structure of proteins and enzymes resulting in potential disease onset.[172] Thus, the investigation of metalloproteins delivers an important insight into processes of the human body. Due to its gentle separation conditions and adaptable carrier composition AF4 is ideally suited for protein fractionation, while ICP-MS detection allows for sensitive metal-quantification.

One of the first applications of FlFFF/ICP-MS for the analysis of metal-containing proteins was highlighted and proven to be feasible by Siripinyanond and Barnes. They used a 3 kDa RC membrane and 0.1 M Tris-HNO$_3$ buffer at pH 8 as carrier for the investigation of several metal/heteroatom containing proteins: carbonic anhydrase, alcohol dehydrogenase (Zn, Cu), rabbit liver metallothionein (Cd, Cu), bovine ceruplasmin (Cu, Zn), bovine thyroglobulin (I).[173] Furthermore, the authors suggested employing ESI-MS/MS coupling for structural information.

Recently a complementary mass-spectrometric approach was presented by Kim *et al.*[172] investigating metalloproteins for comparison of plasma samples from patients with lung cancer and healthy controls. For AF4 separations a 10 kDa RC membrane was used with a carrier of 10 mM ammonium bicarbonate and ICP-MS detection provided relative quantities of 16 protein bound metals. Mn, Ni, Cu, Zn, Zr, I and Ba showed substantial changes in patients with lung cancer. Mn, Ni and Cu decreased in samples from lung cancer patients compared to healthy control samples, while Ba, Zn and I increased.[172] In addition protein fractions were collected from AF4 and quantified by nanoLC-ESI-MS/MS. Comparison of the resulting relative changes in serum proteins from patients with lung cancer with the changes of associated metals obtained from ICP-MS detection revealed common trends although the two analytical approaches were based on different detection principles. The method proposed by the authors is beneficial in terms of a rapid screening of metalloproteins related to diseases once metalloprotein biomarkers are well established.[172]

Metals are essential for maintaining functions within the human body, but can also show adverse effects for example when introduced unintentionally by implants such as hip replacements in case of metal-on-metal arthroplasty. Wear particles were generated in the surroundings of such hip replacements, which can lead to localised inflammation and loss of the hip due to necrosis of the tissue and bone. Loeschner *et al.* used AF4/ICP-MS as well as sp-ICP-MS to investigate released nanosized particles as well as the interaction of released dissolved metals with proteins.[174] Target elements included Cr, Co and Mo but also further elements. The proteins investigated were albumin (Alb) and transferrin (Tf). Serum and hip aspirate samples were analysed using a 10 kDa RC membrane with a carrier of either 0.05% SDS (pH 6) or 50 mM NH$_4$NO$_3$ (pH 7.2-7.4).[174] Hip aspirates required enzymatic digestion prior to AF4 separation. In serum samples AF4/ICP-MS suggests that Cr was associated with Tf and Co with Alb. In hip aspirate samples it seems that Cr was associated with Alb and Tf; Co was associated with Alb and two unidentified compounds. AF4/ICP-MS analysis suggested sizes of Cr-, Co-, and Mo-containing wear particles in a hip aspirate sample in the range of 40-150 nm (for Cr- and Co-containing nanoparticles confirmed by sp-ICP-MS). The results highlight the applicability of nanoanalytical techniques to study relevant medicinal questions.

5.1.4.4 Environment

Initial examples of environmental applications of FFF/ICP-MS are focusing on the investigation of various natural colloid size fractions and their interaction with metal ions. In this context, the migration of radionuclides associated to colloids is of special interest regarding safety aspects of disposal sites. Geckeis *et al.* developed a symmetric FlFFF/ICP-MS method to investigate the interaction of U, Th and rare earth elements (REE) with smectitic colloids as well as groundwater humic/fulvic colloids for samples taken near a nuclear waste repository (Gorleben, Lower Saxony, Germany).[175] A Tris-buffer carrier (5 mM, pH 9) including 0.01 wt.% Tween 20 (Polyethoxysorbitanlaurate) as detergent and a 5 kDa RC membrane were applied for Fl-FFF fractionation. A 5% nitric acid solution containing Rh as internal standard is

mixed with the FFF effluent post-channel via a T-piece prior to ICP-MS detection. Size calibration was conducted by polystyrene particles based on UV-Vis detection. The FFF/ICP-MS fractograms suggest the association of Th and REE mainly with inorganic colloids (>17 nm, containing also Fe and/or Al), while U and Ca appear to be distributed between larger colloids and the fulvic/humic acid fraction (<3 nm). The results demonstrate that even in environments with high humic/fulvic content (acting as potential metal-chelates) inorganic colloids play an important role as carrier for metal ions.[175] Colloid related transport of critical metals need to be taken into account with regard to safety aspects of e.g. permanent disposal sites.

Due to the presence of natural nanomaterials (e.g. colloids) comprising the same elemental constituents as ENPs, unambiguous tracing as well as quantification of nanoparticles in complex matrices is a big challenge. ENPs analysis in complex matrices becomes more and more important, especially considering that the rapid development and growth of nanotechnology increases the probability of releasing substantial amounts of ENPs into the (aquatic) environment. As mentioned previously, a promising strategy suggested by Gulson and Wong is based on the application of stable (metal) isotope tracing of ENPs.[54] Gigault and Hackley combined stable isotope tracing with AF4/ICP-MS. Isotopically labelled [109]Ag nanoparticles were spiked into an estuarine sediment matrix and enabled an unambiguous tracing based on their isotopic signature.[176] Furthermore, isotopic shift gives further indication of fate and transformation processes of Ag nanoparticles in the environment. However, the authors applied their approach for qualitative purposes only. Recently, Meermann *et al.* combined AF4/ICP-SFMS with stable isotope labelling of Fe-oxide nanoparticles ([57]Fe labelled) and "reverse" post-channel on-line isotope dilution for tracing and quantification of [57]Fe-oxide nanoparticles spiked in a sediment-slurry matrix filtrate. The combined approach allowed for an unambiguous tracing as well as sensitive mass-based quantification of the [57]Fe-oxide nanoparticles next to natural iron containing colloids.[60]

A smart application alienating the Fl-FFF/ICP-MS system as an "on-line filtration unit" for sample preconcentration and matrix removal was introduced by Al-Ammar *et al.*.[177] Thereby a commercial FFF system was modified enabling large volume injections (up to 50 mL). Upon injection the sample is mixed with an ethylene imine polymer forming strong metal-complexes with most elements while no/weak complexes with alkaline and alkaline earth elements. Due to their high molecular weight the metal-complexes remain in the FFF channel, while non-complexed matrix constituents (e.g. Na, Ca) were removed via the FFF membrane during the preconcentration step. Afterwards, the preconcentrated sample is directly introduced into the ICP-MS for analysis. Preconcentration factors of 50-1,400 fold could be achieved allowing for ultra-trace analysis in the presence of high matrix concentrations. The approach is promising for trace-metal analysis of samples containing high salt concentrations, such as biological, geological or environmental sample (e.g. sea-water samples).[178]

5.2 Hydrodynamic chromatography (HDC) on-line with ICP-MS

5.2.1 Theory

The separation principle of HDC was first described by Small in 1974 who observed that the rate of transport of colloidal particles through packed beds of spherical non-porous particles is dependent on the size of the colloids, the size of the packing material and the ionic composition of the aqueous carrier.[179] The mechanism involves hydrodynamic effects in the void volume of the packed bed as well as electrostatic and van der Waals interactions between the colloid and the packing material.[180]

Giddings attempted a simple theoretical model of HDC based on adaption of equations previously developed for FFF (compare chapter 5.1). However, he found severe complications for the calculation of the displacement velocity in HDC due to the packed bed compared to FFF where the channel is always free from obstructions.[181] A simple model describes the solute velocity v, that means the velocity of the analyte particles through the column, as sum of the carrier velocity v_0 and the core velocity v^* multiplied by the retention factor R_f (equation 11).[181]

$$v = v_0 + R_f \cdot v^* \qquad \text{(Eq. 11)}$$

The retention factor R_f, defined as the ratio of the rate of transport of the colloid through the "bed" and the rate of transport of the carrier, characterises the elution behaviour of the particles (by analogy with the retention ratio R in FFF - refer to chapter 5.1, equation 7). In FFF the retention ratio R is always below 1 due to the application of a separation force causing retention of the particles.[181] However, for HDC, Small reported that R_f is always larger than 1 for latex particles meaning that the colloids pass faster through the column than the carrier.[179] This is explained by the theory that the particles due to their size are excluded from the slow laminar flow close to the column wall and thus reaching higher average velocity than the carrier. This wall effect is increasing with increasing ratio of particle size to column diameter. For the example of polystyrene latex particles Small found increasing R_f with decreasing ionic strength of the aqueous sodium chloride carrier due to ionic double layers affecting the wall effect. For high ionic strength he found that R_f is increasing with increasing particle size according to the wall effect but then decreasing for very large particles leading even to deposition on the column bed.[179] Further theoretical approaches to calculation of R_f and correction equations for axial dispersion to obtained particle size distributions from the chromatographic elution profiles are reviewed and discussed by Husain *et al.*.[182]

Regarding method development and optimisation, the number of commercially available separation columns reported in various applications is rather small. Due to the low or lacking interaction of the analyte particles with the packed bed of the column, specific adaption of the column is typically not required. Suitable carriers contain low ionic strength buffers with addition of a surfactant, for example 5 mM sodium phosphate at pH 7.0 with 0.5 g L^{-1} sodium lauryl sulphate, to achieve reliable elution and recovery of particles from the column bed.[179] More specific conditions for HDC separations are discussed in the following summary of applications.

5.2.2 Applications
5.2.2.1 Consumer products
Sunscreen is a frequently analysed commercial product containing high concentration of nanoparticles in complex fatty matrix and thus is suitable and challenging to explore the capabilities of nano-analytical techniques. In case of HDC, Philippe *et al.* suspended sunscreen in a mixture of deionised water and Triton-X100 followed by filtration (1 µm syringe filter) and injection of the filtrate. Zn and Ti were monitored by on-line hyphenation with ICP-MS. The obtained chromatograms showed one Ti peak which was assigned to particle size range from about 150 to 1,000 nm and 80 to 900 nm, respectively for the two analysed samples. According to the authors the results are only qualitative due to incomplete suspension of particles and losses during filtration. Unfortunately, no attempt was made to determine and report the extraction efficiency of the chosen sample preparation which would allow a comparison of the HDC results to other studies using alternative techniques for

quantifying TiO_2 particles in sunscreen.[183] The size calibration based on Au-nanoparticles is only valid for spherical particles of similar surface properties and thus may result in significant bias for the sunscreen particles of unknown shape and surface. The study concludes that the HDC-UV/Vis-ICP-MS setup is very useful for analysis of TiO_2 particles in matrix with high content of organic compounds, but fails to compare the results and performance with previous studies (e.g. see chapter 5.1.4.1).

5.2.2.2 Food

Mattarozzi *et al.* reviewed HDC applications for nanoparticle characterisation in food and beverages and found few relevant studies.[37] Only one of them used on-line ICP-MS detection for studying the presence and risk of nano-silica.[184] With one exception all reviewed studies use the same column PL-PSDA-type1 and also the carrier of 10 mM SDS is used in nearly all these studies indicating that method optimisation is of minor relevance for HDC separation.[37] Reported main limitations are the lower resolution of particle size separation compared to FFF, moderate sensitivity for the lower size limit of 1 nm as required for analyses according to the EU definition of nanoparticles and the less ambiguous distinction between particles and dissolved low molecular weight species.[37] Advantageous are the higher separation speed compared to FFF and the fact that the non-particulate dissolved species/fractions are also potentially eluted and thus offer the chance for facilitated mass balance compared to Fl-FFF where this fraction is lost with the cross flow (see chapter 5.1). In particular for food the high load of large particulate matrix components (up to the low micrometer range) is likely to be critical regarding clogging of the HDC column, damaging the non-porous beads and shortening column life time. Pre-fractionation of the sample, for example by centrifugation is required.[185]

5.2.2.3 Medicine

Ag nanoparticles are frequently applied in medicine due to their anti-bacterial properties. Roman *et al.* applied HDC with a phosphate buffered SDS containing aqueous mobile phase for the size-separation of Ag fractions in blood plasma from burn patients.[186] The low resolution of HDC did not allow separation of the dissolved (ionic) silver from 20 nm particulate Ag. However, efficient combination of HDC with sp-ICP-MS using a novel deconvolution algorithm enabled individual evaluation of dissolved and particulate Ag. Thus, from a single injection it was possible to determine the amount of dissolved Ag as well as hydrodynamic diameter, number and mass concentration of the Ag nanoparticles. The analysis of blood samples from four patients revealed an average of 94% dissolved Ag (standard deviation 9%) and was thus not statistically different from the total Ag concentration.

5.2.2.4 Environment, natural colloids

HDC for environmental applications was reviewed by Leopold *et al.* highlighting the simple separation mechanism with the advantage of straightforward method development, improved column recoveries compared to FFF and rather stable separation being less affected by particle coating, particle density and temperature.[187] Combination of HDC with complementary detectors like MALLS, viscometer and differential refractometer allows in addition to determination of the size-related elemental composition by ICP-MS detailed size and shape characterisation. Such studies demonstrated for example that HDC is less structure disrupting for agglomerates than size exclusion chromatography (SEC). The majority of environmental applications is related to the characterisation of Au or Ag

nanoparticles in spiked or natural water samples.[187,188,189] Philippe *et al.* demonstrated in a detailed study that the HDC retention factor is hardly affected by particle properties, in particular surface coating, for the example of citrate and tannate stabilised Ag and Au particles as well as for silica particles provided that a carrier with sufficiently high ionic strength is used.[188] Tiede *et al.* reported suitability of HDC also for environmental samples with high matrix content like sludge supernatant for Ag nanoparticles. Main focus was on size calibration and size determination which achieved good agreement with TEM data considering the broad size distribution of Ag particles in the supernatant.[189] Complementary to this, Lewis *et al.* focussed on improved quantification of Ag and TiO_2 nanoparticles using a post-column injection approach for calibration with ionic standards as well as for determination of column recoveries by comparison of sample injection pre- and post-column. Nearly quantitative recovery (97.7%) was achieved. Results from quantification, particle size determination and calculation of particle number concentration were validated using a PVP-stabilised Ag nanoparticle reference sample previously characterised in other studies. Limits of detection were 10 μg L^{-1} for Ag and 2 μg L^{-1} for Ti which were considered as major drawback of the method preventing application for determination of ultra-low levels in environmental waters.[190]

5.2.2.5 Nanoparticle standards and model solutions

Combinations of HDC with additional separation or detection techniques were developed to overcome some of the mentioned limitations. In particular the combination of HDC on-line with sp-ICP-MS is a promising approach to significantly extend the performance by enabling the determination of number-based particle distributions in addition to particle size and particulate elemental mass fraction.[191] Using the model of NIST gold nanoparticles of 30 nm and 60 nm Pergantis *et al.* demonstrated the incomplete size resolution of these particles in a mixture, but compensated this by the second dimension obtained from sp-ICP-MS detection leading to separate signals in the resulting 2D contour plot. Regarding size determination the calibration with standard particles of known size is a feasible approach. However, due to the fast elution and low resolution even small variations in the elution time lead to rather high uncertainty of the particle size determination. Alternative calculation of the particle size from sp-ICP-MS data matched well with the certified size given by NIST. The developed setup provided quantitative recovery of nanoparticle number for bottled drinking water spiked with 30 nm gold particles at the 50 ng L^{-1} level.[191]

Detailed investigation of HDC for separation of the NIST citrate stabilised gold-nanoparticles was performed by Pitkänen *et al.* in comparison with size exclusion chromatography.[192] Their special focus was on quantitative elution of the particles from the column. For this purpose a specially adapted aqueous mobile phase containing 0.5 mmol L^{-1} Na_2HPO_4, 0.05% Triton X-100, 0.013% SDS and 0.05% formaldehyde (pH 7.5) was employed to minimise particle aggregation and adsorption on the column material (PS-1 HDC). Previously discussed low separation efficiency of HDC is illustrated by the inability to achieve baseline separation for 10 nm and 60 nm gold particles (resolution 0.62). Separation of a mixture of 10 nm, 30 nm and 60 nm as reported for FFF-ICP-MS[38] (see chapter 5.1.4.1) was not even attempted with HDC in this study. However, quantitative recovery of both the gold nanoparticles and ionic gold was achieved with recoveries ranging from 93% to 99% with exception of the 10 nm gold particles with 124% recovery. The latter was explained by potential aggregation and instability of the 10 nm gold particle suspension after multiple opening of the vial. This instability has been also observed

in the author's own work[38] and can be avoided by aliquoting the standard solution after first opening into several small vials for later use. Detailed comparison of HDC and FFF for Au nanoparticles in size range from 5 to 100 nm by Gray *et al.* clearly demonstrated the much better column recovery for HDC and the much better size resolution for Fl-FFF.[193]

5.3 High performance liquid chromatography (HPLC) on-line with ICP-MS
5.3.1 Theory
While separation in HDC is based on particle transport in the void volume of non-porous particles, size exclusion chromatography (SEC) is utilising distribution of the particles into the pore volume of porous particles and often achieves better resolution.[182] Also for SEC specific interaction of the particle surface with the stationary phase is usually not desired and often leads to poor column recoveries. These interactions are typically minimised by increasing the ionic strength of the mobile phase.[194] A detailed review on advantages as well as potential artifacts and limitations of SEC was published by Berek using the example of synthetic polymers [195] while Fekete *et al.* summarised theory and practical application of this technique for the analysis of protein aggregates.[196] SEC is usually operated in isocratic elution mode coupled to UV/Vis detection. However, many studies on biomedical elemental speciation analysis employed SEC on-line with ICP-MS for the characterisation of metallo-proteins and other metal-containing macromolecules.[197] Kostanski *et al.* reviewed direct calibration strategies based on polymer standards as well as molecular weight sensitive detection for SEC applications.[198]

Apart from SEC also reverse phase chromatography (RPC) has been employed for separation of (nano)particles. Retention and separation is based on interaction of the particle surface with the non-polar stationary phase which is in particular interesting for surface coated particles. This approach requires specific adaption to particle properties and matrix composition and is therefore less generally applicable compared to HDC or FFF separation/fractionation.

5.3.2 Applications
There is a broad variety of HPLC-ICP-MS applications in the biomedical field focussing on characterisation of high molecular weight metal binding proteins which is well-known and well-established. The following section aims at a brief summary of novel applications targeting on ENPs in relevant matrices.

5.3.2.1 Medicine
The size of high molecular weight proteins like bovine serum albumin (BSA, 69 kDa) equals the low nanometer range and thus the research fields of biomedical elemental speciation analysis and size-resolved elemental determination of nanoparticles are overlapping and can benefit from each other regarding analytical instrumentation and methods. For example BSA can be separated both by SEC and by FFF with on-line detection of bound metals by ICP-MS.[197,199] Recently, SEC was applied for the characterisation and quantification of virus-like particles demonstrating the broad application range. Detection was performed by UV/Vis, light scattering and nanoparticle tracking analysis and could significantly benefit from complementary on-line sensitive element-selective detection by ICP-MS.[200]

Sötebier *et al.* developed a RPC separation method on-line with ICP-MS for Ag nanoparticles and Au nanoparticles based on a Nucleosil C18 column with 7 µm particle size and 1,000 Å or 4,000 Å pore size. The mobile phase was optimised to achieve adequate resolution between particles and dissolved low molecular weight

species while stabilising both the metal nanoparticles and the dissolved metal ions to maintain the percentage ratio of particulate and dissolved metal originally present in the sample and to ensure good column recoveries. This resulted in a carrier at pH 6.7 containing 10 mmol L^{-1} sodium dodecyl sulfate (SDS), 10 mmol L^{-1} ammonium acetate and 500 µmol L^{-1} penicillamine. Resolution was sufficient for NIST 10 nm and 30 nm Au-particles but not for the 60 nm particles. Column recovery above 80% was achieved for the investigated Ag nanoparticles up to a size of 60 nm and decreased then rapidly. Calibration by post-column isotope dilution was employed for improved Ag quantification.[201] This method was applied by Soto-Alvaredo et $al.$ for the speciation/fractionation analysis of Au-nanoparticles and low molecular weight Au metabolites in tissue samples from Wistar rats after intraperitoneal injection of 10 nm Au nanoparticles. Critical aspect was the extraction of the Au species/fractions from the tissue without changing the particle properties, aggregation and dissolution state. Alkaline extraction of the tissue was found to be incompatible with RPC separation but enzymatic extraction with proteinase K showed good results of intact nanoparticles. Therefore, it was possible to study the gradual dissolution of the Au nanoparticles in liver tissue as a function of the incubation time. Complementary analysis of the tissue by transmission electron microscopy (TEM) confirmed the results obtained by RPC/ICP-MS.[202]

Zhou et $al.$ developed an SEC method on-line with ICP-MS for elemental mass size distribution i.e. in one run of 8 minutes the particle size, particle mass and composition is obtained. Complete elution of Au and Ag nanoparticles was achieved with a high ionic strength eluent (2% FL-70, 2 mM $Na_2S_2O_3$). Mathematical correction by Gaussian fitting was applied to the SEC elution profiles to correct for instrumental peak broadening and thus obtain the correct size distribution. The developed method was employed to study the transformation of Ag nanoparticles in bovine serum. Also in this case TEM was used for validation of the obtained size distribution.[203]

5.3.2.2 Environment, natural colloids

Separation of CdSe/ZnS quantum dots from dissolved Cd^{2+} and Zn^{2+} cations was achieved by adding ammonium lauryl sulfate for efficient elution of the quantum dots and ethylenediaminetetraacetate (EDTA) for complexation of the metal cations into the mobile phase in combination with a SEC column of smallest available pore size. The robustness of the method was demonstrated by analysis of spiked natural water and urban river water samples.[204]

5.3.2.3 Nanoparticle standards and model solutions

Pitkänen et $al.$ reviewed several studies on the application of SEC for the characterisation of Au nanoparticles, Ag nanoparticles and quantum dots. Adequate separation was achieved but adsorption on the stationary phase is often resulting in low column recoveries. However, column recovery was reported only in one of the reviewed studies. This is likely due to the predominant use of UV/Vis detection which does not provide species/fraction-independent response and quantification. Surprisingly, on-line detection by ICP-MS has rarely been used for SEC separation of ENPs and quantum dots.[205] The SEC separation of Au nanoparticles and nanorods according to their shape was highlighted in a review on various nanoseparation techniques by Kowalczyk et $al.$. In this case the combined use of an anionic and a non-ionic surfactant (SDS and polyoxyethylene-dodecanol) improved the resolution of Au particles of similar size but different shape obviously due to different effective surface charge of the particles with mixed surfactants attached to their surface.[206] Such studies are currently mostly performed with UV/Vis detection, but the mobile

phase is usually compatible with ICP-MS detection and thus the applications could benefit from improved selectivity in particular when transferring the methods to other nanoparticles with lower sensitivity in UV/Vis absorption compared to Au nanoparticles. Kowalczyk also identified a novel approach called "recycling SEC" a promising option to improve SEC performance for nanoparticle separations. By feeding the eluate from the column back into the column inlet for several column volumes the resolution was much better and it was even claimed that alkyl-thiol-stabilised gold nanoparticles with size difference of only 6 Å (0.6 nm) were separated.[206]

5.4 Capillary Electrophoresis (CE) on-line with ICP-MS

5.4.1 Theory

Capillary electrophoresis is operated in an electrolyte filled thin capillary. In most cases, fused silica capillaries are used, which have the disadvantage of a charged inner surface. However, the capillaries can be coated on the inner surface to minimise interaction of the analytes with the charged silica. In general, CE combines the advantage of FFF that there is no stationary phase which could lower the recovery due to adsorption and the advantage of column chromatography that the whole sample including the dissolved fraction is kept in the separation system and in theory can be detected in addition to the monitoring of the particulate fraction for complete mass balance. The separation force is achieved by an electric field along the capillary causing migration of the electrolyte and charged analytes. At voltages of 20-30 kV a non-laminar flow of the electrolyte (>pH 3) within the capillary (typically 30-100 µm internal diameter) is generated, comprising a flat-flow profile, which is referred to as electroosmotic flow (EOF). The flow rate of the EOF is depending on capillary coating and can thus be modified either to speed up the migration of the analytes to the detector end of the capillary or to flow in opposite direction and thus increase the effective capillary length and separation time for the analytes.[207,208] In any case effects of the EOF and the matrix composition of the sample in particular the ionic strength on analyte migration need to be well controlled and balanced to achieve robust separation at high resolution. The separation buffer needs to be adapted to the sample matrix. Several separation modes are possible, most common is capillary zone electrophoresis. Non-charged particles will not respond to the electric field as separation force and could only be transported with the EOF. Modification of the electrolyte in the capillary by addition of ionic surfactants provides a possibility to form charged micelles with the neutral particles in the core. This is an elegant way to adapt the migration behaviour of such particles. In case of strong interaction of the surfactant with the (nano-)particle surface this can be considered as capillary zone electrophoresis (CZE) of a new surface coated particle. In case of weaker interaction there is a kinetic equilibrium between the nanoparticle and the micelle, which is leading to another CE operation mode referred to as micellar electrokinetic chromatography (MEKC).[209] In any case the sample injection volume is very low (nL to sub-µL range) compared to chromatographic separation and FFF (µL to mL range). Advantages are the high separation efficiency and fast separation.[207,208] On the other hand, disadvantages are the relatively high limits of detection and low robustness to complex matrix of real samples.[209]

5.4.2 Coupling interfaces

In case of FFF, HDC, SEC and RPC the interface of the separation system to the ICP-MS is simple provided that the carrier/mobile phase composition is compatible with direct introduction into the ICP-MS and the flow rate is within the typical range of

commercial nebulisers (about 0.1 to 2 mL min^{-1}). Connection is achieved by a PEEK capillary from the channel or column outlet to the nebuliser inlet. Optionally a T-piece is inserted in this transfer line for introduction of an internal standard or for special calibration strategies[201,199] (see also chapter 5.1.1). However, the coupling of CE to ICP-MS is less straightforward due to the flow rates in the nL min^{-1} range and the need for closing the electric circuit. Several interfaces were published mostly using a sheath flow to supply enough liquid to the nebuliser to avoid suction effects within the CE capillary (in case of self-aspirating nebulisers) and to provide conductive contact to the counter electrode placed within the sheath liquid flow path.[207,210]

5.4.3 Applications
Up to now CE/ICP-MS hyphenation has been rarely applied for nanoparticle characterisation. Some applications for model solutions and in the biomedical field are summarised in the following section.

5.4.3.1 Medicine
Aleksenko *et al.* reviewed the characterisation of interactions between metal containing nanoparticles and biomolecules by CE. Such studies include incubation of nanoparticles with biomolecules in simulated physiological media (e.g. 10 mM phosphate buffer pH 7.4 containing 100 mM NaCl) as well as real biological medium, e.g. serum. However, the latter poses significant challenges due to the high load of proteins in serum which requires adequate dilution prior to injection. These investigations aim at monitoring both the free and the bound nanoparticles in the same CE run. The predominant criteria for selecting the most suitable background electrolyte are the stability of the nanoparticles and maintaining the interaction between nanoparticles and biomolecules, while improving separation efficiency is of secondary importance. Physiological buffers like HEPES are typically suitable electrolytes. High salt contents would be better matching the physiological conditions, but are typically avoided due to incompatibility with the detection system. In the past UV and laser induced fluorescence (LIF) detection were mostly used, but their sensitivity and selectivity are not sufficient for nanoparticle interaction at physiologically relevant concentrations. Therefore, ICP-MS detection is applied in a rising number of such studies due to the metal selectivity, high signal stability, broad linear detection range and excellent limits of detection down to $2 \cdot 10^{-15}$ mol for Au nanoparticles compared to $8 \cdot 10^{-5}$ mol with UV/Vis absorption at 530 nm (plasmon resonance). Promising applications are the monitoring of the biotransformation of CdSeS/ZnS-quantum dots in ten times diluted human serum and the time dependent speciation/fractionation analysis of Au nanoparticles in human serum showing conjugates with transferrin and albumin, although at a rather high Au level of 19 mg L^{-1}.[211]

5.4.3.2 Nanoparticle standards and model solutions
Franze *et al.* developed CE on-line with sp-ICP-MS (CE-sp-ICP-MS) for the separation and detection of Au nanoparticles. The CE buffer contained 70 mmol L^{-1} SDS and N-cyclohexyl-3-aminopropanesulfonic acid to achieve conditions for MEKC separation mode.[212] The developed method was applied for separation of the NIST Au nanoparticles of 10 nm, 30 nm and 60 nm (see Table 1). Baseline separation was not achieved, but in particular the separation of the 60 nm particles from the 30 nm particles was much better compared to RPC[201], SEC[192] and HDC[192]. Separation speed is higher (10 minutes runtime) than for HDC (15 to 30 minutes) and for SEC (30 to 60 minutes), but lower compared to RPC (7 minutes). CE-sp-ICP-MS detection

enabled 3-dimensional plots of migration time *versus* nanoparticle size and particle number concentration.[212]

Significant improvement of CE-sp-ICP-MS performance was achieved by Mozhayeva *et al.* by two innovations. First, the data acquisition system was modified to allow 5 µs time resolution and second the use of stacking allowed on-line pre-concentration of the analytes in the capillary and much larger injection volumes. The achieved dwell time of 5 µs is 20 to 2,000 times lower than using routine commercial ICP-MS data acquisition and was realised by continuously monitoring one isotope and modified detector readout procedure. The great advantage is that no nanoparticle escapes detection and that the probability of detecting more than one particle within the same dwell time is minimised. Slight disadvantage is that the multi-element capability is sacrificed. Hopefully, this prototype data acquisition system will inspire instrument manufactures to improve detector readout and signal processing for future commercial systems. The stacking approach enabled detection of approximately 14-fold to 28-fold (depending on particle size) higher number of nanoparticles. The separation time including stacking increased to 28 minutes.[213] This instrumental setup was applied for the analysis of mixtures of nanoparticles with same size but different surface coatings. For example, 40 nm citrate coated Ag nanoparticles could be separated from polyvinylpirrolidone coated Ag particles of same size using an electrolyte containing 60 mmol L^{-1} SDS and 10 mmol L^{-1} 3-(cyclohexylamino)-1-propanesulfonic acid (CAPS) at pH 10.[214] Previous studies on noble metal nanoparticles and quantum dots were reviewed by Lopez-Lorente *et al.* highlighting the advantages of CE such as fast analysis times, less surface effects causing issues with recovery and size-resolved separation as well as low consumption of sample and reagents. The electrophoretic mobility of nanoparticles is dependent on their surface charge, mass to charge ratio, hydrodynamic diameter and the orientation of non-symmetric particles within the electric field. Therefore, information about the surface coating, size and shape can be derived from electrophoretic separation behaviour provided that suitable standards with known properties are available for comparison.[209]

5.5 Laser ablation (LA) on-line with ICP-MS
5.5.1 Theory
In contrast to the previously discussed hyphenated techniques the main focus and capability of LA-ICP-MS is not on separation of (nano)particles in a mixed suspension according to their size but on the imaging of the spatial distribution of (particulate) elemental contents within the surface layer of a solid material. The sample is placed on a three-dimensionally (x,y and z direction) adjustable stage within a gas purged ablation cell. Via line scanning with a laser beam across the surface of the sample, material is ablated i.e. released as an aerosol due to the high energy of the laser. The generated aerosol is transported with a continuous gas stream out of the ablation cell through a transfer line into the plasma of an ICP-MS. A polymer tubing is typically suitable as transfer line. Helium is most frequently used as carrier gas but also argon is possible which simplifies the experimental setup because the nebuliser gas of the ICP-MS can be used.

Critical aspects are the spatial resolution, the ablation efficiency of the target particles from the surface, the transport efficiency from the ablation cell to the ICP-MS as well as the detection and quantification of the particulate elemental contents within the background of the surface matrix of the sample. Routine ablation of tissue samples is operating the laser with a spot size of about 60 µm and a speed of 70 µm per second. These conditions are sufficient for elemental imaging of, for example, brain

tissue showing various anatomical sub-structures. However, such spatial resolution is by far not suitable for imaging of individual nanoparticles embedded in tissues or similar matrices. Improvement was achieved by reducing the laser spot size and the scan speed, which is on the other hand affecting the amount of ablated material per time and thus signal intensity and stability. Current commercial instrumentation enables spot sizes in the low µm range with scan speeds equal to the spot size diameter per s.[215] The new Hyperion imaging system achieves laser spot size of 1 µm.[216] Examples will be discussed in the application section. Equally important is modifying the ablation cell for fast washout of the ablated material to minimise broadening of the signal. Van Malderen *et al.* reviewed various strategies for cell design including modelling of flow profiles to achieve minimum dispersion of the ablated material as compared by the peak width.[217] Optimised construction of miniaturised ablation cells combined with improved flow path and composition of the carrier gas (argon-helium mixtures) achieved signal peak width from a single laser pulse down to 10 ms while standard commercial ablation cells require wash-out times of up to 2-3 seconds.[217,218] However, it needs to be considered that such low volume cells have a very limited capacity for samples and are only suitable for scanning areas of a few square-millimeters. Introduction and scanning of calibration standards in the same work flow together with the sample without venting the ablation cell is most likely not possible any more with exception of the Hyperion system combining fast wash out with a cell dimension sufficient to host a standard microscopic slide.[216] Regarding the connection of the ablation cell to the ICP-MS a polymer tubing of minimum length and low inner diameter (few millimeter) is recommended to be installed in a straight way without sharp bends.[217]

Investigation of ablation efficiencies requires detailed insight into the ablation process. Depending on the sample matrix the high energy of the laser focussed on a small area causes heating far above the melting and boiling point. Consequently, the surface material is evaporated or decomposed including atomisation to a significant degree. However, the atomised material cannot be transported over longer distances as required to reach the ICP-MS. Several studies found that an aerosol with particle size in the nm range is generated which allows adequate transport efficiency from the ablation cell into the plasma.[219] It is important to note that small particles are enriched with elements of high vapour pressure while larger particles are depleted of these elements. For example, a typical bi-modal aerosol size distribution shows a fraction <100 nm enriched with Cu and Zn and a second fraction from 100 nm to 10 µm with depleted Cu and Zn.[220] Provided that the whole size range of generated particles is transported, atomised and ionised in the same way full quantification is possible. Therefore, it is vital that adequate matrix-matched calibration standards are available and ablated in the same way as the sample to minimise artefacts in aerosol generation and transport leading to a bias in the quantitative results. Hergenröder proposed a theoretical model to explain and understand the generation of a fine aerosol with size up to 100 nm during LA-ICP-MS using helium or argon atmosphere.[219] He concludes that the formation of large particles needs to be minimised to achieve optimum performance by short laser pulses with high energy using UV-laser or femtosecond laser. The use of helium as purge gas of the ablation cell also supports generation of smaller aerosol particles compared to argon. A detailed review on laser generated aerosols during LA-ICP-MS is available from the same author.[220] In case nanomaterials are present in the sample it is likely that their structure is significantly changed during the ablation and that the information on their size, shape and elemental composition is lost and there will be a summed elemental signal of the particles and the surrounding matrix obtained.

ICP-MS dwell times and scan speed need to be minimised to enable reliable multielement monitoring for the fast transient signals generated in the above discussed novel ablation cells. Most studies apply quadrupole or ICP-SFMS instruments, in some cases with modified (plug-in) detector readout for short dwell times. Instrument manufacturers improve dwell times of commercial quadrupole instruments. Alternatively, ICP-ToF-MS instruments provide fast data acquisition and readout, and recent instrumental developments enable new applications with LA hyphenation.[217,216]

5.5.2 Applications
5.5.2.1 Medicine

Rapid response laser ablation cells as discussed in section 5.5.1 and spot sizes in the order of 4 µm are suitable for imaging of single cells (diameter approximately 50 µm).[217] Several studies focussed on (quantitative) imaging of nanoparticles in cells. Drescher *et al.* monitored the sub-cellular distribution of 25 nm gold and 50 nm silver particles in individual fibroblast cells using a NWR 213 laser ablation system and a sector-field Element XR ICP-MS in low resolution mode. Based on a laser spot size of 4 µm and a scan speed of 5 µm per second a pixel width of 1 µm and height of 6 µm was obtained. According to the authors each peak in the recorded line scans represents either single metal nanoparticles or nanoparticle aggregates. Quantification was performed by calibration with dried nanoparticle droplets on nitrocellulose membrane. The achieved limit of detection was 20 particles of silver and 190 particles of gold.[221] Mahmoud *et al.* determined the distribution of surface functionalised gold nanorods in human skin using a home-built ablation cell with 0.5 seconds washout time, 10 µm spot size and 20 µm per second scan speed. Calibration was performed with spiked gelatine slices, which resulted in a limit of detection of 0.02 µg g^{-1} for gold using a quadrupole ICP-MS. Accumulation of Au in stratum corneum and in follicular hair was observed.[222] Niehoff *et al.* applied similar LA-ICP-MS conditions to monitor the distribution of palladium-tagged nanoparticles used for delivery of a photosensitiser to tumor cells. The porphyrin-based photosensitiser complexed Pd as the central ion and was embedded in poly(lactic-co-glycolic acid) nanoparticles with average diameter of 250 nm.[223]

Pozebon *et al.* reviewed recent applications of LA-ICP-MS for biological sample analysis including a section on nanoparticle imaging and quantification. They mainly highlighted the fact that the signal response at least in some reported applications was found to depend on nanoparticle size in particular when metal nanoparticles are distributed in organic tissue matrix. This requires suitable calibration strategies and further fundamental studies on the behaviour of nanoparticles during laser ablation to achieve reliable quantification.[224] Hsiao *et al.* studied the cellular uptake of TiO_2 and Ag nanoparticles by combined use of LA-ICP-MS with sp-ICP-MS and direct introduction conventional ICP-MS measurements. LA-ICP-MS with spot size of 4 µm could distinguish between nanoparticle adsorption to the outer surface of the cells and nanoparticles taken up into the cells. Sp-ICP-MS provided direct information on nanoparticle size and number and thus could reveal formation of particle agglomerates.[225]

Dual-Mode mass spectrometric imaging was recently proposed as novel approach to investigate the stability of surface-functionalised nanoparticles *in vivo*. In this case LA-ICP-MS provides spatially resolved imaging of the metal from the nanoparticle core in cryo-sections of organs while laser desorption ionisation (LDI) mass spectrometry imaging monitors the surface monolayer of the particle. Spot size of the laser for ablation (LA) was 50 µm while the step width for LDI was 25 µm. It was

reported that the monitored LDI ions are specific for the monolayer ligand while it is still attached to the nanoparticle core. Overlay of the images from both techniques allows calculating the percentage of intact surface-coated nanoparticles as demonstrated for Au nanoparticles in organ tissue slices from a mouse model.[226] The same LA-ICP-MS conditions were previously applied to study differences in the uptake and distribution of 2 nm gold nanoparticles with positive, neutral or anionic surface charge in mice organs.[227] Büchner et al. combined LA-ICP-MS imaging of Au nanoparticle exposed fibroblast cells with surface enhanced Raman scattering to correlate spatial distribution of the nanoparticles with their molecular nanoenvironment. Laser spot size of 1.5 µm was used for both techniques.[228]

In summary, both spatial resolution and sensitivity are not yet sufficient to monitor single nanoparticles in cells or tissues.

5.5.2.2 Environment, natural colloids

The characterisation of individual fly ash particles by elemental imaging with LA-ICP-MS using commercial laser ablation instrumentation with a standard fast-washout-cell shows the capabilities but also limitations. The particles with size range from 25 µm to 100 µm were sprayed as dry aerosol onto a glass surface and fixed with anti-static spray and subsequently with two layers of hair spray. First, a laser beam with spot size larger than the particle diameter was focussed with low energy onto the individual particles to generate a cross section of the particles by ablating approximately half of the particle. Subsequently the obtained cross section was line-scanned with laser spot sizes of 3 µm to 20 µm depending on particle size to obtain an elemental image. Using this setup a lateral resolution of 2 µm was reported, which was suitable for the analysed particles but not for imaging of the distribution of individual nano-objects unless they are located in larger than 2 µm distance. Validation of the LA-ICP-MS imaging was performed by prior non-destructive imaging of the same particles using scanning electron microscopy with energy dispersive X-ray analysis (SEM-EDX).[215]

Böhme et al. studied the uptake of various metal nanoparticles (Ag, Au, CuO, ZnO) and the dissolved ionic form of the same metals by zebrafish embryos, which are frequently used for eco-toxicological assessments. 40 µm thick slices of the frozen samples were analysed with 50 µm spot size. Although routine laser ablation conditions were employed it was possible to distinguish different distribution and uptake kinetics between various elements as well as between nanoparticles and ionic form of the same element. LA-ICP-MS did not provide information about the rate of dissolution of the nano-particles after uptake. Complementary analysis by SEM-EDX enabled detection of some particles but in case of Ag and ZnO, particles could hardly be distinguished from the background due to high dissolution rate of these nanoparticles.[229]

5.5.2.3 Nanoparticle standards and model solutions

Yan et al. combined thin layer chromatography with LA-ICP-MS for quantitative characterisation of surface stabilised gold nanoparticles. The use of 0.2 mol L^{-1} phosphate buffer at pH 6.8, 0.4% Triton X-114 and 10 mmol L^{-1} EDTA in the mobile phase enabled the separation of ionic gold as well as nanoparticles of 13 nm, 34 nm and 47 nm size. The separation efficiency was claimed to be similar to FFF and the surface coating had minor effect on the separation. Limits of detection were in the pg range. Recoveries for tap water, river water and lake water spiked with Au-nanoparticles were in a range from 74% to 105%.[230]

6 Aspects of quality assurance

The discussed hyphenated techniques with a broad variety of applications require thorough optimisation and operation to ensure reliable results at high quality with minimised risk of artifacts. Apart from laser ablation the sample needs to be injected as liquid suspension which needs to be obtained by extraction in case of solid samples (see chapter 2). During separation interaction with the inner surface of the separation unit (channel, column or capillary) and with the liquid carrier/mobile phase/buffer may cause changes on particles´ surface or agglomeration/aggregation state, possibly cause partial dissolution and may lead to incomplete recovery due to adsorption. The latter is in particular critical when being size-dependent and thus affecting the obtained particle size distribution. Therefore, mass balance is an important tool for quality control. After separation, the particles need to be structurally and chemically characterised for identification and accurately quantified. Selected quality control aspects of this analytical process will be briefly discussed in the following.

6.1 Criteria for method development and validation

The overall priority needs to be on preserving the particles´ properties of interest as originally present in the sample without significant change. For particle standards with known properties this can be checked by suitable on-line detection techniques after the fractionation/separation. However, in case of real samples with unknown composition, it is rather challenging to prove that this criterion was met. The use of an alternative particle fractionation/separation technique in parallel could provide reference data in case a suitable matrix-matched reference material is not available. Secondary priority is on particle size resolution and recovery of particles from the separation device. Usually, a compromise needs to be established because these parameters behave in opposing way. For example, in FFF the maximum recovery is achieved with zero cross flow i.e. no separation force. With increasing cross flow the separation is improved but also the interaction with the membrane is stronger and thus the recovery is often decreasing (see chapter 5.1.2.2). Careful adaption of the carrier composition usually helps to minimise this problem by modifying the surface charge of the particles and/ or of the separation device and thus counteracting ionic interactions. Mixed model solutions of standards of the target particles with or without sample matrix are suitable for optimisation and validation. However, in particular with partially non-polar sample matrices (e.g. extracts of fatty sunscreen) it is likely that the particle standards without matrix behave rather differently due to lacking surface stabilisation by matrix components. In case of LA-ICP-MS the main priorities for optimisation are the improvement of the spatial resolution and of the ablation as well as transport efficiencies for nanoparticles from the solid sample into the plasma (see chapter 5.5.2).

6.2 Mass balance

Establishing a mass balance accounting for the whole amount of the particles of interest injected onto the separation device is a basic criterion for method performance and validation. Using ICP-MS detection the mass balance is typically referring to the total mass of the element of interest in the sample independent of its speciation/fractionation that means including particulate and dissolved forms. In case of chromatographic techniques there are only two components to be accounted for: the eluting fraction and the fraction remaining bound to the stationary phase. In case of CE there might be a third fraction escaping detection due to migration towards the

other end of the capillary. Also in Fl-FFF there is a further fraction to be considered because the low molecular weight fraction is lost with the cross flow (see chapter 5.1). Usually the basic mass balance is established by calculating the ratio of the quantified eluting species/fractions and the total amount of the injected sample (see chapter 5.1.2.2). Typically, the obtained percentage ratio is below 100%. The missing fraction is then assigned to particles/species remaining in the fractionation/separation device or for example being lost with the cross flow in FFF. Of course the (strongly) retained fraction bears the risk of accidental elution leading to contamination of subsequently analysed samples and overestimation of their recovery. Attempts were made to quantify the i.e, dissolved fraction in FFF either by collection of the cross flow or by ultrafiltration of another aliquot of the sample using centrifugal filtration devices with the same or similar membrane as in the FFF separation channel.[231]

6.3 Identification / size calibration using multiple detectors

The complexity of (nano)particles´ properties including size, shape, elemental composition, aggregation state etc. requires efficient combined use of multiple detection techniques. While ICP-MS provides reliable data on the elemental composition of the particles, for example light scattering provides complementary on-line data on particle size. Further options are fraction collection for the liquid based fractionation/separation techniques and analysis for example by scanning electron microscopy or TEM. Critical aspect of the size resolved separation techniques is proper calibration of particle size to convert the elution time axis into particle size axis. To some extent this conversion can be done via a theoretical function assuming ideal separation conditions for example when using Fl-FFF with constant cross flow and no specific interaction of the particles with the membrane. More realistic is the calibration with well characterised particle size standards thus including effects of carrier composition and separation force on the particle transport (see chapter 5.1.3). A substantial source of uncertainty of this approach can be the difference in particle properties of the standards and of the target particles in the sample because in most cases sufficiently characterised standards of the target particles are not available. Therefore, additional size information for example from light scattering detection is highly recommended for reliable size determination and validation. Also in this case adequate modeling of the obtained data is required to derive a valid particle size.

6.4 Quantification by ICP-MS including suitable calibration

Elemental detection of the eluting nanoparticles is usually straightforward for liquid fractionation/separation techniques. Special interfaces are required for CE and LA hyphenation. However, accurate calibration and quantification is challenging. In rare cases well characterised standards of the target particles are available (see Table 1) in sufficient purity to be used for calibration. Such calibration standards can be analysed at varying dilution in the same way as the samples to establish a species/fraction-specific calibration for each target particle size. Provided that the standard particles are stable, i.e. neither significant dissolution nor aggregation/agglomeration is occurring, this approach includes all system parameters like exact volume of the injection loop, recovery from the separation system and ICP-MS response to particulate species and should therefore achieve most accurate results. To minimise matrix effects either standard addition of the samples or matrix matching of the standards can be performed. The utmost accuracy can be achieved by spiking the sample with isotopically enriched particles of same size, shape and composition.[58]

Due to the lack of adequate particulate standards, calibration is in most applications performed with conventional commercial stock solutions of dissolved elemental species. This species/fraction-unspecific calibration could be also done by injection of the standards via the separation system using the same method as for the samples in case the dissolved fraction is eluting or by using a modified method for example with zero cross flow in case of Fl-FFF. This approach has the advantage of using the same injection conditions (eliminating the exact injection volume) but requires that the dissolved standard passes with high recovery through the separation unit. The latter is for Fl-FFF not generally the case due to interaction with the membrane or residual sample components attached to the membrane. Alternatively, post-column or post-channel introduction of calibration standards is possible with the advantage of avoiding interaction with the separation unit and thus potential incomplete recovery of the standard and contamination of the separation unit. This approach can be easily combined with a constant introduction of an internal standard for drift correction of the ICP-MS signal and as indicator for any instability of the carrier flow rate eluting from the separation unit.[199] Short-circuiting the fractionation/separation device (channel, column) via a cross-piece is also possible. The principle drawback of using dissolved standards for calibration is the potentially different atomisation and ionisation efficiency for the dissolved elemental species in the standard compared to the particulate target species/fractions in the sample. Up to a particle size of approximately 600-800 nm there is typically no significant bias reported.[39] For more detailed discussion of this aspect compare chapters 3.1 as well as 4.1.4. Using the described calibration strategies the particulate elemental content is obtained in concentration units without providing information on the stoichiometry of the particles. With complementary information on the amount of the target element per particle, for example derived from size and shape information for purely metallic particles or from sp-ICP-MS data, it is possible to convert the mass-based elemental quantity into a number based quantity as demanded in legislation on nanoparticles.[24]

7. Conclusion and Future perspective

ICP-MS based techniques have evolved as one of the leading approaches in metal-based nanoparticle analysis. Especially hyphenated techniques such as FFF/ICP-MS and HDC/ICP-MS turned out as powerful tools. Hyphenated techniques allow for size-fractionation as well as mass- & number-based quantification of nanoparticles. However, crucial aspects are (i) (still) a lack of nanoparticle CRMs certified in size and number-based concentration allowing for appropriate size-calibration and, (ii) especially with regard to FFF missing standardised method-development guidelines.

A technique featuring size-number based quantification of nanoparticles is sp-ICP-MS. During recent years sp-ICP-MS evolved as a trend technique in metal-based nanoparticle analysis in such a way that also suppliers of ICP-MS systems integrated data assessment tools within their ICP-MS software making method development as well as data interpretation easier. Sp-ICP-ToF-MS for multi-element analysis as well as µs-dwell time options in current ICP-MS systems are driving forces for further single particle applications. However, although sp-ICP-MS is widely applied, still some crucial aspects need to be taken into account: (i) determination of nebulisation/transport efficiency is not straightforward; (ii) size detection limits are restricted by sensitivity of current ICP-MS systems down to about 10 nm; (iii) the theoretical considerations in sp-ICP-MS rely on spherical nanoparticles, thus further complementary techniques (e.g. TEM) are needed for sample characterisation. However, despite the aforementioned limitations, it is to be expected that sp-ICP-MS

(especially sp-ICP-ToF-MS) will take a leading role in metal-based nanoparticle analysis in the near future.

To benefit from "the best of both worlds" some research groups started to combine separation/fractionation systems on-line with sp-ICP-MS detection. This enables a higher size resolution of the separation/fractionation system and increases the information content obtained within one measurement. Ongoing technical developments (e.g. fast data processing) are a driving force of this trend and a rising number of publications are expectable in the near future.

Since a few years a reversal in application trends started: from "standard" nanoparticle suspensions with low matrix load to nanoparticle analysis in real matrices. However, still one of the key challenges in the field of nanoparticle analysis is sample preparation. From the authors´ opinion, this is mainly because of the fact that nanoparticles are not a distinct class of analytes (in contrast to e.g. elemental species). Thus, nanoparticles can comprise the same elemental composition, but e.g. different surface coatings and thus behave in a different manner. In addition they comprise a relatively large surface area, hence high reactivity, thus numerous possibilities for interaction with e.g. matrix constituents do exist. In this context, a further particular challenge is tracing as well as quantification of metal-based nanoparticles in the presence of high background concentrations. A promising approach is the application of stable isotopes and monitoring of isotope ratios. However, up to now only a few publications in this field of research exist. As the potential of stable isotope applications is large an ongoing research is expected.

During (about) the recent decade several technical developments in the field of ICP-MS were made, such as the release of tandem ICP-MS (triple quad), a new generation of ICP-ToF-MS as well as µs-dwell time ICP-MS systems. The potential for further developments is not exhausted yet. On the authors´ personal "wish list" are (i) instruments with increased ion transmission, enabling higher sensitivity, to push size-detection limits in sp-ICP-MS down to 1 nm; (ii) ICP-MS systems combining high mass resolution and the possibilities of reaction/collision cells to tackle all kinds of isobaric interferences; (iii) straightforward software interfaces allowing for an easier integration of fractionation/separation systems. Apart from technical developments a larger set of certified nanoparticle reference materials, certified in size as well as number-concentration, are a heart´s desire to meet requirements related to method validation.

Nanoparticle analysis is a highly complex research field and the "everything in one" technique does not exist. ICP-MS represents an important pillar in metal-based nanoparticle analysis, but a set of complementary analytical techniques is inevitable to obtain a "complete picture" (see also Figure 2). Especially, in case of e.g. dissolution of nanoparticles the situation is getting more complicated; due to the authors´ opinion merging fractionation and speciation tools is the only way to meet this situation. This is particularly required for environmental and medical samples with complex matrices.

As a summary, a decision flow-chart is provided in Figure 6 including all ICP-MS based techniques covered within this tutorial review. This decision flow-chart is intended to provide a hands-on overview for users. The available techniques are linked with the desired information required for the respective analytical requests: mass-based quantification, number-based quantification, number- & size-distribution. Furthermore, cross-references to chapters/sections within this tutorial review are provided. This enables a targeted selection of the most appropriate ICP-MS based technique for the current sample.
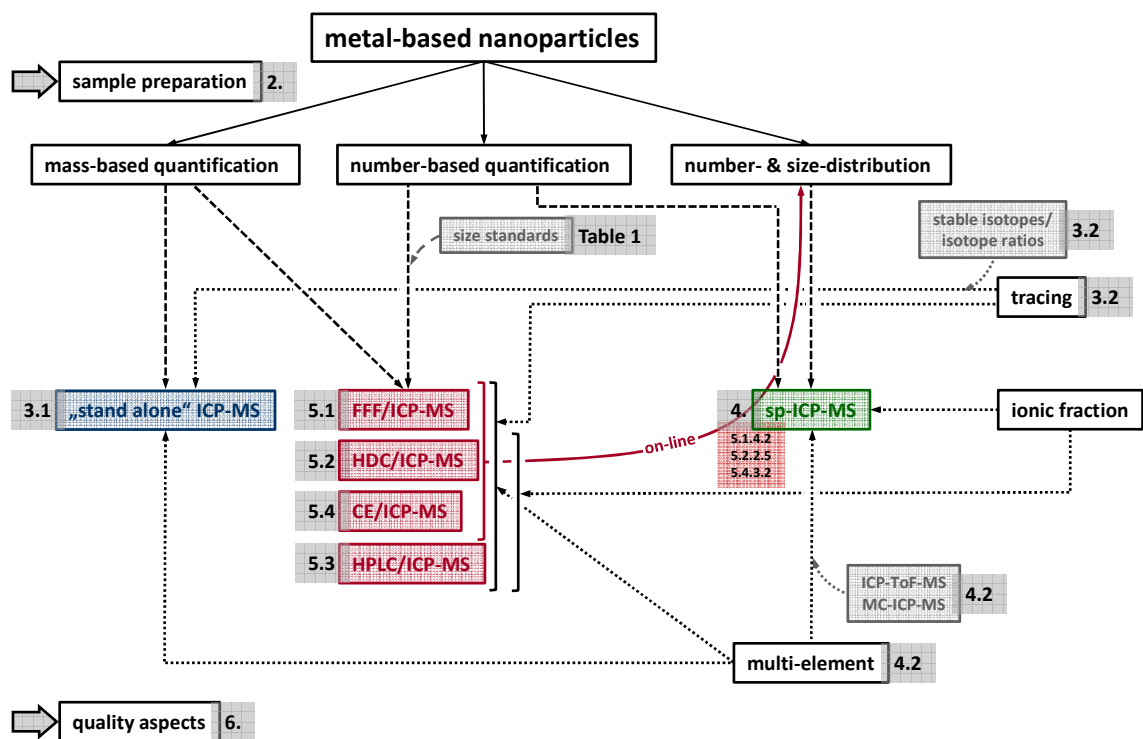
Figure 6: Decision flow-chart for ICP-MS based techniques for nanoparticle analysis depending on the information envisaged (mass-based quantification, number-based quantification, number- & size-distribution). Numbers indicate cross-references to the respective chapters of this tutorial review. Intersections of arrow tips indicate the need for additional tools (e.g. size standards, ICP-ToF-MS) to obtain the envisaged information. The red arrow indicates the possibility of on-line coupling of separation systems (FFF, HDC, CE) with sp-ICP-MS - cross-references to related applications highlighted within this tutorial review are given in the red box.

In conclusion, we are well on track in nanoparticle analysis and made a lot of significant progress, but the community is still far away from real world routine applicability - the good news is that there is still enough work for each scientist to do.

8. Acknowledgement

9. References

[1] A. J. Waldner and P. A. Freedman, *J. Anal. At. Spectrom.*, 1992, **7**, 571-575.

[2] F. Vanhaecke, L. Balcaen and D. Malinovsky, *J. Anal. At. Spectrom.*, 2009, **24**, 863-886.

[3] M. Costas-Rodriguez, J. Delanghe and F. Vanhaecke, *Trends Anal. Chem.*, 2016, **76**, 182-193.

[4] J. T. Rowan and R. S. Houk, *Appl. Spectrosc.*, 1989, **43**, 976-980.

[5] G. C. Eiden, C. J. Barinaga and D. W. Koppenaal, *J. Anal. At. Spectrom.*, 1996, **11**, 317-322.

[6] S. D. Tanner, V. I. Baranov and D. R. Bandura, *Spectrochim. Acta, Part B*, 2002, **57**, 1361-1452.

[7] L. Balcaen, E. Bolea-Ferndandez, M. Resano and F. Vanhaecke, *Anal. Chim. Acta*, 2015, **894**, 7-19.

[8] D. P. Myers and G. M. Hieftje, *Microchem. J.*, 1993, **48**, 259-277.

[9] F. Vanhaecke, L. Moens, R. Dams, L. Allen and S. Georgitis, *Anal. Chem.*, 1999, **71**, 3297-3303.

[10] D. M. Templeton, F. Ariese, R. Cornelis, L. G. Danielsson, H. Muntau, H. P. van Leeuwen and R. Lobinski, *Pure Appl. Chem.*, 2000, **72**, 1453-1470.

[11] J. J. Thompson and R. S. Houk, *Anal. Chem.*, 1986, **58**, 2541-2548.

[12] M. Montes-Bayón, K. DeNicola and J. A. Caruso, *J. Chromatogr. A*, 2003, **1000**, 457-476.

[13] O. Butler, H. Evans, A. Fisher, S. Hill, C. Harrington, A. Taylor, M. West and A. Ellis, *J. Anal. At. Spectrom.*, 2010, **25**, 1546-1566.

[14] S. Mounicou, J. Szpunar and R. Lobinski, *Chem. Soc. Rev.*, 2009, **38**, 1119-1138.

[15] J. S. Becker and N. Jakubowski, *Chem. Soc. Rev.*, 2009, **38**, 1969-1983.

[16] P. Rodríguez-González, J. M. Marchante-Gayón, J. I. García Alonso and A. Sanz-Medel, *Spectrochim. Acta, Part B*, 2005, **60**, 151-207.

[17] H. R. Hansen, R. Pickford, J. Thomas-Oates, M. Jaspars and J. Feldmann, *Angew. Chem. Int. Ed.*, 2004, **43**, 337-340.

[18] Z. A. Quinn, V. I. Baranov, S. D. Tanner and J. L. Wrana, *J. Anal. At. Spectrom.*, 2002, **17**, 892-896.

[19] D. R. Bandura, V. I. Baranov, O. I. Ornatsky, A. Antonov, R. Kinach, X. Lou, S. Pavlov, S. Vorobiev, J. E. Dick and S. D. Tanner, *Anal. Chem.*, 2009, **81**, 6813-6822.

[20] J. L. Neilsen, A. Abildtrup, J. Christensen, P. Watson, A. Cox and C. W. McLeod, *Spectrochim. Acta, Part B*, 1998, **53**, 339-345.

[21] L. Waentig, N. Jakubowski, S. Hardt, C. Scheler, P. H. Roos and M. W. Linscheid, *J. Anal. At. Spectrom.*, 2012, **27**, 1311-1320.

[22] J. S. Becker, A. Matusch and B. Wu, *Anal. Chim. Acta*, 2014, **835**, 1-18.

[23] C. Giesen, H. A. O. Wang, D. Schapiro, N. Zivanovic, A. Jacobs, B. Hattendorf, P. J. Schueffler, D. Grolimund, J. M. Buhmann, S. Brandt, Z. Varga, P. J. Wild, D. Guenther and B. Bodenmiller, *Nat. Methods*, 2014, **11**, 417-422.

[24] European Commision, Commission recommendation of 18 October 2011 on the definition of nanomaterial (2011/696/EU). *Off. J.*, 2011a, L 275, 38-40.

[25] F. Laborda, E. Bolea, G. Cepriá, M. T. Gómez, M. S. Jiménez, J. Pérez-Arantegui and J. R. Castillo, *Anal. Chim. Acta*, 2016, **904**, 10-32.

[26] EC, Communication from the Commission to the European Parliament, the Council and the European Economic and Social Committee, Second Regulation Review on Nanomaterials, COM(2012) 572, 2012.

[27] S. K. Brar and M. Verma, *Trends Anal. Chem.*, 2011, **30**, 4-17.

[28] D. R. Baer, D. J. Gaspar, P. Nachimuthu, S. D. Techane and D. G. Castner, *Anal. Bioanal. Chem.*, 2010, **396**, 983-1002.

[29] A. Lapresta-Fernandez, A. Salinas-Castillo, S. A. de la Llana, J. M. Costa-Fernandez, S. Dominguez-Meister, R. Cecchini, L. F. Capitan-Vallvey, M. C. Moreno-Bondi, M. P. Marco, J. C. Sanchez-Lopez and I. S. Anderson, *Crit. Rev. Solid State*, 2014, **39**, 423-458.

[30] R. Brydson, A. Brown, C. Hodges, P. Abellan and N. Hondow, *J. Microsc.*, 2015, **260**, 238-247.

[31] A. Dudkiewicz, K. Tiede, K. Loeschner, L. H. S. Jensen, E. Jensen, R. Wierzbicki, A. B. A. Boxall and K. Molhave, *Trends Anal. Chem.*, 2011, **30**, 28-43.

[32] P. L. Stewart, *WIREs Nanomed. Nanobiotechnol.*, 2017, **9**, 1-16.

[33] S. Wagner, S. Legros, K. Koeschner, J. Liu, J. Navratilova, R. Grombe, T. P. J. Linsinger, E. H. Larsen, F. von der Kammer and T. Hofmann, *J. Anal. At. Spectrom.*, 2015, **30**, 1286-1296.

[34] D. Bitounis, J. Pourchez, V. Forest, D. Boudard, M. Cottier and J. P. Klein, *Biomaterials*, 2016, **76**, 302-312.

[35] S. M. Rodrigues, T. Trindade, A. C. Duarte, E. Pereira, G.F. Koopmans and P.F.A.M. Römkens, *Trends Anal. Chem.*, 2016, **75**, 129-140.

[36] I. de la Calle, M. Menta and F. Seby, *Spectrochim. Acta Part B*, 2016, **125**, 66-96.

[37] M. Mattarozzi, M. Suman, C. Cascio, D. Calestani, S. Weigel, A. Undas and R. Peters, *Anal. Bioanal. Chem.*, 2017, **409**, 63-80.

[38] V. Nischwitz and H. Goenaga-Infante, *J. Anal. At. Spectrom.*, 2012, **27**, 1084-1092.

[39] S. Doubascoux, I. Le Hécho, M. Hassellöv, F. von der Kammer, M. Potin Gautier and G. Lespes, *J. Anal. At. Spectrom.*, 2010, **25**, 613-623.

[40] R. Sanchez, C. Sanchez, J. L. Todoli, C. P. Lienemann and J. M. Mermet, *J. Anal. At. Spectrom.*, 2014, **29**, 242-248.

[41] L. Halicz and I. B. Brenner, *Spectrochim. Acta*, 1987, **42B**, 207-217.

[42] D. A. Laird, R. H. Dowdy and R. C. Munter, *Soil Sci. Soc. Am. J.*, 1989, **55**, 274-278.

[43] L. Halicz, I. B. Brenner and O. Yoffe, *J. Anal. At. Spectrom.*, 1993, **8**, 475-480.

[44] P. Goodall, M. E. Foulkes and L. Ebdon, *Spectrochim. Acta*, Part B, 1993, **48**, 1563-1577.

[45] L. Ebdon, M. Foulkes and K. Sutton, *J. Anal. At. Spectrom.*, 1997, **12**, 213-229.

[46] R. Allabashi, W. Stach, A. de la Escosura-Muniz, L. Liste-Calleja and A. Merkoci, *J. Nanopart. Res.*, 2009, **11**, 2003-2011.

[47] S. Motellier, A. Guiot, S. Legros and B. Fiorentino, *J. Anal. At. Spectrom.*, 2014, **29**, 2294-2301.

[48] J. A. Hubbard and J. A. Zigmond, *Spectrochim Acta Part B*, 2016, **119**, 50-64.

[49] P. Krystek, A. Ulrich, C. C. Garcia, S. Manohar and R. Ritsema, *J. Anal. At. Spectrom.,* 2011, **26**, 1701-1721.

[50] E. Bolea-Fernandez, L. Balcaen, M. Resano and F. Vanhaecke, *J. Anal. At. Spectrom.*, 2017, **32**, 1660-1679.

[51] M. Menendez-Miranda, M. T. Fernandez-Arguelles, J. M. Costa-Fernandez, J. Ruiz Encinar and A. Sanz-Medel, *Anal. Chim. Acta*, 2014, **839**, 8-13.

Journal of Analytical Atomic Spectrometry Accepted Manuscript

[52] F. Larner and M. Rehkämper, *Environ. Sci. Technol.*, 2012, **46**, 4149-4158.

[53] Y. Yin, Z. Tan, L. Hu, S. Yu, J. Liu and G. Jiang, *Chem. Rev.,* 2017, **117**, 4462-4487.

[54] B. Gulson and H. Wong, *Environ. Health Perspect.*, 2006, **114**, 1486-1488.

[55] A. Laycock, B. Stolpe, I. Römer, A. Dybowska, E. Valsami-Jones, J. R. Lead and M. Rehkämper, *Environ. Sci.:Nano*, 2014, **1**, 271-283.

[56] B. Meermann, *Anal. Bioanal. Chem.*, 2015, **407**, 2665-2674.

[57] CIAAW - Commission on Isotope Abundances and Atomic Weights. Website: http://www.ciaaw.org/index.htm (website accessed: 22th November 2017).

[58] M. Pálmai, R. Szalay, D. Bartczak, Z. Varga, L. N. Nagy, C. Gollwitzer, M. Krumrey and H. Goenaga-Infante, *J. Colloid Interface Sci.*, 2015, **445**, 161-165.

[59] A. D. Dybowska, M.-N. Croteau, S. K. Misra, D. Berhanu, S. N. Luoma, P. Christian, P. O´Brian and E. Valsami-Jones, *Environ. Pollut.*, 2011, **159**, 266-273.

[60] B. Meermann, K. Wichmann, F. Lauer, F. Vanhaecke and T. A. Ternes, *J. Anal. At. Spectrom.*, 2016, **31**, 890-901.

[61] S. K. Misra, A. D. Dybowska, D. Berhanu, M. N. Croteau, S. N. Luoma, A. R. Boccaccini and E. Valsami-Jones, *Environ. Sci. Technol.*, 2012, **46**, 1216-1222.

[62] B. Gulson, M. McCall, M. Korsch, L. Gomez, P. Casey, Y. Oytam, A. Taylor, M. McCulloch, J. Trotter, L. Kinsley and G. Greenoak, *Toxicol. Sci.*, 2010, **118**, 140-149.

[63] B. Gulson, H. Wong, M. Korsch, L. Gomez, P. Casey, M. McCall, M. McCulloch, J. Trotter, J. Stauber and G. Greenoak, *Sci. Total Environ.*, 2012, **420**, 313-318.

[64] F. Larner, B. Gulson, M. McCall, Y. Oytam and M. Rehkämper, *J. Anal. At. Spectrom.*, 2014, **29**, 471-477.

[65] F. R. Khan, A. Laycock, A. D. Dybowska, F. Larner, B. D. Smith, P. S. Rainbow, S. N. Luoma, M. Rehkämper and E. Valsami-Jones, *Environ. Sci. Technol.*, 2013, **47**, 8532-8539.

[66] F. Larner, Y. Dogra, A. D. Dybowska, J. Fabrega, B. Stolpe, L. J. Bridgestock, R. Goodhead, D. J. Weiss, J. Moger, J. R. Lead, E. Valsami-Jones, C. R. Tyler, T. S. Galloway and M. Rehkämper, *Eviron. Sci. Technol.*, 2012, **46**, 12137-12145.

[67] A. Laycock, M. Diez-Ortiz, F. Larner, A. D. Dybowska, D. Spurgeon, E. Valsami-Jones, M. Rehkämper and C. Svendsen, *Environ. Sci. Technol.*, 2016, **50**, 412-419.

[68] A. Laycock, A. Romero-Freire, J. Najorka, C. Svendsen, C. A. M. van Gestel and M. Rehkämper, *Environ. Sci. Technol.*, 2017, **51**, 12756-12763.

[69] S. Yu, Y. Yin, X. Zhou, L. Dong and J. Liu, *Environ. Sci.: Nano*, 2016, **3**, 883-893.

[70] M.-N. Croteau, A. D. Dybowska, S. N. Luoma, S. K. Misra and E. Valsami-Jones, *Environ. Chem.*, 2014, **11**, 247-256.

[71] A. Bourgeault, C. Cousin, V. Geertsen, C. Cassier-Chauvat, F. Chauvat, O. Durupthy, C. Chanéac and O. Spalla, *Environ. Sci. Technol.*, 2015, **49**, 2451-2459.

[72] T. Ramskov, A. Thit, M.-N. Croteau and H. Selck, *Aquat Toxicol.*, 2015, **164**, 81-91.

[73] A. Thit, T. Ramskov, M.-N. Croteau and H. Selck, *Aquat Toxicol.*, 2016, **180**, 25-35.

[74] A. Laycock, B. Coles, K. Kreissig and M. Rehkämper, *J. Anal. At. Spectrom.*, 2016, **31**, 297-302.

[75] D. Lu, Q. Liu, T. Zhang, Y. Cai, Y. Yin and G. Jiang, *Nat. Nanotechnol.*, 2016, **11**, 682-686.

[76] A. R. Montoro Bustos and M. R. Winchester, *Anal. Bioanal. Chem.*, 2016, **408**, 5051-5052.

[77] C. Degueldre and P.-Y. Favarger, *Colloids Surf. A*, 2003, **217**, 137-142.

[78] C. Degueldre, P.-Y. Favarger and C. Bitea, *Anal. Chim. Acta*, 2004, **518**, 137-142.

[79] C. Degueldre, P.-Y. Favarger and S. Wold, *Anal. Chim. Acta*, 2006, **555**, 263-268.

[80] C. Degueldre, P.-Y. Favarger, R. Rossé and S. Wold, *Talanta*, 2006, **68**, 623-628.

[81] M. D. Montano, J. W. Olesik, A. G. Barber, K. Challis and J. F. Ranville, *Anal. Bioanal. Chem.*, 2016, **408**, 5053-5074.

[82] F. Laborda, E. Bolea and J. Jiménez-Lamana, *Anal. Chem.*, 2014, **86**, 2270-2278.

[83] F. Laborda, J. Jiménez-Lamana, E. Bolea and J. R. Castillo, *J. Anal. At. Spectrom.*, 2013, **28**, 1220-1232.

[84] https://ec.europa.eu/jrc/en/scientific-tool/jrc-nanomaterials-repository (assessed January 29th 2018).

[85] H. E. Pace, N. J. Rogers, C. Jarolimek, V. A. Coleman, C. P. Higgins and J. R. Ranville, *Anal. Chem.*, 2011, **83**, 9361-9369.

[86] D. D. Smith and R. F. Browner, *Anal. Chem.*, 1982, **54**, 533-537.

[87] W.-W. Lee and W.-T. Chan, *J. Anal. At. Spectrom.*, 2015, **30**, 1245-1254.

[88] L. Telgmann, C. D. Metcalfe and H. Hintelmann, *J. Anal. At. Spectrom.*, 2014, **29**, 1265-1272.

[89] C. A. Sötebier, D. J. Kutscher, L. Rottmann, N. Jakubowski, U. Panne and J. Bettmer, *J. Anal. At. Spectrom.*, 2016, **31**, 2045-2052.

[90] S. Gschwind, L. Flamigni, J. Koch, O. Borovinskaya, S. Groh, K. Niemax and D. Günther, *J. Anal. At. Spectrom.*, 2011, **26**, 1166-1174.

[91] S.-I. Miyashita, A. S. Groombridge, S.-I. Fujii, A. Minoda, A. Takatsu, A. Hioki, K. Chiba and K. Inagaki, *J. Anal. At. Spectrom.*, 2014, **29**, 1598-1606.

[92] H. Wang, M. Wang, B. Wang, L. Zheng, H. Chen. Z. Chai and W. Feng, *Anal. Bioanal. Chem.*, 2017, **409**, 1415-1423.

[93] S.-I. Miyashita, H. Mitsuhashi, S.-I. Fujii, A. Takatsu, K. Inagaki and T. Fujimoto, *Anal. Bioanal. Chem.*, 2017, **409**, 1531-1545.

[94] K. Kanaki and S. A. Pergantis, *J. Anal. At. Spectrom.*, 2016, **31**, 1041-1046.

[95] J. W. Olesik and P. J. Gray, *J. Anal. At. Spectrom.*, 2012, **27**, 1143-1155.

[96] A. Hineman and C. Stephan, *J. Anal. At. Spectrom.*, 2014, **29**, 1252-1257.

[97] J. Tuoriniemi, G. Cornelis and M. Hassellöv, *J. Anal. At. Spectrom.*, 2015, **30**, 1723-1729.

[98] I. Strenge and C. Engelhard, *J. Anal. At. Spectrom.*, 2016, **31**, 135-144.

[99] M. D. Montano, B. J. Majestic, A. K. Jämting, P. Westerhoff and J. F. Ranville, *Anal. Chem.*, 2016, **88**, 4733-4741.

[100] G. Cornelis and M. Hassellöv, *J. Anal. At. Spectrom.*, 2014, **29**, 134-144.

[101] M. Hadioui, C. Peyrot and K. J. Wilkinson, *Anal. Chem.*, 2014, **86**, 4668-4674.

[102] J. Tan, J. Liu, M. Li, H. El Hadri, V. A. Hackley and M. R. Zacharia, *Anal. Chem.*, 2016, **88**, 8548-8555.

[103] S. Lee, X. Bi, R. B. Reed, J. F. Ranville, P. Herckes and P. Westerhoff, *Environ. Sci. Technol.*, 2014, **48**, 10291-10300.

[104] K.-S. Ho, K.-O. Lui, K.-H. Lee and W.-T. Chan, *Spectrochim. Acta, Part B*, 2013, **89**, 30-39.

[105] K.-S. Ho, W.-W. Lee and W.-T. Chan, *J. Anal. At. Spectrom.*, 2015, **30**, 2066-2073.

[106] R. J. Peters, Z. Herrera-Rivera, A. Undas, M. van der Lee, H. Marvin, H. Bouwmeester and S. Weigel, *J. Anal. At. Spectrom.*, 2015, **30**, 1274-1285.

[107] Wageningen, The Netherlands, https://www.wur.nl/en/show/Single-Particle-Calculation-tool.htm (assessed December 22nd 2017).

[108] http://blogg.slu.se/Nanocount (assessed January 11th 2018).

[109] K. E. Murphy, J. Liu, A. R. Montoro Bustos, M. E. Johnson and M. R. Winchester, NIST Special Publication 1200-21, Version 1.0, December 2015.

[110] http://dx.doi.org/10.6028/NIST.SP.1200-21; further information/updates: https://www.nist.gov/mml/nano-measurement-protocols (assessed December 29th 2017).

[111] M. Yamanaka, K. Yamanaka, T. Itagaki, S. Wilbur and E. McCurdy, Application note, 5991-5891EN, 2015. https://www.agilent.com/cs/library/applications/5991-5891EN_AppNote_7900_ICP-MS_spNP.pdf (assessed December 30th 2017).

[112] D. Kutscher, J. D. Wills and S. McSheehy Ducos, Technical Note 43279-EN 0316S, 2016. https://tools.thermofisher.com/content/sfs/brochures/TN-43279-LC-MS-nanoparticles-spICP-MS-npQuant-Qtegra-TN43279-EN.pdf (assessed December 30th 2017).

[113] C. Stephan and K. Neubauer, White paper, 011649_01, 2014. https://www.perkinelmer.com/lab-solutions/resources/docs/Nanomaterials_SP-ICP-MS_Compendium(012982_01).pdf (assessed December 30th 2017).

[114] P. Shaw and A. Donard, *J. Anal. At. Spectrom.*, 2016, **31**, 1234-1242. http://www.cameca.com/company/news/2016/may/detection-and-characterisation-of-sub-10nm-au-nanoparticles-using-nu-attom-es (assessed December 30th 2017).

[115] O. Borovinskaya and M. Tanner, Multi-Element Detection of Single Nanoparticles with icp-TOF: Application Note, 2016. https://www.tofwerk.com/application/nanoparticles/ (assessed December 30th 2017).

[116] S. Yongyang, W. Wei, L. Zhiming, D. Hu, Z. Guoqing, X. Jiang and R. Xiangjun, *J. Anal. At. Spectrom.*, 2015, **30**, 1184-1190.

[117] O. Borovinskaya, B. Hattendorf, M. Tanner, S. Gschwind and D. Günther, *J. Anal. At. Spectrom.*, 2013, **28**, 226-233.

[118] A. Praetorius, A. Gundlach-Graham, E. Goldberg, W. Fabienke, J. Navratilova, A. Gondikas, R. Kaegi, D. Günther, T. Hofmann and F. von der Kammer, *Environ. Sci.: Nano*, 2017, **4**, 307-314.

[119] L. Hendriks, A. Gundlach-Graham, B. Hattendorf and D. Günther, *J. Anal. At. Spectrom.*, 2017, **32**, 548-561.

[120] I. de la Calle, M. Menta, M. Klein and F. Séby, *Talanta*, 2017, **171**, 291-306.

[121] Y. Dan, H. Shi, C. Stephan and X. Liang, *Microchem. J.*, 2015, **122**, 119-126.

[122] A. Mackevica, M. E. Olsson and S. F. Hansen, *J. Hazard. Mater.*, 2017, **322**, 270-275.

[123] B. Kollander, F. Widemo, E. Agren, E. H. Larsen and K. Loeschner, *Anal. Bioanal. Chem.*, 2017, **409**, 1877-1885.

[124] E. Verleysen, E. van Doren, N. Waegeneers, P.-J. de Temmerman, M. Abi Daoud Francisco and J. Mast, *J. Agric. Food Chem.*, 2015, **63**, 3570-3578.

[125] A. Mackevica, M. E. Olsson and S. F. Hansen, *J. Nanopart. Res.*, 2016, 18:5.

[126] S. V. Jenkins, H. Qu, T. Mudalige, T. M. Ingle, R. Wang, F. Wang, P. C. Howard, J. Chen and Y. Zhang, *Biomaterials*, 2015, **51**, 226-237.

Journal of Analytical Atomic Spectrometry Accepted Manuscript

[127] S. Zhang, G. Han, Z. Xing, S. Zhang and X. Zhang, *Anal. Chem.*, 2014, **86**, 3541-3547.

[128] K. Folens, T. van Acker, E. Bolea-Fernandez, G. Cornelis, F. Vanhaecke, G. Du Laing and S. Rauch, *Sci. Total Environ.*, 2018, **615**, 849-856.

[129] J. Jiménez-Lamana, J. Wojcieszek, M. Jakubiak, M. Asztemborska and J. Szpunar, *J. Anal. At. Spectrom.*, 2016, **31**, 2321-2329.

[130] M. A. Gomez-Gonzalez, E. Bolea, P. A. O´Day, J. Garcia-Guinea, F. Garrido and F. Laborda, *Anal. Bioanal. Chem.*, 2016, **408**, 5125-5135.

[131] J. C. Giddings, *Sep. Sci.*, 1966, **1**, 123-125.

[132] G. Yohannes, M. Jussila, K. Hartonen and M.-L. Riekkola, *J. Chromatogr. A*, 2011, **1218**, 4104-4116.

[133] P. S. Fedotov, M. S. Ermolin, E. Y. Savonina, V. A. Kronrod and B. Y. Spivakov, *J. Anal. Chem.*, 2010, **65**, 1209-1214.

[134] B. Y. Spivakov, T. A. Maryutina, P. S. Fedotov, S. N. Ignatova, O. N. Katasonova, J. Dahmen and R. Wennrich, *J. Anal. Chem.*, 2002, **57**, 928-934.

[135] O. N. Katasonova, P. S. Fedotov, B. Y. Spivakov and M. N. Filippov, *J. Anal. Chem.*, 2003, **58**, 473-477.

[136] P. S. Fedotov, M. S. Ermolin and O. N. Katasonova, *J. Chromatogr. A*, 2015, **1381**, 202-209.

[137] M. Schimpf, K. Caldwell and J. C. Giddings, Field-flow fractionation handbook, 2000. Wiley-Interscience, New York.

[138] J. A. Jönsson and A. Carlshaf, *Anal. Chem.*, 1989, **61**, 11-18.

[139] A. Zattoni, S. Casolari, D. C. Rambaldi and P. Reschiglian, *Curr. Anal. Chem.*, 2007, **3**, 310-323.

[140] H. Dou, E. C. Chang Jung and S. Lee, *J. Chromatogr. A*, 2015, **1393**, 115-121.

[141] R. Beckett, *At. Spectrosc.*, 1991, **12**, 228-232.

[142] D. M. Murphy, J. R. Garbarino, H. E. Taylor, B. T. Hart and R. Beckett, *J. Chromatogr. A*, 1993, **642**, 459-467.

[143] M. Hassellöv, B. Lyvén, C. Haraldsson and W. Sirinawin, *Anal. Chem.*, 1999, **71**, 3497-3502.

[144] E. Bolea, J. Jimenez-Lamana, F. Laborda and J. R. Castillo, *Anal. Bioanal. Chem.*, 2011, **401**, 2723-2732.

[145] M. Bouby, H. Geckeis and F. W. Geyer, *Anal. Bioanal. Chem.*, 2008, **392**, 1447-1457.

[146] S. Dubascoux, I. Le Hecho, M. P. Gautier and G. Lespes, *Talanta*, 2008, **77**, 60-65.

[147] B. Meermann, A.-L. Fabricius, L. Duester, F. Vanhaecke and T. A. Ternes, *J. Anal. At. Spectrom.*, 2014, **29**, 287-296.

[148] T. Lang, K. A. Eslahian and M. Maskos, *Macromol. Chem. Phys.*, 2012, **213**, 2353-2361.

[149] J. Heroult, V. Nischwitz, D. Bartczak and H. Goenaga-Infante, *Anal. Bioanal. Chem.*, 2014, **406**, 3919-3927.

[150] C. A. Sötebier, F. S. Bierkandt, S. Rades, N. Jakubowski, U. Panne and S. M. Weidner, *J. Anal. At. Spectrom.*, 2015, **30**, 2214-2222.

[151] H. Hagendorfer, R. Kaegi, J. Traber, S. F. L. Mertens, R. Scherrers, C. Ludwig and A. Ulrich, *Anal. Chim. Acta*, 2011, **706**, 367-378.

[152] S. Podzimek, Light Scattering, Size Exclusion Chromatography and Asymmetric Flow Field Flow Fractionation, 2011, Wiley, Hoboken, New Jersey.

[153] S. Dubascoux, F. von der Kammer, I. Le Hécho, M. Potin Gautier and G. Lespes, *J. Chromatogr. A*, 2008, **1206**, 160-165.

[154] T. J. Cho and V. A. Hackley, *Anal. Bioanal. Chem.*, 2010, **398**, 2003-2018.

[155] K. Loeschner, J. Navratilova, S. Legros, S. Wagner, R. Grombe, J. Snell, F. von der Kammer and E. H. Larsen, *J. Chromatogr. A*, 2013, **1272**, 116-125.

[156] T. K. Mudalige, H. Qu and S. W. Linder, *Langmuir*, 2017, **33**, 1442-1450.

[157] L. Sanchez-Garcia, E. Bolea, F. Laborda, C. Cubel, P. Ferrer, D. Gianolio, I. da Silva and J. R. Castillo, *J. Chromatogr. A*, 2016, **1438**, 205-215.

[158] S. Schachermeyer, J. Ashby, M. J. Kwon and W. Zhong, *J. Chromatogr. A*, 2012, **1264**, 72-79.

[159] Q. Du and M. E. Schimpf, *Anal. Chem.*, 2002, **74**, 2478-2485.

[160] B. Meisterjahn, S. Wagner, F. von der Kammer, D. Hennecke and T. Hofmann, *J. Chromatogr. A*, 2016, **1440**, 150-159.

[161] N. Bendixen, S. Losert, C. Adlhart, M. Lattuada and A. Ulrich, *J. Chromatogr. A*, 2014, **1334**, 92-100.

[162] A. Ulrich, S. Losert, N. Bendixen, A. Al-Kattan, H. Hagendorfer, B. Nowack, C. Adlhart, J. Ebert, M. Lattuada and K. Hungerbühler, *J. Anal. At. Spectrom.*, 2012, **27**, 1120-1130.

[163] T. K. Mudalige, H. Qu, G. Sánchez-Pomales, P. N. Sisco and S. W. Linder, *Anal. Chem.*, 2015, **87**, 1764-1772.

[164] M. E. Hansen and J. C. Giddings, *Anal. Chem.*, 1989, **61**, 811-819.

[165] H. Dou, G. Bai, L. Ding, Y. Li and S. Lee, *J. Chromatogr. A*, 2015, **1422**, 253-259.

[166] A. Koliadima, *J. Liq. Chrom. & Rel. Technol.*, 1999, **22**, 2763-2777.

[167] M. Martin and F. Feuillebois, *J. Sep. Sci.*, 2003, **26**, 471-479.

[168] E. Neubauer, F. von der Kammer and T. Hofmann, *J. Chromatogr. A*, 2011, **1218**, 6763-6773.

[169] H. Qu, I. R. Quevedo, S. W. Linder, A. Fong and T. K. Mudalige, *J. Nanopart. Res.*, 2016, **18**, 292.

[170] C. Cascio, O. Geiss, F. Franchini, I. Ojea-Jimenez, F. Rossi, D. Gilliland and L. Calzolai, *J. Anal. At. Spectrom.*, 2015, **30**, 1255-1265.

[171] B. Hetzer, A. Burcza, V. Gräf, E. Walz and R. Greiner, *Food Control*, 2017, **80**, 113-124.

[172] J. Y. Kim, H. B. Lim and M. H. Moon, *Anal. Chem.*, 2016, **88**, 10198-10205.

[173] A. Siripinyanond and R. M. Barnes, *J. Anal. At. Spectrom.*, 1999, **14**, 1527-1531.

[174] K. Loeschner, C. F. Harrington, J. L. Kearney, D. J. Langton and E. H. Larsen, *Anal. Bioanal. Chem.*, 2015, **407**, 4541-4554.

[175] H. Geckeis, Th. Ngo Manh, M. Bouby and J. I. Kim, *Colloids and Surfaces A: Physicochem. Eng. Aspects*, 2003, **217**, 101-108.

[176] J. Gigault and V. A. Hackley, *Anal. Chim. Acta*, 2013, **763**, 57-66.

[177] A. Al-Ammar, A. Siripinyanond and R. M. Barnes, *Spectrochim. Acta, Part B*, 2001, **56**, 1951-1962.

[178] S. Sangsawong, J. Shiowatana and A. Siripinyanond, *J. Anal. At. Spectrom.*, 2006, **21**, 1336-1339.

[179] H. Small, *J. Colloid Interface Sci.*, 1974, **48**, 147-161.

[180] H. Small, F.L. Saunders and J. Solc, *Adv. Colloid Interface Sci.*, 1976, **6**, 237-266.

[181] J. C. Giddings, *Sep. Sci. Technol.*, 1978, **13**, 241-254.

[182] A. Husain, A. E. Hamielec and J. Vlachopoulos, *J. Liquid Chrom.*, 1981, **4**, 295-320.

<div style="text-align: right; writing-mode: vertical">Journal of Analytical Atomic Spectrometry Accepted Manuscript</div>

[183] A. Philippe and G. E. Schaumann, *PLOS one*, 2014, **9**, DOI: 10.1371/journal.pone.0090559.

[184] S. Dekkers, P. Krystek, R. J. Peters, D. P. Lankveld, B. G. Bokkers, P. H. van Hoeven-Arentzen, H. Bouwmeester and A. G. Oomen, *Nanotoxicology*, 2011, **5**, 393-405.

[185] Y. J. Chang, Y. H. Shih, C. H. Su and H. C. Ho, *J. Hazard. Mat.*, 2017, **322**, 95-104.

[186] M. Roman, C. Rigo, H. Castillo-Michel, I. Munivrana, V. Vindigni, I. Micetic, F. Benetti, L. Manodori and W. R. L. Cairns, *Anal. Bioanal. Chem.*, 2016, **408**, 5109-5124.

[187] K. Leopold, A. Philippe, K. Wörle and G. E. Schaumann, *Trends Anal. Chem.*, 2016, **84**, 107-120.

[188] A. Philippe, M. Gangloff, D. Rakcheev and G. E. Schaumann, *Anal. Methods*, 2014, **6**, 8722-8728.

[189] K. Tiede, A. B. A. Boxall, X. Wang, D. Gore, D. Tiede, M. Baxter, H. David, S. P. Tear and J. Lewis, *J. Anal. At. Spectrom.*, 2010, **25**, 1149-1154.

[190] D. J. Lewis, *Analyst*, 2015, **140**, 1624-1628.

[191] S. A. Pergantis, T. L. Jones-Lepp and E. M. Heithmar, *Anal. Chem.*, 2012, **84**, 6454-6462.

[192] L. Pitkänen, A. R. Montoro Bustos, K. E. Murphy, M. R. Winchester and A. M. Striegel, *J. Chromatogr. A*, 2017, **1511**, 59-67.

[193] E. P. Gray, T. A. Bruton, C. P. Higgins, R. U. Halden, P. Westerhoff and J. F. Ranville, *J. Anal. At. Spectrom.*, 2012, **27**, 1532-1539.

[194] T. Arakawa, D. Ejima, T. Li and J. S. Philo, *J. Pharm. Sci.*, 2010, **99**, 1674-1692.

[195] D. Berek, *J. Sep. Sci.*, 2010, **33**, 315-335.

[196] S. Fekete, A. Beck, J. L. Veuthey and D. Guillarme, *J. Pharm. Biomed. Anal.*, 2014, **101**, 161-173.

[197] V. Nischwitz, A. Berthele and B. Michalke, *Anal. Chim. Acta*, 2008, **627**, 258-269.

[198] L. K. Kostanski, D. M. Keller and A. E. Hamielec, *J. Biochem. Biophys. Methods*, 2004, **58**, 159-186.

[199] V. Nischwitz, N. Gottselig, A. Missong, T. Meyn and E. Klumpp, *J. Anal. At. Spectrom.*, 2016, **31**, 1858-1868.

[200] P. Steppert, D. Burgstaller, M. Klausberger, A. Tover, E. Berger and A. Jungbauer, *J. Chromatogr. A*, 2017, **1487**, 89-99.

[201] C. A. Sötebier, S. M. Weidner, N. Jakubowski, U. Panne and J. Bettmer, *J. Chromatogr. A*, 2016, **1468**, 102-108.

[202] J. Soto-Alvaredo, C. Lopez-Chaves, C. Sanchez-Gonzalez, M. Montes-Bayon, J. Llopis and J. Bettmer, *J. Anal. At. Spectrom.*, 2017, **32**, 193-199.

[203] X. Zhou, J. Liu and G. Jiang, *Environ. Sci. Technol.*, 2017, **51**, 3892-3901.

[204] P. Paydary and P. Larese-Casanova, *Intern. J. Environ. Anal. Chem.*, 2015, **95**, 1450-1470.

[205] L. Pitkänen and A. M. Striegel, *Trends Anal. Chem.*, 2016, **80**, 311-320.

[206] B. Kowalczyk, I. Lagzi and B. A. Grzybowski, *Curr. Opin. Colloid Interface Sci.*, 2011, **16**, 135-148.

[207] B. Michalke, *Electrophoresis*, 2005, **26**, 1584-1597.

[208] A. R. Timerbaev, *Trends Anal. Chem.*, 2009, **28**, 416-425.

[209] A. I. Lopez-Lorente, B. M. Simonet and M. Valcarcel, *Trends Anal. Chem.*, 2011, **30**, 58-71.

[210] G. Alvarez-Llamas, M. del Rosario Fernandez de la Campa and A. Sanz-Medel, *Trends Anal. Chem.*, 2005, **24**, 28-36.

[211] S. S. Aleksenko, M. Matczuk and A.R. Timerbaev, *Electrophoresis*, 2017, **38**, 1661-1668.

[212] B. Franze, I. Strenge and C. Engelhard, *J. Anal. At. Spectrom.*, 2017, **32**, 1481-1489.

[213] D. Mozhayeva, I. Strenge and C. Engelhard, *Anal. Chem.*, 2017, **89**, 7152-7159.

[214] D. Mozhayeva and C. Engelhard, *Anal. Chem.*, 2017, **89**, 9767-9774.

[215] G. Bauer, B. Achleitner, M. Bonta, G. Friedbacher and A. Limbeck, *RSC Adv.*, 2017, **7**, 20510-20519.

[216] R.N. Straus, A. Carew, D. Sandkuijl, T. Closson, V. I. Baranov and A. Loboda, *J. Anal. At. Spectrom.*, 2017, **32**, 1044-1051.

[217] S. J. M. Van Malderen, A. J. Managh, B. L. Sharp and F. Vanhaecke, *J. Anal. At. Spectrom.*, 2016, **31**, 423-439.

[218] H. A. O. Wang, D. Grolimund, C. Giesen, C. N. Borca, J. R. H. Shaw-Stewart, B. Bodenmiller and D. Günther, *Anal. Chem.*, 2013, **85**, 10107-10116.

[219] R. Hergenröder, *J. Anal. At. Spectrom.*, 2006, **21**, 1016-1026.

[220] R. Hergenröder, *Spectrochim. Acta B*, 2006, **61**, 284-300.

[221] D. Drescher, C. Giesen, H. Traub, U. Panne, J. Kneipp and N. Jakubowski, *Anal. Chem.*, 2012, **84**, 9684-9688.

[222] N. N. Mahmoud, A. M. Alkilany, D. Dietrich, U. Karst, A.G. Al-Bakri and E. A. Khalil, *J. Colloid Interface Sci.*, 2017, **503**, 95-102.

[223] A. C. Niehoff, A. Moosmann, J. Söbbing, A. Wiehe, D. Mulac, C. A. Wehe, O. Reifschneider, F. Blaske, S. Wagner, M. Sperling, H. von Briesen, K. Langer and U. Karst, *Metallomics*, 2014, **6**, 77-81.

[224] D. Pozebon, G. L. Scheffler and V. L. Dressler, *J. Anal. At. Spectrom.*, 2017, **32**, 890-919.

[225] I. L. Hsiao, F. S. Bierkandt, P. Reichardt, A. Luch, Y. J. Huang, N. Jakubowski, J. Tentschert and A. Haase, *J. Nanobiotechnol.*, 2016, **14**, 50.

[226] S. G. Elci, G.Y. Tonga, B. Yan, S. T. Kim, C. S. Kim, Y. Jiang, K. Saha, D. F. Moyano, A. L. M. Marsico, V. M. Rotello and R. W. Vachet, *ACS Nano*, 2017, **11**, 7424-7430.

[227] S. G. Elci, Y. Jiang, B. Yan, S. T. Kim, K. Saha, D. F. Moyano, G. Y. Tonga, L. C. Jackson, V. M. Rotello and R. W. Vachet, *ACS Nano*, 2016, **10**, 5536-5542.

[228] T. Büchner, D. Drescher, H. Traub, P. Schrade, S. Bachmann, N. Jakubowski and J. Kneipp, *Anal. Bioanal. Chem.*, 2014, **406**, 7003-7014.

[229] S. Böhme, M. Baccaro, M. Schmidt, A. Potthoff, H. J. Stärk, T. Reemtsma and D. Kühnel, *Environ. Sci.: Nano*, 2017, **4**, 1005-1015.

[230] N. Yan, Z. Zhu, L. Jin, W. Guo, Y. Gan and S. Hu, *Anal. Chem.*, 2015, **87**, 6079-6087.

[231] V. Nischwitz, N. Gottselig, M. Bläsing, A. Missong and E. Klumpp, *J. Anal. At. Spectrom.*, submitted.